TECHNICAL REPORT 89-07

STRIPA PROJECT

INTERIM REPORT ON THE ROCK SEALING PROJECT (STAGE 1)

R. Pusch (Principal investigator)[1)]
L. Börgesson[1)]
A. Fredrikson[1)]
I. Markström[2)]
M. Erlström[2)]
G. Ramqvist[3)]
M. Gray[4)]
B. Coons[5)]

SEPTEMBER 1988

Nagra
Nationale
Genossenschaft
für die Lagerung
radioaktiver Abfälle

Cédra
Société coopérative
nationale
pour l'entreposage
de déchets radioactifs

Cisra
Società cooperativa
nazionale
per l'immagazzinamento
di scorie radioattive

TECHNICAL REPORT 89-07

STRIPA PROJECT

INTERIM REPORT ON THE ROCK SEALING PROJECT (STAGE 1)

R. Pusch (Principal investigator)[1)]
L. Börgesson[1)]
A. Fredrikson[1)]
I. Markström[2)]
M. Erlström[2)]
G. Ramqvist[3)]
M. Gray[4)]
B. Coons[5)]

[1)]Clay Technology, Sweden
[2)]Swedish Geological AB, Sweden
[3)]Eltekno, AB, Sweden
[4)]AECL, Canada
[5)]IT Corp, USA

SEPTEMBER 1988

Parkstrasse 23 5401 Baden / Schweiz Telephon 056 / 20 55 11

Der vorliegende Bericht betrifft eine Studie, die für das Stripa-Projekt ausgeführt wurde. Die Autoren haben ihre eigenen Ansichten und Schlussfolgerungen dargestellt. Diese müssen nicht unbedingt mit denjenigen des Auftraggebers übereinstimmen.

Le présent rapport a été préparé pour le projet de Stripa. Les opinions et conclusions présentées sont celles des auteurs et ne correspondent pas nécessairement à ceux du client.

This report concerns a study which was conducted for the Stripa Project. The conclusions and viewpoints presented in the report are those of the authors and do not necessarily coincide with those of the client.

Das Stripa-Projekt ist ein Projekt der Nuklearagentur der OECD. Unter internationaler Beteiligung werden im Rahmen einer 3. Phase dieses Projektes von 1986-1991 Forschungsarbeiten in einem unterirdischen Felslabor in Schweden durchgeführt. Unter Anwendung des in den vorhergehenden Phasen 1 und 2 Gelernten sollen folgende Arbeiten realisiert werden:

- Anwendung verschiedener Felduntersuchungs- und Berechnungsmethoden, um den Wasserfluss und Nuklidtransport in einem unbekannten Felsvolumen des Stripagranites vorherzusagen und anschliessend zu überprüfen
- Evaluation verschiedenster Materialien und Methoden zum Abdichten wasserführender Klüfte im Stripagranit

Seitens der Schweiz beteiligt sich die Nagra an diesen Untersuchungen. Die technischen Berichte aus dem Stripa-Projekt erscheinen gleichzeitig in der NTB-Serie der Nagra.

The Stripa Project is organised as an autonomous project of the Nuclear Energy Agency of the OECD. Over the time period 1986-1991 (Phase 3 of the Project), an international cooperative programme of investigations is being carried out in an underground rock laboratory in Sweden. Building on experience gained in Phases 1 and 2, the following research will be carried out:

- Application of various site characterisation techniques and analysis methods with a view to predicting and validating groundwater flow and nuclide transport in an unexplored volume of Stripa granite
- Verification of the use of different materials and techniques for sealing water-bearing fractures in the Stripa granite

Switzerland is represented in the Stripa Project by Nagra and the Stripa Project technical reports appear in the Nagra NTB series.

Le projet de Stripa est un projet de l'Agence de l'OCDE pour l'Energie Nucléaire. C'est dans le cadre d'une troisième phase de ce projet allant de 1986 à 1991, que des travaux de recherches sont réalisés avec une participation internationale, dans un laboratoire souterrain de Suède. Il s'agit d'effectuer les travaux ci-dessous, en mettant en application ce que l'on a appris au cours des précédentes phases 1 et 2:

- Application de diverses méthodes de recherches sur le terrain et de calcul, pour prévoir puis contrôler l'écoulement de l'eau et le transport des nucléides dans un volume rocheux inconnu du granite de Stripa
- Evaluation des méthodes et des matériaux les plus divers, en vue de colmater des fractures aquifères du granite de Stripa

La Cédra participe à ces recherches pour la Suisse. Les rapports techniques rédigés à propos du projet de Stripa paraissent en même temps dans la série des Rapports Techniques de la Cédra (NTB).

ABSTRACT

The objective of the Sealing Project is to find new ways of sealing finely fractured rock by grouting. This requires development of new injection techniques as well as identification of materials which are sufficiently fluid to be groutable, have an acceptably low permeability and are physically and chemically stable. The present report describes the results of the first two years of investigations (Stage 1) which gave very positive results, as can be concluded from the large-scale field test.

RESUME

L'objectif du Projet de Scellement est de trouver des solutions pour obturer par cimentation des roches finement fracturées. Cela implique la mise au point de nouvelles techniques d'injection ainsi que l'identification de ciments suffisamment fluides pour cette application, d'étanchéité satisfaisante et stables physiquement et chimiquement. Le présent rapport décrit les résultats obtenus au cours des deux premières années d'investigations (phase 1) qui ont donné des résultats très positifs ainsi que l'a confirmé un important essai de terrain à grande échelle.

ZUSAMMENFASSUNG

Ziel des Versiegelungstests ist es, neue Methoden zur Abdichtung von feingeklüftetem Gestein mit Zementmörtel zu entwickeln. Dies bedingt sowohl die Entwicklung neuer Injektionstechniken als auch die Identifizierung von Mörteln, die für diesen Zweck genügend flüssig sind, eine annehmbar tiefe Permeabilität zeigen und auch physisch und chemisch stabil sind. Dieser Bericht präsentiert die Untersuchungsresultate der ersten zwei Jahre (Phase 1); sie sind als sehr positiv zu betrachten, wie aus dem grossräumigen Feldtest hervorgeht.

LIST OF CONTENTS

CHAPTER I

SUMMARY

The most essential goal of the Rock Sealing Project, i.e.to develop a technique to bring grout into fractures with a "hydraulic" aperture of less than 100 µm, has been reached. Actually, it has been demonstrated that clay and cement grouts of considerable density penetrate fractures with an aperture of 10-20 µm by applying the "Dynamic Injection Technique". The distribution of grouts in fractures can be reasonably well predicted on the basis of Lugeon testing and fracture mapping, applying a flow model that has been developed in the course of the project. This theory requires that suitable flow parameters are used, which depend on the grout density, the applied frequency, and the geometry of the system (fracture aperture, borehole diameter). The flow parameters have been deduced from systematic viscometer tests, with special respect to the influence of vibrations.

Two major grout materials have been found to be the most promising candidate materials, i.e. finely ground cement with 10 % silica fume and 1 % superplasticizer (w/c ~0.4), and 50/50 Na bentonite and finely ground quartz powder. Their hydraulic conductivity appears to be sufficiently low to yield a net hydraulic conductivity of any grouted rock of about 10^{-10} m/s and they offer a reasonably high resistance to piping and erosion. Lab percolation tests simulating widening of a sealed fracture by 10-30 % at 90°C show that the conductivity of the expanded system is significantly increased, but that it is still not higher than 10^{-6} m/s. As to the choice of clay grout compositions it is clear that there are options, a major one being clay/brine which has a high fluidity at a consistency corresponding to 1.5 times the liquid limit and which is expected to consolidate very quickly in the rock, yielding a fresh- or brackish-water smectite with a density of about 1.3 t/m^3 and a high resistance to percolation, piping and erosion. The matter of longevity of the candidate grouts has been investigated but needs more attention. However, a preliminary estimate is that the chemical stability may be extremely long-lasting, i.e. tens or hundreds of thousand years depending on the temperature and percolation rates. Thus, it is felt that there is a very good basis for continuing the Stripa sealing project.

A large-scale Pilot Field Test was conducted in January, comprising Lugeon tests for hydraulic characterization of the test rock area and for predicition of the grout penetration. The test, which had the form of grouting using four 1.5 m long holes,

two 7 m long ones and two 40 m long holes, was concluded to be successful since the sealing effect turned out to be the expected one, and since the distribution of the grouts in the rock fractures corresponded relatively well to the predictions as demonstrated at a comprehensive excavation of the rock mass. Both cement and clay were used successfully.

The experience from the field test and the basic knowledge extracted from the lab experiments have formed the basis of the planning of a Large Scale Field Test. The intention is to apply the instrument of rock sealing to a number of practical cases, where cutting-off and redirection of groundwater flow in repositories are called for. Five field subtests, which are integrated mutually or with other Stripa projects (3D), are proposed. One of them concerns "near-field" sealing, i.e. sealing of tunnel floors hosting deposition holes, while two involve sealing of "disturbed" rock around tunnels. A fourth one concerns sealing of a natural fracture zone in the 3D area, and this latter test has the expected spin-off effect of obtaining additional information on the general flow pattern around the northeastern wing of the 3 D cross. A fifth test is an option of sealing structures in the Validation Drift. It is also suggested that the longevity of major grout types is focussed on, and detailed plans have been worked out for that purpose. It is foreseen that the continuation of the project, as outlined in this report, will yield suitable methods and grouts for effective and long-lasting sealing of rock for use at strategic points in repositories.

CHAPTER II INTRODUCTION

1 SCOPE OF STUDY

The Rock Sealing Project comprises an investigation of the possibility of effectively blocking or retarding groundwater flow through underground repositories by sealing rock fractures. No particular aperture intervals have been considered since a spectrum of fracture types and widths are expected to require sealing in the construction phase, but strong emphasis has been put on effective sealing of fine fractures with equivalent apertures of down to 10 μm. For this, no technique was available at the start of the study and great effort has therefore been made to develop practically useful techniques and suitable grouts. In particular, the longevity of these substances has been in focus and it is still a major subject in the forthcoming work.

The work started in late 1986 and the present document describes the situation and yields preliminary test results as per February 1988, It forms a basis of the second part of the project that is intended to be conducted in the period 1988-1991 (1992):

1 Physical properties of grouts in the grouting phase

2 Physical properties of grouts in the grouted state

3 Longevity assessment - physical and chemical

4 Development of grout injection technique

5 Pilot Field Test at Stripa for documentation of sealing efficiency and validation of grout flow model for prediction of grout penetration

6 Planning of Large Scale Field Tests

The detailed test programs are defined in the respective chapter.

2 OUTLINE OF THE STUDY

2.1 GENERAL

The major features of the research work reported here were defined in the "General Program for Testing of Rock Sealing Candidates" of April 6, 1987, to which the reader is referred. It defined the form of the six activities specified in the preceding chapter. In principle, the intended test techniques have been found to be relevant and useful and the work is on time. We will point out here a few important findings that have affected the detailed form of the research program and the planning of the Large Scale Field Test.

* The efficiency of the "dynamic" injection technique in lowering the flow resistance ("viscosity") of the grouts has emphasized the importance of developing a theory of grout flow that accounts for the vibratory stress state. Much work with substantial success has been made in this field

* Cement slurries with w/c in the range of 0.35-0.45 can be given a very low viscosity by rather moderate addition of superplasticizer. It appears to be easier to produce very low-viscous cement slurries than smectite suspensions without exceeding the liquid limit too much

* The sealing effect of even very dilute clay gels is significant and sudden expansion by 30 % of fractures filled with clay gels having a water content equal to 1.6 times the liquid limit, does not cause a very dramatic increase in hydraulic conductivity due to the flexibility and bond strength of such gels

* Cement with w/c ~0.4, 10 % silica fume and 1 % superplasticizer, has a substantial reserve hydration potential which is mobilized on heating to 90°C

* A very effective dynamic injection device is at hand today but it is required that further development be made

* The longevity is the key problem that remains to be solved. The work made so far is very promising

2.2 CHOICE OF CANDIDATE MATERIALS

The State of Art review concerning grouts and grouting techniques that formed the basis of the lab and field work reported here, indicated that clay-based and cementitious grouts were major candidate materials. The Task Force then made a preliminary selection namely:

A Finely ground Portland cement with silica fume and superplasticizer

B Finely ground cement (Alofix, Onoda Co, Japan)

C Na montmorillonite-rich clay (Tixoton, Süd-Chemie, West Germany)

D Ca montmorillonite-rich clay (Süd-Chemie, West Germany)

E Mixture of Na montmorillonite-rich clay and quartz filler (<15 µm)

A decision was taken early that candidates A, C and E should be investigated in a first "qualification heat" and that the study should later comprise also B and D. This plan is still valid.

CHAPTER III GROUTING TECHNIQUE

1 BACKGROUND

It is a well known fact from rock construction that while wide fractures can be effectively and easily sealed with cement, apertures smaller than about 100 µm cannot be grouted even with very high w/c-cements or with smectite clay. Rather intense SKB-research in this field was initiated about 4 years ago, leading to the new technique of static pressure superimposed by high frequence percussion pumping. The idea was launched by the principal investigator, the technique and equipment used at the exploratory stage being developed in cooperation with Karl-Erik Nyman, Svensk Grundundersökning AB, Arlöv, Sweden.

Fairly large-scaled lab grouting tests indicated that both clays and cements can be effectively injected in 100 µm slots if the water content is only slightly higher than the liquid limit, and this formed the basis of the present work.

The choice of 100 µm as a standard aperture of slots for lab injection tests, such as the ones referred to and the ones used in the present study, was based on the fact that this measure represents the lower limit for penetration of clayey grouts, as well as on the conclusion that significantly water-bearing rock fractures have the form of sets of channels with apertures ranging between 0 and 200 µm, 100 µm being a reasonable average value.

While the tests preceding the present study mainly served as pilot experiments for identifying the potential and limitations of the dynamic grouting technique, it was clear from the beginning that theoretical models also had to be derived to allow for prediction of the grout penetration. Such modelling therefore forms a significant part of the work.

2 THE DYNAMIC INJECTION TECHNIQUE

The dynamic injection device was manufactured by Svensk Grundundersökning AB. It has been successively developed and improved by theoretical studies and grouting experiences.

The idea of producing a dynamic pressure by percussion has both advantages and disadvantages, one disadvantage being that the duration of the initial stress-wave is very short, another being that it is difficult to change the frequency and the amplitude of the stress wave. However, the advantage which is very important is that the total dynamic energy produced is very high compared to the energy from ordinary vibrators.

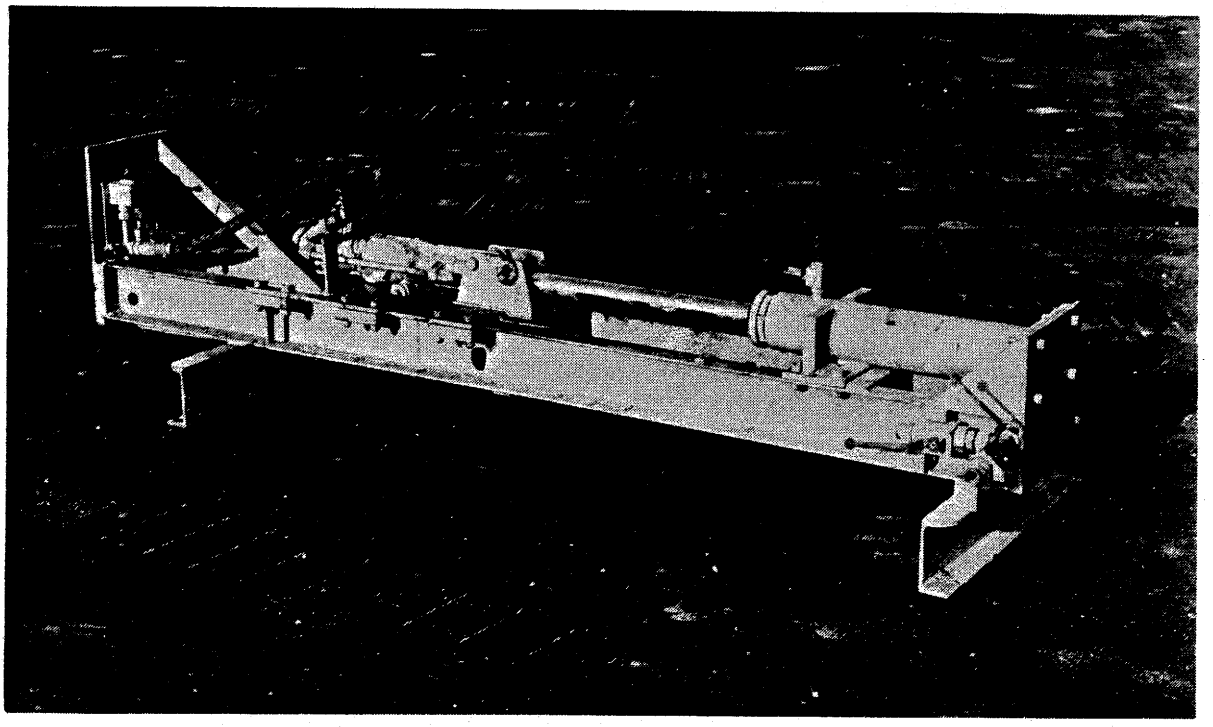

Fig. 2.1 The latest version of the dynamic injection machine

Fig 2.1 shows a picture of the injection machine used in Stripa. The machine is supplied with grouts from a colloid mixer via a pump.

The stress wave produced by the injection machine can be theoretically derived:

A steel hammer with the mass m_1 strikes a steel piston with the velocity v_1. The mass of the piston is m_2 and the velocity of the piston is v after the strike while $v=0$ before the strike. The cross section area of the piston is A_2 leading into a tube with the same inner area. The tube is filled with the grout having an E-modulus E_v.

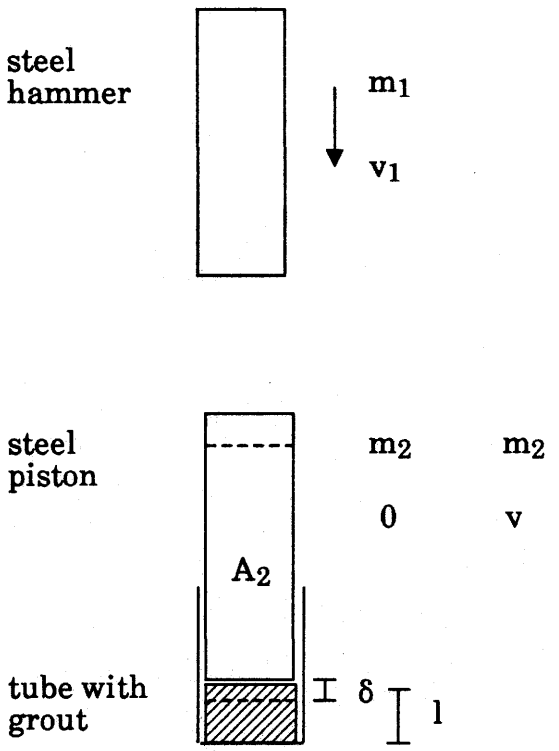

Since $E_{steel} >> E_v$ only the grout is supposed to be compressed.

Constant momentum gives

$$m_1 v_1 = (m_1 + m_2) \cdot v \qquad (1)$$

$$v = \frac{m_1}{m_1 + m_2} v_1$$

Newtons' second law gives

$$-F(t) = (m_1 + m_2) \frac{dv}{dt} \qquad (2)$$

where F(t) is the force from the grout to the piston as a function of the time t.

$$\delta = \int_o^t v\,dt \tag{3}$$

The compression of the grout will be

$$\varepsilon = \frac{\delta}{l} = \frac{p(t)}{E_v} = \frac{F(t)}{A} \cdot \frac{1}{E_v} \tag{4}$$

where p(t) is the pressure in the grout

$$F(t) = \frac{\delta}{l} \cdot A \cdot E_v = \int_o^t v \cdot dt \cdot \frac{A \cdot E_v}{l} \tag{5}$$

$$-\int_o^t v \cdot dt \frac{A \cdot E_v}{l} = (m_1 + m_2) \frac{dv}{dt} \tag{6}$$

Take the derivative of Eq. (6)

$$-v \frac{A \cdot E_v}{l} = (m_1 + m_2) \frac{d^2v}{dt^2} \tag{7}$$

$$\frac{d^2v}{dt^2} + v \frac{A \cdot E_v}{l(m_1 + m_2)} = 0 \tag{8}$$

const

$$\frac{d^2v}{dt^2} + v \cdot const = 0 \tag{9}$$

The solution of the differential Eq. (9) is

$$v = C_1 \cos(\sqrt{const} \cdot t) \tag{10}$$

t = 0 gives

$$v = C_1 = \frac{m_1}{m_1 + m_2} \cdot v_1$$

$$v = \frac{m_1}{m_1 + m_2} v_1 \cdot \cos(\sqrt{const} \cdot t) \tag{11}$$

Take the derivative of Eq. (11) and put it into Eq. (2)

$$F(t) = m_1 v_1 \cdot \sqrt{const} \cdot \sin(\sqrt{const} \cdot t) \tag{12}$$

Considering

$$const = \frac{A_2 E_v}{l(m_1 + m_2)}$$

$$p(t) = \frac{F(t)}{A_2}$$

we arrive at the final solution

$$p(t) = m_1 v_1 \sqrt{\frac{E_v}{A_2 l (m_1 + m_2)}} \cdot \sin\left(\sqrt{\frac{A_2 E_v}{l (m_1 + m_2)}} \cdot t\right) \tag{13}$$

ampl

Thus, theoretically the injection machine will produce a sinusoidal pressure wave with respect to the amplitude:

$$ampl = m_1 v_1 \sqrt{\frac{E_v}{A_2 l (m_1 + m_2)}} \tag{14}$$

and the frequency

$$f = \frac{1}{2\pi} \sqrt{\frac{A_2 E_v}{l (m_1 + m_2)}} \tag{15}$$

The theoretical frequency is much higher than f = 50 Hz which is the percussion frequency of the machine. This means that the time between two strikes is long compared to the duration of the strike. However, measurements of the pressure waves after passing the tubes and connections show that secondary effects will deform the waves and give them a shape which can be approximated by a

sinusoidal curve. The flow modelling for the fracture penetration can thus be made using an oscillatory sinusoidal pressure as boundary condition.

3 BASIC GROUT FLOW THEORY

3.1 SYMBOLS

The symbols used in the theoretical solutions are listed below.

A = inner area (m^2, tube) or area/meter (m, slot)

a = wave velocity (m/s)

d = inner diameter (tube) or slot aperture(m)

d_R = tube thickness (m)

E_R = E-modulus of wall (Pa)

E_v = E - modulus of liquid (Pa) $E = -dp \frac{v}{dv}$

H = total pressure, $H = h_1 + h'$(Pa)

h_1 = constant pressure (Pa)

h' = oscill pressure (Pa)

$|h'|$ = ampl of oscill pressure (Pa)

h_o = initial oscill pressure amplitude (Pa)

L_1 = distance between inflow and front

m = viscosity type of parameter (Pa)

m_1 = $m/\gamma_o n$

n = exponent

P = wet parameter (m)

p = pressure (Pa)

Q = total flow, $Q = q_1 + q'$(m^3/s)

q_1 = constant flow (m^3/s)

q' = oscill flow (m^3/s)

$|q'|$ = ampl of oscill flow (m^3/s)

s = oscill def (m)

t = time (sec)

u = rate of flow (m/s)

w = angular frequency (s^{-1})

x = distance from inflow $(0 \le x \le L_1)$ (m)

δ = attenuation factor

γ = complex constant

$\dot{\gamma}$ = rate of shear (s^{-1})

$\dot{\gamma}_o$ = normalized rate of shear (s^{-1})

ρ_v = liquid density (kg/m^3)

τ = shear stress (Pa)

μ = dynamic viscosity (Newtonian, Pas)

ν = kinematic viscosity (Newtonian) $\upsilon = \frac{\mu}{\rho}$

3.2 FLOW MODEL

An attempt is made to formulate general theoretical solutions of the influence of static pressure superimposed by an oscillating pressure on the static and oscillating flow of a liquid in circular boreholes and thin rectangular fractures in a rock. The study is made in order to evaluate the influence of geometrical parameters and liquid properties of the flow. The study first deals with a perfectly Newtonian liquid and then with a non-Newtonian liquid. The theories are developed in cooperation with Dr Lennart Jönsson at the Department of Water Resources Engineering, University of Lund.

3.2.1 General theory of an oscillating compressible flow

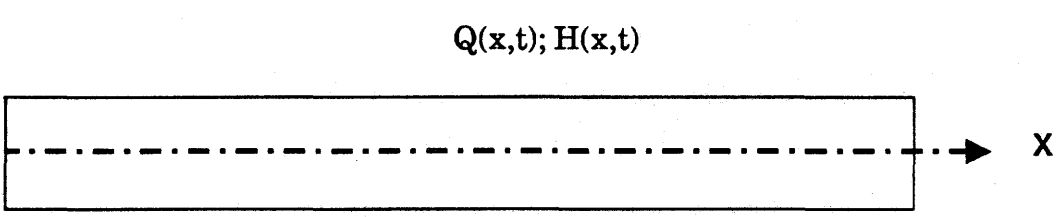

Consider an unsteady flow in a tube of a fluid which is slightly compressible. The general equations for the flow is given by (Wylie and Streeter) [1].

$$C\frac{\delta H}{\delta t}+\frac{\delta Q}{\delta x}=0 \tag{16}$$

$$L\frac{\delta Q}{\delta t}+\frac{\delta H}{\delta x}+RQ=0 \tag{17}$$

where

$$L=\frac{4}{3gA}$$

$$C=\frac{gA}{a^2}$$

$$R=\frac{32\upsilon}{gAd^2}\ \text{(laminar flow)}$$

---

1) Fluid transients, Wylie and Streeter, Mc Graw-Hill Inc., 1978

It is supposed that the friction is described by the linear term $R \cdot Q$ for a Newtonian fluid.

Suppose that the unsteady flow is composed of a quasi-steady flow q_1 and pressure h_1 and an oscillatory smaller component q' resp h'.

$$Q = q_1 + q'$$

$$H = h_1 + h'$$

The oscillating component is described by

$$C \frac{\delta h'}{\delta t} + \frac{\delta q'}{\delta x} = 0 \tag{18}$$

$$L \frac{\delta q'}{\delta t} + \frac{\delta h'}{\delta x} + R\, q' = 0 \tag{19}$$

Elimination of q' in Eq. (3) and Eq. (4) gives:

$$\frac{\delta^2 h'}{\delta x^2} = L\, C \frac{\delta^2 h'}{\delta t^2} + RC \frac{\delta h'}{\delta t} \tag{20}$$

Let

$$h'(x,t) = X(x) \cdot \quad T(t) \tag{21}$$

giving

$$\frac{1}{X} \frac{d^2X}{dx^2} = \frac{1}{T} \left(C L \frac{d^2T}{dt^2} + RC \frac{dT}{dt}\right) = const = \gamma^2 \tag{22}$$

Thus

a

$$\frac{1}{X} \frac{d^2X}{dx^2} = \gamma^2$$

$$X(x) = A_1 e^{\gamma x} + A_2 e^{-\gamma x} \tag{23}$$

b) Suppose that the temporal disturbance is purely sinusoidal and forced on the tube. The angular frequency is considered as fixed -w. The temporal part of the solution is thus of the form:

$$T = A_3 e^{iwt} \tag{24}$$

Eq. (22) and Eq. (24) give:

$$-CLw^2 + iRCw - \gamma^2 = 0 \tag{25}$$

Put

$$\gamma = \sqrt{-CLw^2 + iCRw} = f + ik$$

which gives for the real and imaginary parts respectively:

$$f = \frac{CRw}{2k} \tag{26}$$

$$k = \sqrt{\frac{CLw^2}{2} + \sqrt{\frac{C^2L^2w^4}{4} + \frac{C^2R^2w^2}{4}}} \tag{27}$$

It can be shown that the general solution to Eq. (18) and Eq. (19) with a forced disturbance according to Eq. (24) is given by:

$$h'(x,t) = e^{iwt}(C_1 e^{\gamma x} + C_2 e^{-\gamma x}) \tag{28}$$

$$q'(x,t) = -\frac{Ciw}{\gamma} e^{iwt}(C_1 e^{\gamma x} - C_2 e^{-\gamma x}) \tag{29}$$

where C_1 and C_2 are constants determined by means of the specific boundary conditions. Eq. (28) and Eq. (29) thus describe the attenuation and phase characteristics along a conduit of imposed pressure oscillations.

3.2.2 Circular cross section

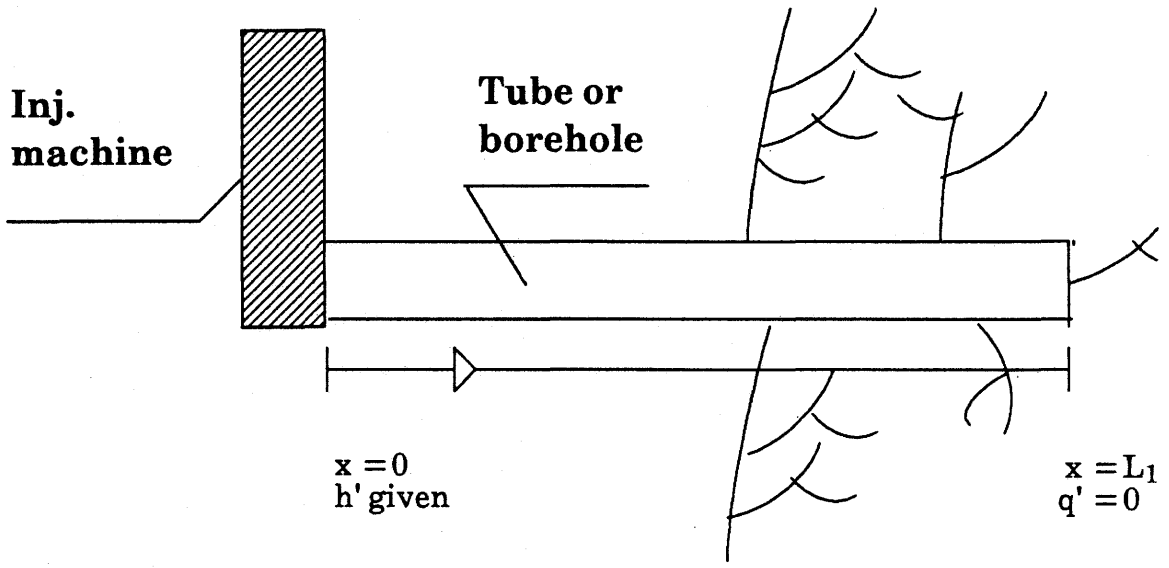

In this chapter the wave propagation in the tube leading from an injection device into the fracture is studied both in order to have the basic equations for further applications on non-Newtonian liquids in fractures and in order to be able to make an optimal design of the equipment. The boundary conditions must in this case be an initial ($x=0$) pressure equal to the pressure produced by the machine:

$$x = 0 \rightarrow h' = h_o e^{iwt} \tag{30}$$

At the end of the tube ($x = L_1$) it is necessary to apply the simplified assumption that the flow is zero:

$$x = L_1 \rightarrow q' = 0 \tag{31}$$

This is a relevant assumption since the cross sectional area of the fracture is very small compared to the cross sectional area of the tube. These conditions give the following values of the constants

$$C_2 = \frac{h_o e^{\gamma L_1}}{e^{\gamma L_1} + e^{-\gamma L_1}} \tag{32}$$

$$C_1 = C_2 e^{-2\gamma L_1} \tag{33}$$

The variation of the pressure will thus be:

$$h'(x,t) = h_o e^{iwt} \frac{e^{-\gamma(L_1 - x)} + e^{\gamma(L_1 - x)}}{e^{\gamma L_1} + e^{-\gamma L_1}} \tag{34}$$

The complex constant $\gamma = f + ik$ can be inserted in Eq. (16). Taking the absolute value of this equation the amplitude of the oscillating pressure is:

$$\left| h'(x,t) \right| = h_o \sqrt{\frac{\cosh(2f(L_1 - x)) + \cos(2k(L_1 - x))}{\cosh(2fL_1) + \cos(2kL_1)}} \tag{35}$$

The constants f and k are given by Eq. (11).

The rate of the wave propagation a can be calculated by the general Eq. (18):

$$a = \sqrt{\frac{E_v/\rho_v}{1 + \frac{E_v}{E_R} \cdot \frac{d}{d_R}}} \tag{36}$$

The amplitude of the oscillatory flow will be

$$|q'(x,t)| = \frac{h_o}{g\rho_v} \frac{Cw}{\sqrt{f^2 + k^2}} \sqrt{\frac{\cosh(2f(L_1 - x)) - \cos(2k(L_1 - x))}{\cosh(2fL_1) + \cos(2kL_1)}} \tag{37}$$

and the corresponding maximum oscillatory deformation

$$\left| s_{ampl} \right| = \frac{|q'(x_1 t)|}{Aw} \tag{38}$$

3.2.3 Thin rectangular cross-section

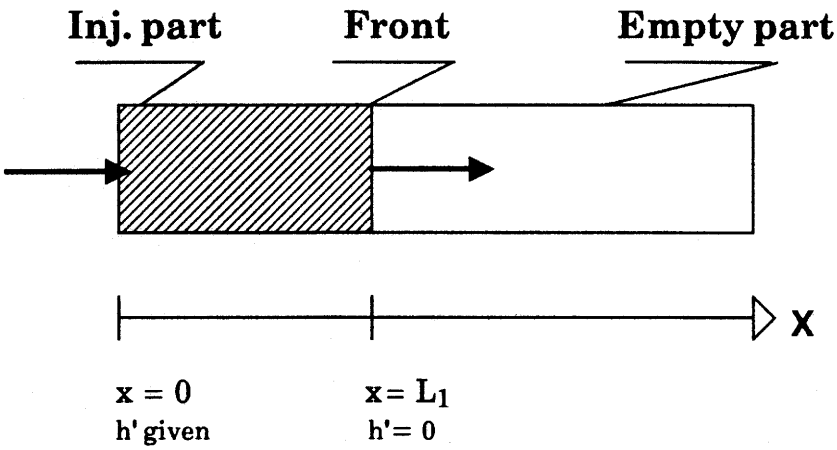

The liquid is injected from the beginning of the fracture, $x = 0$, and the flow is one-dimensional which means that the front is straight. The basic solution of h' and q' in Chapter 2 is still valid but with different values of C_1 and C_2. The boundary conditions in the beginning of the slot will be

$$x = 0 \rightarrow h' = h_o e^{iwt} \tag{39}$$

At the front of the penetrating liquid $(x = L_1)$ there is no limitation on the flow but the pressure is zero:

$$x = L_1 \rightarrow h' = 0$$

These boundary conditions give the following values of the constants

$$C_1 = -\frac{h_o e^{-2\gamma L_1}}{1 - e^{-2\gamma L_1}} \tag{40}$$

$$C_2 = \frac{h_o}{1 - e^{-2\gamma L_1}} \tag{41}$$

The variation of the pressure will thus be:

$$h'(x,t) = h_o e^{iwt} \quad \frac{e^{\gamma(L_1-x)} - e^{-\gamma(L_1-x)}}{e^{\gamma L_1} - e^{-\gamma L_1}} \tag{42}$$

Eq. (42) can be transformed in an identical way as Eq. (34). This transformation gives:

$$|h'(x,t)| = h_o \sqrt{\frac{\cosh(2f(L_1-x)) - \cos(2k(L_1-x))}{\cosh(2fL_1) - \cos(2kL_1)}} \tag{43}$$

The solution for the oscillating flow, using the new values of C_1 and C_2 is, according to (13):

$$q' = \frac{h_o}{g\rho_v} e^{iwt} \quad \frac{Ciw}{\gamma} \quad \frac{e^{-\gamma(L_1-x)} + e^{\gamma(L_1-x)}}{e^{\gamma L_1} - e^{-\gamma L_1}} \tag{44}$$

Using $\gamma = f + ik$ in the same way as earlier we arrive at Eq. (45):

$$|q'| = \frac{h_o}{g\rho_v} \quad \frac{Cw}{\sqrt{f^2+k^2}} \sqrt{\frac{\cosh(2f(L_1-x)) + \cos(2k(L_1-x))}{\cosh(2fL_1) - \cos(2kL_1)}} \tag{45}$$

The oscillatory flow and pressure in a fracture can thus be solved according to Eq. (43) and (45) using the values of the parameters shown in Chapter 3.2.1 and Chapter 3.2.2.

3.2.4 Non-Newtonian flow

Viscosity measurements show that the gels of interest for injection do not follow the traditional Newtonian viscosity law:

$$\tau = \mu \dot{\gamma} \tag{46}$$

but a modified much less rate dependent power law:

$$\tau = m_1 \dot{\gamma}^n \ (n<1) \tag{47}$$

where n according to preliminary test results depends on the composition of the granules while m_1 depends on the water content.

Eq. (47) is suitably written as:

$$\tau = m \left(\frac{\dot{\gamma}}{\dot{\gamma}_o}\right)^n \tag{48}$$

in order to have the same unit of m and τ (kPa) which means that

$$m_1 = \frac{m}{\dot{\gamma}_o^{\,n}}$$

This law may be included in the theory in the following way

Consider a layer with the thickness d!

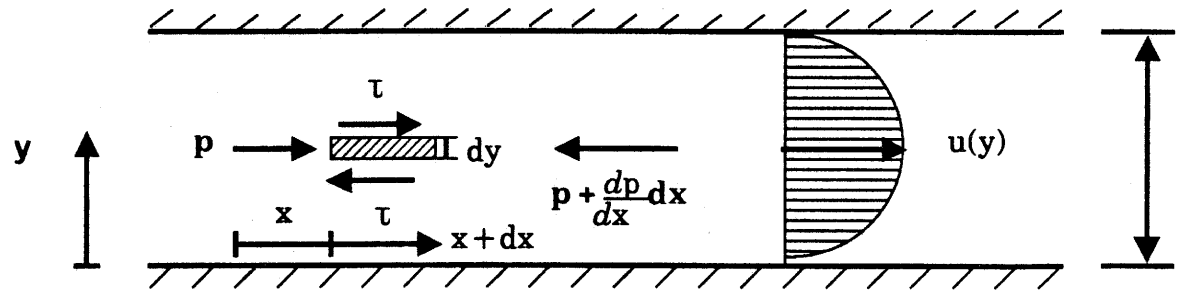

A pressure gradient $\frac{dp}{dx}$ gives a rate distribution $u\,(y)$. Equilibrium between forces on a small element in the x-direction at steady state gives

$$p\,dy - (p + \frac{\delta p}{\delta x}\,dx)\,dy - \tau(y)dx + \tau(y+dy)\,dx = 0 \tag{49}$$

where

$$\tau(y) = m_1(\dot{\gamma})^n = m_1\,(\frac{du}{dy})^n$$

giving

$$-\frac{\delta p}{\delta x} + \frac{d\tau}{dy} = 0$$

$$\frac{d}{dy}\,[m_1(\frac{du}{dy})^n] = \frac{dp}{dx}$$

A double integration with respect to y gives

$$u(y) = \frac{1}{m_1^{1/n}} \cdot \frac{1}{\frac{dp}{dx}}\,[y\,\frac{dp}{dx} + A_1]^{(\frac{1}{n}+1)} \cdot \frac{1}{\frac{1}{n}+1} + B_1 \tag{50}$$

Assume a raw surface which gives $u = 0$ at $y = 0$ and at $y = d$. These boundary conditions give the values of A_1 and B_1, the rate distribution being:

$$u(y) = \frac{1}{m_1^{1/n}}(-\frac{dp}{dx})^{\frac{1}{n}} \frac{1}{\frac{1}{n}+1}\left[\,(\frac{d}{2})^{\frac{1}{n}+1} - (\frac{d}{2}-y)^{\frac{1}{n}+1}\,\right] \tag{51}$$

The total flow is given by an integration

$$Q = 2\int_0^{d/2} u(y)\,dy \tag{52}$$

resulting in

$$Q = B(-\frac{dp}{dx})^{\frac{1}{n}} \cdot\; d^{(\frac{1}{n}+2)} \tag{53}$$

where

$$B = \frac{2}{m_1^{1/n}} \cdot \frac{(\frac{1}{n}+1)}{(\frac{1}{n}+1)(\frac{1}{n}+2)\,2^{(\frac{1}{n}+2)}} \tag{54}$$

Eq. (53) gives:

$$-\frac{dp}{dx} = \left(\frac{Q}{B} \cdot \frac{1}{d^{\left(\frac{1}{n}+2\right)}} \right)^n = Q^n \frac{1}{B^n} \frac{1}{d^{(1+2n)}} \tag{55}$$

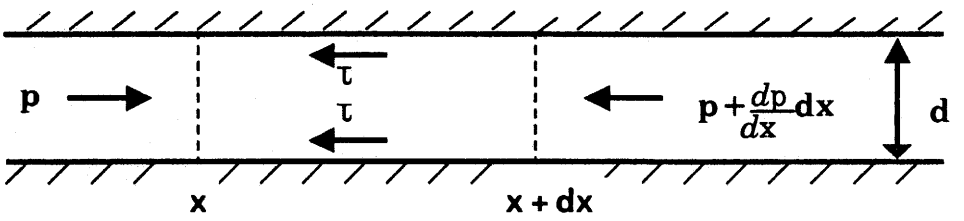

But force equilibrium in the slot yields

$$-\frac{dp}{dx}\, d = 2\tau$$

giving

$$\tau = \frac{d}{2} Q^n \frac{1}{B^n} \cdot \frac{1}{d^{(1+2n)}} \tag{56}$$

We will now consider the unsteady motion of the non-Newtonian liquid in the fracture (Eq. 17):

$$-\frac{\delta H}{\delta x} - \frac{\tau P}{\rho g A} = \frac{1}{Ag} \cdot \frac{\delta Q}{\delta t}$$

where $Q = Q(x,t)$ = unsteady flow

τ = shear stress at the boundary between the liquid and the fracture

Using Eq. (56) one obtains

$$\frac{1}{Ag} \frac{\delta Q}{\delta t} + \frac{\delta H}{\delta x} + \frac{dQ^n}{2B^n} \cdot \frac{1}{d^{(1+2n)}} \cdot \frac{1}{g\rho} \cdot \frac{2}{d} = 0 \tag{57}$$

where as usual one supposes that friction in the unsteady state can be approximated by the corresponding instantaneous steady-state value.

$$\frac{1}{Ag}\frac{\delta Q}{\delta t} + \frac{\delta H}{\delta x} + Q^n \cdot \frac{1}{g\rho B^n d^{(1+2n)}} = 0 \tag{58}$$

We suppose that the total flow and the pressure are composed of a basic component and a superimposed oscillating part.

$$Q = q_1 + q'$$

$$H = h_1 + h'$$

giving

$$Q^n = (q_1+q')^n \simeq q_1\,(1+\frac{q'}{q_1}) \simeq q_1^{\,n}\,(1+\frac{nq'}{q_1}) = q_1^n + nq' \cdot \; q_1^{\,(n-1)} \tag{59}$$

giving

$$\frac{1}{Ag}\frac{\delta q'}{\delta t} + \frac{\delta h'}{\delta x} + Rq' = 0 \tag{60}$$

$$R = nq_1^{\,(n-1)} \cdot \frac{1}{B^n} \cdot \frac{1}{d^{(1+2n)}} \cdot \frac{1}{g\rho} \tag{61}$$

Eq. (60) is equal to Eq. (17) which means that the non-Newtonian flow can be solved by Eqs. (43) and (45) considering the values of f and k given in Eq. (26) and Eq. (27) and R, Q and B given in Eqs. (61), (53) and (54). Since Eq. (53) is general, the non-oscillating part q_1 can be expressed according to this equation, putting $\frac{dp}{dx}$ as the static pressure gradient.

3.3 ESSENTIAL GROUT PARAMETERS

The equations describing the inflow and wave propagation in fractures are, as seen in Chapter III 3.2, quite complicated. There are several parameters controlling the inflow and some of them are difficult to determine. Altogether 9 parameters must be determined in order to predict the depth and amount of inflow:

* The E-modulus (the compressibility) of the grout E_v. E_v is a critical parameter since the rate of the wave propagation is depending on it.

The compressibility of the saturated grout is very low or about the same as the compressibility of water $E_v = 2.1 \cdot 10^9$. However a small amount of air or air-bubbles trapped in the grout will strongly decrease the E-modulus and thus change the conditions for the wave propagation. Air-bubbles are probably inevitable but the high constant backpressure during injection compress and dissolve them and no problems that can be directly related to air has yet been seen.

* The E-modulus of the rock E_R. E_R is strongly dependent of the volume of the involved rock mass and the amount and properties of the fractures. A rough estimate of E_R is:

$E_R = 5 \cdot 10^{10}$ Pa	small samples of intact granite
$E_R = 5 \cdot 10^9$ Pa	fairly fracture free rock masses
$E_R = 5 \cdot 10^8$ Pa	extremely fractured rock masses

A sensitivity analysis shows that, within the extremes shown above, the influence of E_R is fairly small. In the forthcoming calculations $E_R = 5 \cdot 10^9$ Pa has been used.

* The static backpressure h_1. The maximum static pressure is rarely higher than $h_1 = 3$ MPa. The backpressure used in the tests has varied a little depending on the type of machine (the slot injection tests) and the type of fracture (the pilot tests). As an average $h_1 = 2$ Mpa has been used in the calculations if not otherwise stated.

* The frequency f of the vibrations. The frequency of the percussion is 40 - 50 Hz but the frequency of the stress waves penetrating into the fractures varies depending on the dynamic response of the borehole. Unless else notified the frequency 40 Hz has been used in the calculations.

* The density of the grout ρ_v. The density varies between 1.1 t/m^3 for the lightest bentonite and 1.9 t/m^3 for the heaviest cement. The influence on the attenuation is about direct proportional to the density. The values 1.1 and 1.9 t/m^3 has been used for the respective material.

* The oscillating pressure h'. This pressure is like the frequency depending on the response of the borehole. If not otherwise stated $h' = 2.5$ MPa has been used.

* The fracture aperture d. This is an essential parameter which is of course very difficult to determine. In the artificial slot the geometrical fracture aperture is to be used in the calculations. In a real fracture the geometrical fracture aperture is usually larger than the effective aperture open for injection due to irregularities. This problem is overcome by using the hydrological fracture width determined from Lugeon tests.

* The two flow property parameters m and n in the expression for the rate dependence of the shear stress:

$$\tau = m \left(\frac{\dot{\gamma}}{\dot{\gamma}_o}\right)^n \tag{62}$$

As will be shown in Chapter IV the flow properties are highly dependent of the material composition, the water content, the thixotropy and the amplitude of the oscillating shear strain. The oscillating shear strain is decreasing with increasing penetration depth, meaning that the flow properties are changing with time. This complication is further dealt with in Chapter IV.

3.4 EXPECTATIONS

The grout flow theory has its advantages and limitations. The dynamic penetration of grouts into fractures is a very complicated process and it is important to know how to evaluate the calculations and what possibilities they give. The theories can be used in order to:

* Increase the general understanding of the process of grouts penetrating into different types of fractures.

* Increase the general understanding of wave propagation and wave attenuation in grout-filled boreholes and fractures.

* Make sensitivity analyses in order to study the influence of changes in grout materials, grouting techniques, fracture properties etc. Such studies are very useful at technique developments.

* Make predictions of grout penetration at injections. If the amount and depth of the grouts can be fairly well calculated it will serve two purposes:

  1 The most effective grout composition can be chosen
  2 The sealing efficiency and thus the usefulness of the injection can be estimated

Of course the complex process of injecting fractures, especially when using dynamic techniques, puts a lot of limits to the applicability of these theories. The nature is more complicated than what can be simulated mathematically. The major weaknesses are the following:

* The fracture is simulated as being plane-parallel. The real fracture has an unknown variation in aperture, width and extension. It is not possible to know from the hydraulic testing whether the water flow originates from a channel-like fracture with similar width and aperture or a very wide fracture with small aperture

* The flow properties vary with the amplitude of the oscillating shear deformation of the grout and the amplitude is a function of the penetration depth and the shape of the fracture.

* The shape of the oscillating pressure waves deviates from the modelled, sinusoidal one.

* The actual amplitude and frequency of the pressure waves in the fracture opening cannot be predicted with a high accuracy, since the original pressure oscillation curve for the grout that leavs the injection machine is irregular. It is possible to investigate the change of the pressure wave in the borehole caused by a change in frequency or borehole length but the irregularity of the oscillation curve makes the study very complicated.

The uncertainty of some parameters and the simplifying assumptions especially of the fracture appearance of course puts a limit to the possibility of predicting the effect of an injection. However, in Chapter IV a technique to make such a prediction in spite of the difficulties is suggested and tested.

4 PRACTICALITY, POTENTIAL

Although the present study is not yet finished, it is clear that a technique is now available for sealing of fractrues that are too narrow to be grouted by conventional techniques. The matter is further discussed in Chapter VII.

CHAPTER IV GROUT MATERIALS

1 GENERAL ASPECTS

The purpose of sealing is to fill the major part of water-bearing fractures with low-permeable grout of sufficient physical and chemical longevity. These matters are described in this chapter.

A major point is that the penetration power of any grout can be predicted, provided that proper grout flow parameters have been selected. This means that it is the fluidity, expressed in terms of such parameters, that is essential and not empirically deduced properties that are related to the certain mineralogical, granulometric or chemical compositions, provided that the fracture aperture is significantly wider than the maximum particle size. The laboratory tests which yield the flow data will be described in detail in this chapter.

2 SEALING PROPERTIES

2.1 INTRODUCTION

While clays in general represent low-permeable media, smectites in sodium form are known to have an extremely low permeability and a self-healing ability, and they have therefore been selected as major sealing component in several repository concepts. The reason for this beneficial property, and possible processes that may have a deteriorating effect on it, are described in this chapter.

As to cement the conditions are similar, i.e. the hydrated substance is known to be almost impermeable in non-fissured form. For ordinary high w/c cements there is no spare hydration potential on mechanical breakage or fracture expansion, but the presently studied version, characterized by w/c around 0.4, turns out to have a certain swelling and self-healing ability.

For both types of grouts it is required that their longevity can be safely estimated. The associated research work is presently focussed on this matter, the major current ideas being reported in this chapter.

2.2 CLAY

2.2.1 General

The microstructure of clays, i.e. the geometrical arrangement of the phyllosilicate constitutents, is a determinant of the hydraulic conductivity and diffusivity. In smectite clays this arrangement is particularly tortuous, which explains that such clays have a hydraulic conductivity that is two to four orders of magnitude lower than that of illitic or kaolinitic clays. Also, the special phenomenon of interlamellar hydration has an influence on the hydraulic conductivity in bulk although it is very small for grouts of low density. However, it is essential for the chemical longevity as discussed at the end of the chapter.

2.2.2 Microstructure

2.2.2.1 Basic concepts

As for most other clay types, the multiple-plate microstructure concept holds also for Na montmorillonite. Thus, this type of smectite clay consists of stacks which are thick and comprise several flakes at high bulk densities and which persist after expansion but with a smaller number of flakes (Fig IV:1). It is concluded from ongoing studies that the continuity of the particle network is preserved even at large expansion, which has a great impact on the erodability of soft gels such as those used for rock grouting.

2.2.2.2 Internal/external pore space

It is of fundamental importance to distinguish between interlamellar space holding "internal" water, and voids which host "external" water. The first-mentioned space contains immobile, hydrate water that forms a large fraction of the total pore volume in smectite-rich clays of high density, while it is only about 5-10 % of soft clay gels ($\rho_d = 0.15\text{-}0.5$ t/m^3). Fig IV:2 illustrates the relation between bulk density and the amount of internal water, indicating that it is very small for clay grouts with water contents around the liquid limit ($\rho_m < 1.1$ t/m^3).

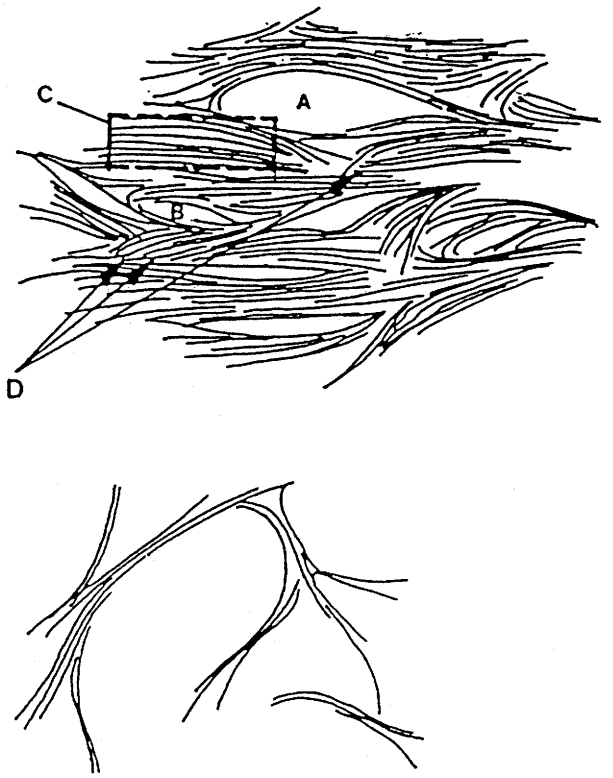

Fig IV:1. Upper: Dense Na montmorillonite clay. A) Large pore, B) Small void with external water, C) Stack or "quasicrystal" with organized interlamellar water, D) Interface between stacks. Lower: Expanded Na montmorillonite gel with very thin stacks and practically only external water

2.2.2.3 Physical state of the water in Na-montmorillonite

While the water in external pores is in free form, the internal or interlamellar water is concluded to be organized and adsorbed, either by forming hydrates of interlamellar cations, which is certainly the case for Ca montmorillonite, or by forming a water lattice that grows directly on the basal planes of the flakes. The latter case, which implies that hydrogen bonds and van der Waals bonds are responsible for the water lattice strength and the mineral/water interaction, fits well with Forslind's concept of water association in montmorillonite gels at temperatures below about 100°C and with the conclusion that at least the first hydrate layer has the form of a strained, significantly deformable ice-like lattice. The low density of the interlamellar water that has been determined experimentally, i.e. about 0.9 t/m^3, is also in support of this model. Forslind's view, as illustrated in Fig IV:3, is that the crystal structure of montmorillonite at temperatures lower than a certain critical range is equivalent to that forwarded by Edelman & Favejee (EF) and that higher temperatures cause breakdown of the apical tetra-

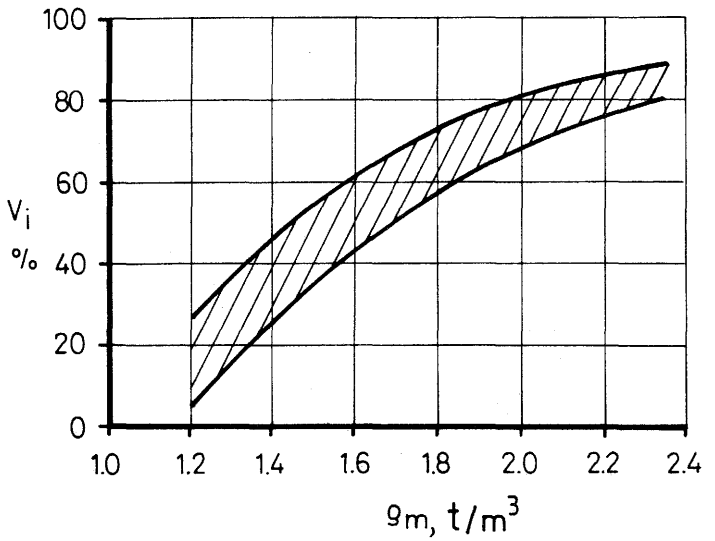

Fig IV:2 General relationship between bulk density and content of internal water in percent of the total porewater volume of smectite clays

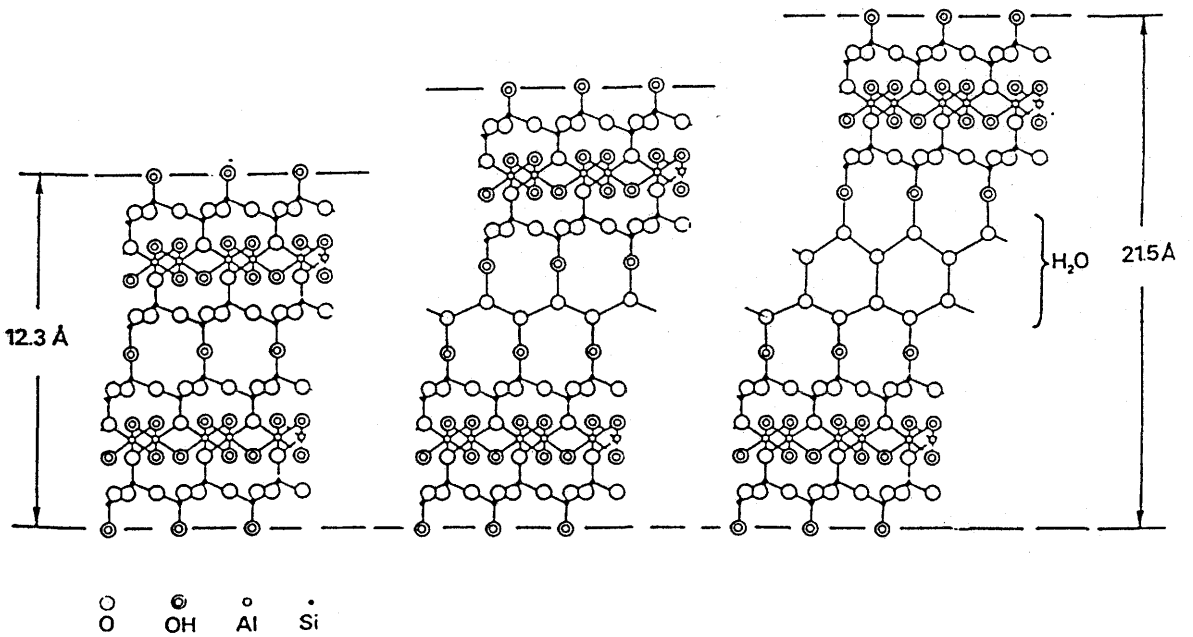

Fig IV:3 Schematic picture of regular H-bonded water lattices formed between apical OH:s of opposing basal planes in interlamellar space following Forslind's concept

hedrons, thus yielding the traditional Hoffman, Endell & Wilm (HEW) structure (cf. Fig IV:4).

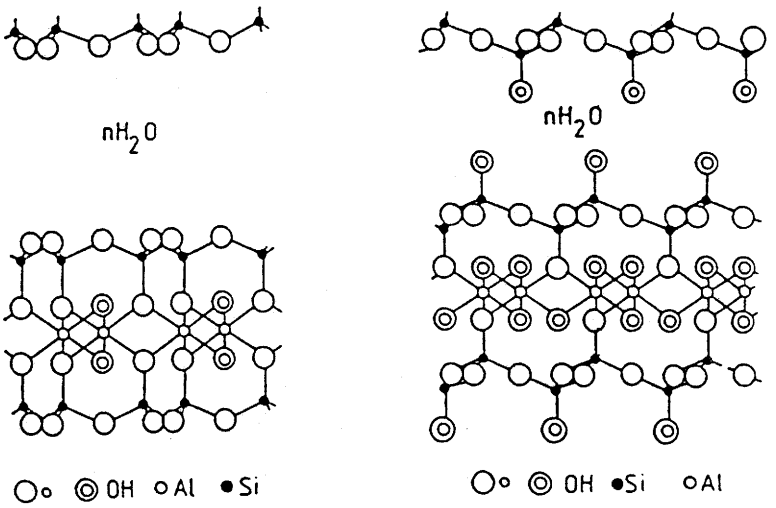

Fig IV:4. Crystal lattice states of montmorillonite. Left: The Endell/ Hoffman/Wilm structure. Right: The Edelman/Favejee structure

2.2.3 Implications

It is clear from Fig IV:1 that the interwoven system of smectite flakes yields very tortuous passages for percolating water, which explains the low hydraulic conductivity. As discussed later in this chapter (4.1.2) the interaction of the crystal lattices and interlamellar water may be a determinant of the longevity of Na montmorillonite at higher temperatures than about 100°C.

2.3 CEMENT

The sealing properties of non-fractured cement are very effective after a sufficient hydration time. Thus, the permeability of hydrated cement is known to be very low with hydraulic conductivities around $k = 10^{-12}$ m/s.

Canadian tests

A lot of experiments where the hydraulic conductivity of different cement mixtures are tested have been performed by Gerard Ballivy, Sheerbrooke University, Canada, in connection with the grouting experiments carried out at the URL in

Canada. We have considered it unnecessary to repeat those experiments since they are very reliable and the measured hydraulic conductivity well below what is necessary in narrow fractures. The results will be reported in an AECL Report.

The Canadian tests concern cement with different fineness (350-600 m^2/kg), different mixtures of silica fume (0 and 10 %), with or without superplasticizer and with different water/cement ratios (0.4-0.8). The tests were conducted with water of different salinity and with different times of curing. The tests show that the best sealing properties are reached using the highest fineness and the lowest water/cement ratio. An increased salinity of the pore water has no drastic effect on the hydraulic conductivity. The tests also show that the hydraulic conductivity of the cement with w/c = 0.4 falls below $k = 10^{-10}$ m/s already after a few days and then continues to drop to $k = 10^{-12} - 10^{-14}$ m/s.

Critical to the sealing properties of cement is probably a potential flow in the contact zone between the cement and the rock. The Canadian measurements also show that a cement-filled slot does not reach a hydraulic conductivity as low as the solid cement.

Tests within the present project

A few basic tests of the hydraulic conductivity of cement have been performed within this project. The so called "cone-in-cone" tests in which the effect of fracture dilation and the thermal effects are tested will be accounted for in Chapter 4.1.1.

The low permeability of the cement mixtures have been confirmed by percolation tests in both oedometers and triaxial cells. The Canadian cement type 50 with a fineness number of 600 and w/c 0.41 were used in the tests. The cement contained 10 % silica fume and 1.1 % superplasticizer.

The strength of cement and the effect of high shear stresses on the permeability of cement have been checked by a triaxial test where the sample with a height of 10 cm and the diameter 5 cm was subjected to an increasing deviator stress. Simultaneously a constant hydraulic gradient was maintained across the sample and the resulting water flow into and out from the sample were measured. A cell pressure of 1 MPa surrounding the sample guaranteed that no water could flow between the membrane and the surface of the sample.

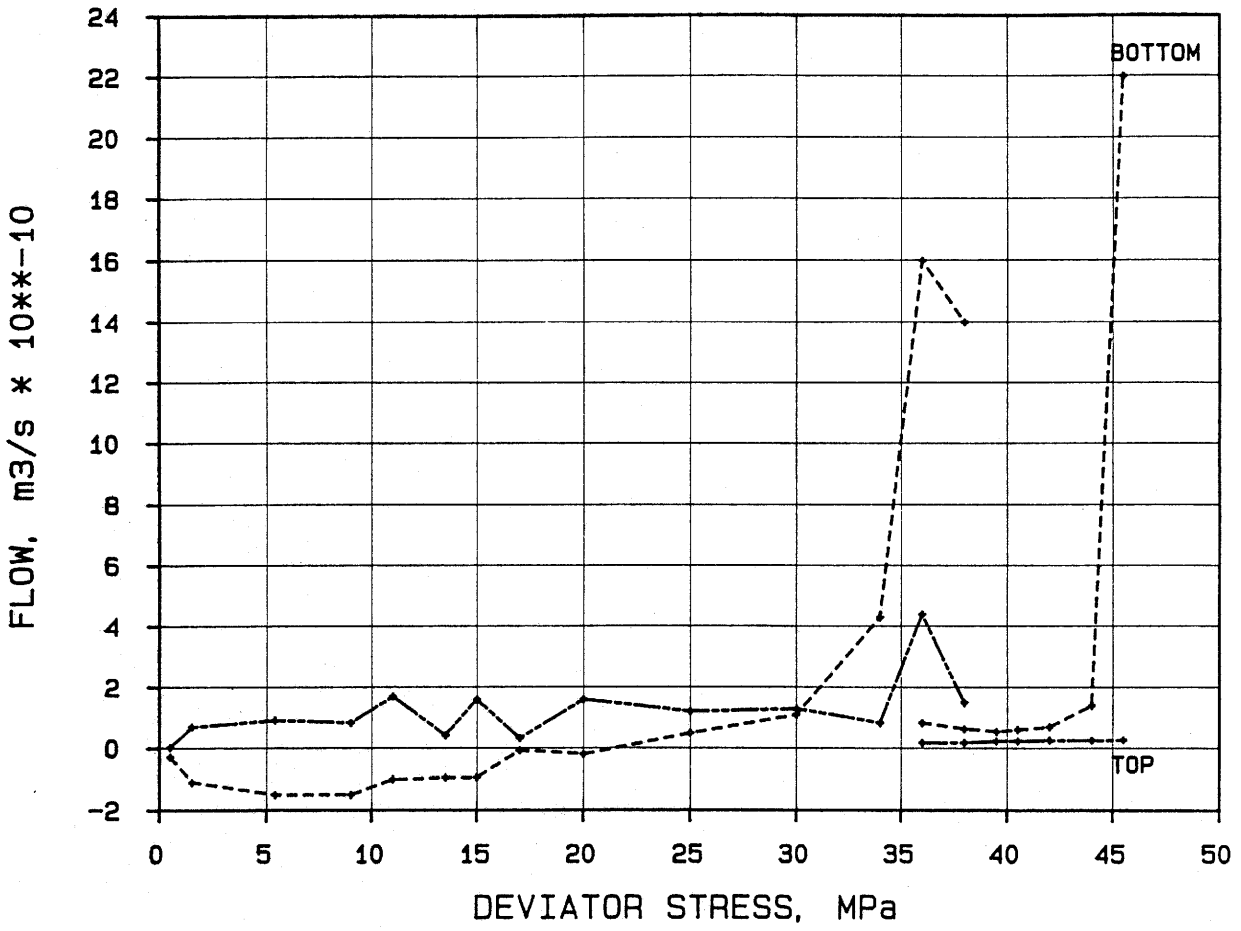

Fig IV:5. Water flow through a cement/sample as a function of the applied deviator stress. The flow was directed from the bottom to the top

After 60 days of hydration the shearing of the sample started. Prior to the shearing the measured hydraulic conductivity was determined giving $k \approx 10^{-13}$ m/s. The increased deviator stress immediately changed the percolation rate. Fig IV:5 shows the change in measured in- and outflow as a function of the applied deviator stress. Failure occurred at the deviator stress 46 MPa. The permeability measurements were somewhat complicated in the beginning of the test due to volume change of the sample. A real increase in flow meaning a permeability higher than 10^{-10} m/s did not occur until 65 % of the failure stress was reached, i.e. 25-30 MPa. At 36 MPa the sample was unloaded and then reloaded. At failure, the permeability was $\sim 10^{-8}$ m/s.

The curing of the cement after failure was also measured. Fig. IV:6 shows the evaluated permeability as a function of time after failure. About 20% of the failure load was left to rest on the sample.

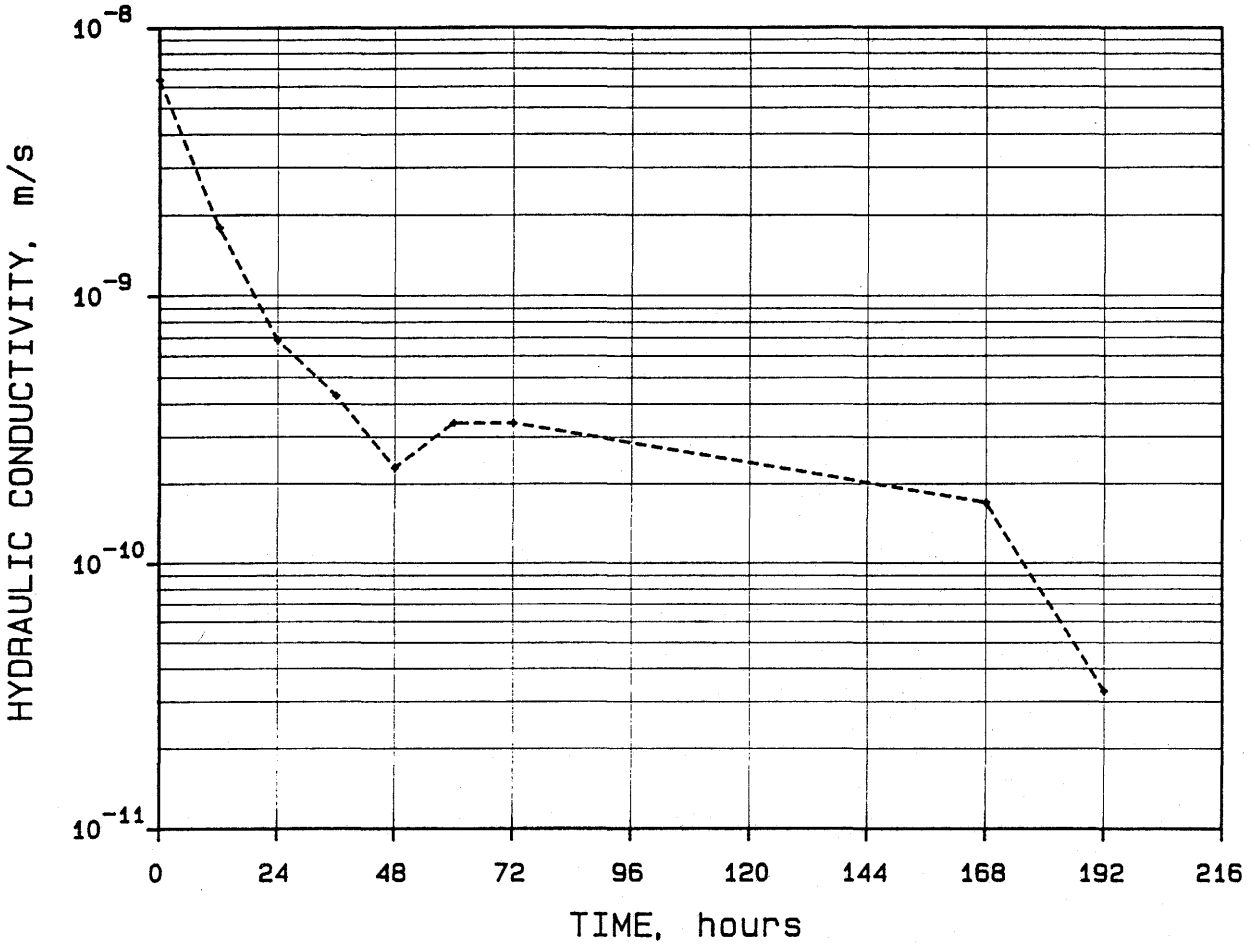

Fig IV:6 Curing of the cement sample after failure

The figure shows that the sample clearly has a curing ability by which the permeability decreases by more than 100 times in 8 days.

An experiment was also made to test the potential risk of percolation in the contact zone between the rock and the cement. Pieces of solid cement and solid, "fracture-rich" rock were tested in the triaxial cell giving $k = 6.7 \cdot 10^{-13}$ m/s for the rock and $k = 4.2 \cdot 10^{-13}$ m/s for the cement. Then, an axial hole with a diameter of 1 cm was bored in the cylindrical rock and filled with cement. After 2 months of hydration the axial permeability of the rock-cement matrix was tested giving $k = 5.6 \cdot 10^{-13}$ m/s, which means that no percolation took place along the rock/cement contact zone.

The shear strength of the contact zone between the rock and the cement, i.e. the bond strength, was also tested by applying an axial force on the cement plug.

These tests showed that the strength of this interface zone was as high as the strength of the cement itself.

3 PHYSICAL PROPERTIES IN THE INJECTION PHASE

3.1 FLOW PROPERTIES

3.1.1 General

A low viscosity of the material is necessary the make it groutable. Vibration and superplasticizers are techniques to lower the viscosity. A deep understanding of the flow properties is essential for both the flow modelling and the possibility of developing the best grout composition and grouting technique.

3.1.2 "Static" Flow Properties

Experimental set-up

The rheological properties of non-vibrated cement and bentonite were measured with a Bohlin VOR Rheometer. Fig IV:7 shows a picture of the equipment. All

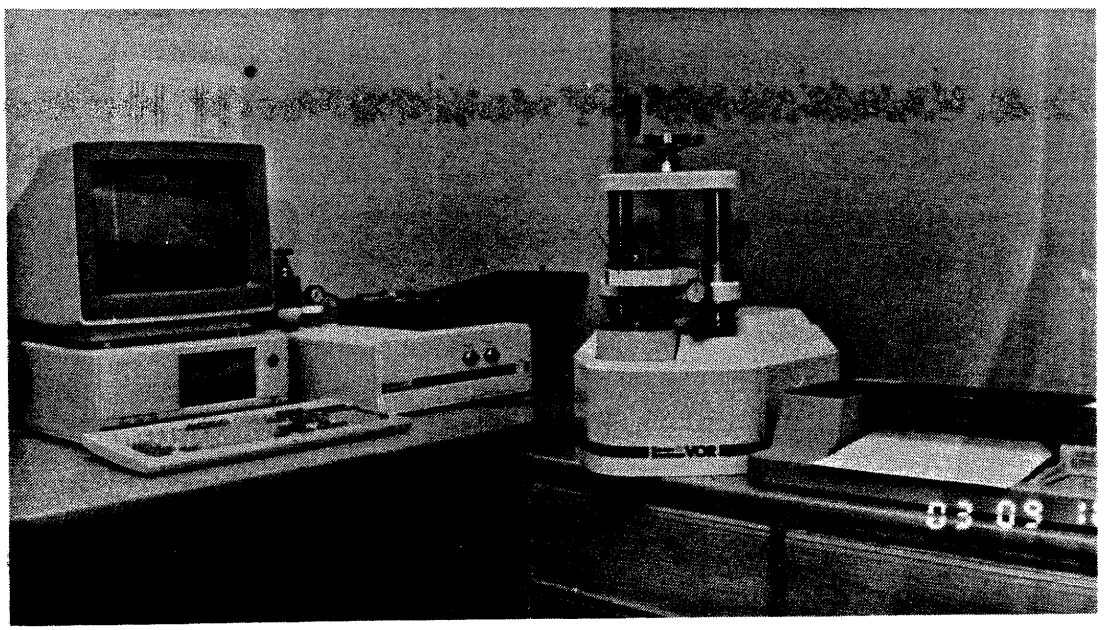

Fig IV:7. The Bohlin VOR Rheometer

measurements, except the pressure tests, were made by use of a concentric cylinder system with a fixed bob located in a rotating cup. The pressure tests were performed with both cup and bob attached to the torsion bar and the rotation transmitted to the bob by magnets.

Flow properties

The VOR Rheometer covers a wide range of shear rates. The flow curves of cement and bentonite are very different, which can be seen in Fig IV:8. While the cement

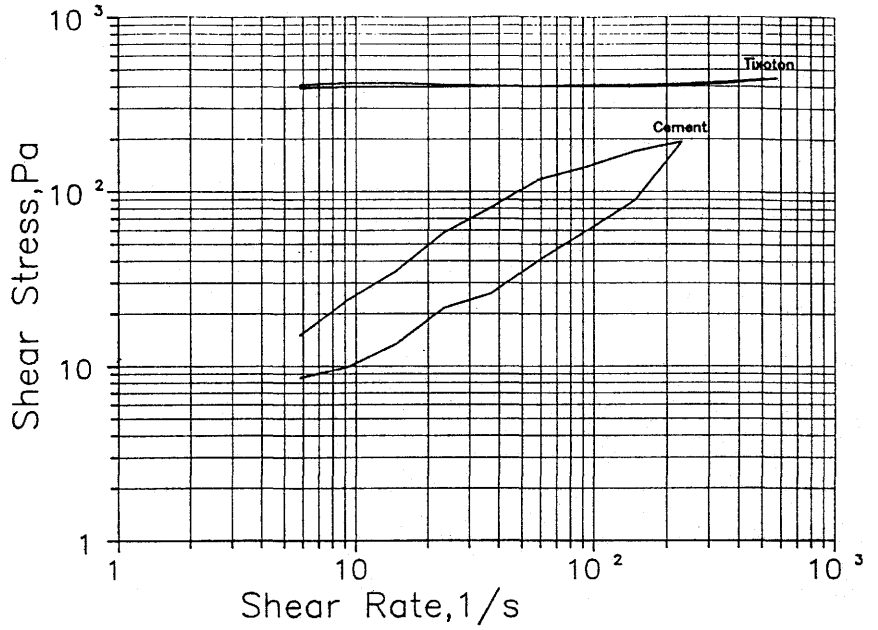

Fig IV:8. Flow curves for bentonite and cement. The bentonite was Tixoton, having w = 705 % and the cement was mixed with 10 % condensed silica fume and 1.7 % superplasticizer at w/c 0.32.

has a Bingham-plastic behavior, the bentonite shows an extremely small influence of shear rate on the shear stress. This demonstrates very clearly that the use of the conventionally defined viscosity, i.e. shear stress divided by the shear rate, is not suitable since increasing the shear rate by a factor 10 will decrease viscosity by almost the same factor, as can be concluded from Fig IV:9. The term viscosity, referred to in the text, is therefore only used to describe the consistency of the paste in general.

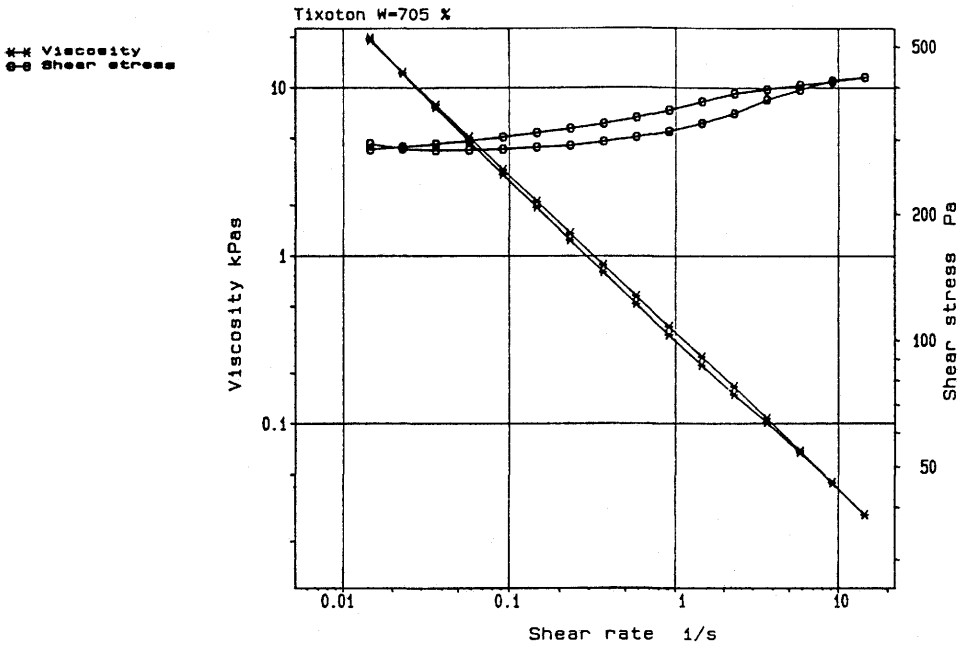

Fig IV:9. Flow curve for bentonite at w = 705 %.

Visco-Elastic behaviour

The influence of strain on the visco-elastic behavior was determined by performing strain sweep tests. In these tests sinusoidally varying strain of different amplitudes were applied, and the response in stress was monitored. Of special interest is the phase angle between the applied strain and the monitored stress (Fig IV:10), since it shows the relation between elastic and viscous response of the material. If the phase angle is low, the elastic component dominates over the viscous one. Thus, the tests show the minimum strain needed for the material to be "fluid". It seems as if the shear strain must exceed 10 % in order to break the structure and create a dominating viscous behaviour.

Influence of temperature

The measurements included both temperature-sweep tests at constant shear rate and flow curves at different temperatures. In the temperature-sweep the shear stress was measured while the temperature was continuosly increased. The flow curve method had to be used because of the rapidly increasing hydration rate of cement without superplasticizer at increasing temperatures.

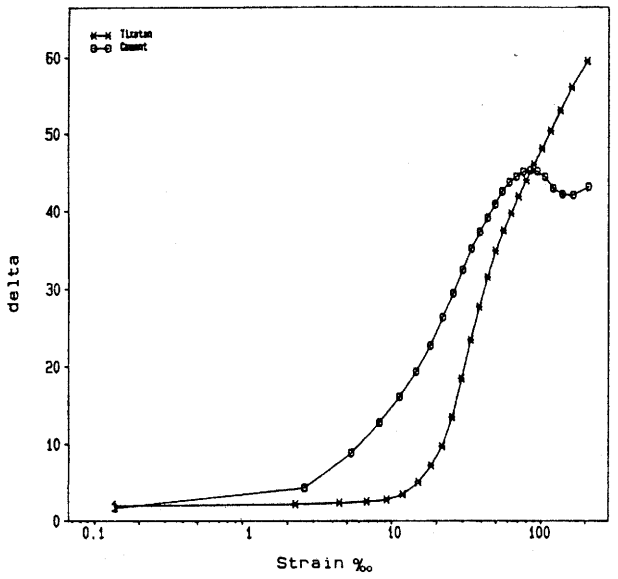

Fig IV:10. Strain sweep tests for bentonite at w = 705 % and cement mixed with 10 % silica fume and 1.7 % superplasticizer at w/c 0.23

The results show that the viscous behavior of bentonite is not temperature-dependent between 5 and 90°C. For cement, the shear resistance was found to decrease with increasing temperature (Fig IV:11). In contrast to cement without superplasticizer, the hydration rate of cement with superplasticizer did not increase with temperature during the first 30 min after mixing.

Influence of pressure

Tests have been made with pressures varying between 100 kPa and 900 kPa. The cement showed no pressure-dependence on viscosity, while the viscosity of bentonite decreased by 20 % when the pressure was increased by 900 kPa.

Influence of superplasticizer

The decrease in viscosity of cement pastes when adding superplasticizers was found to depend on the water/cement ratio and the amount of condensed silica fume. Addition of 1.7 % of superplasticizer allowed the water/cement ratio to be reduced to half its original value without changing the viscosity, as demonstrated by Fig IV:12. The presence of condensed silica fume normally increased the viscosity, but at water/cement ratios below 0.3 the viscosity was decreased.

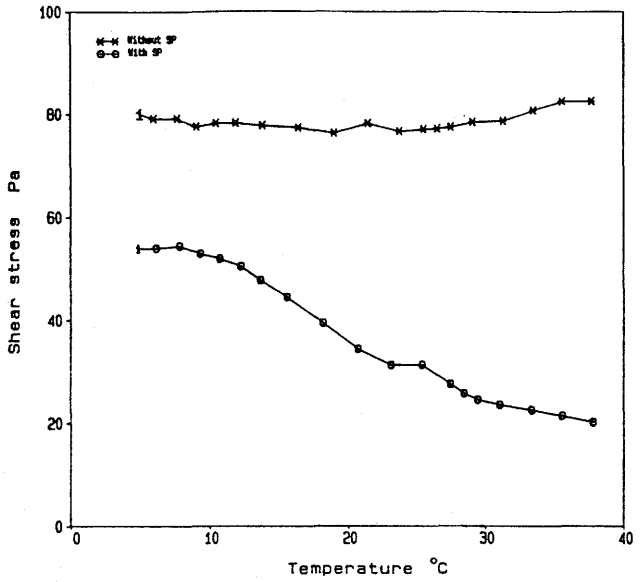

Fig IV:11. Temperature sweep for cement mixed with 10 % silica fume at w/c 0.60 (upper curve) and cement mixed with 10 % silica fume and 1 % superplasticizer at w/c 0.40 (lower curve)

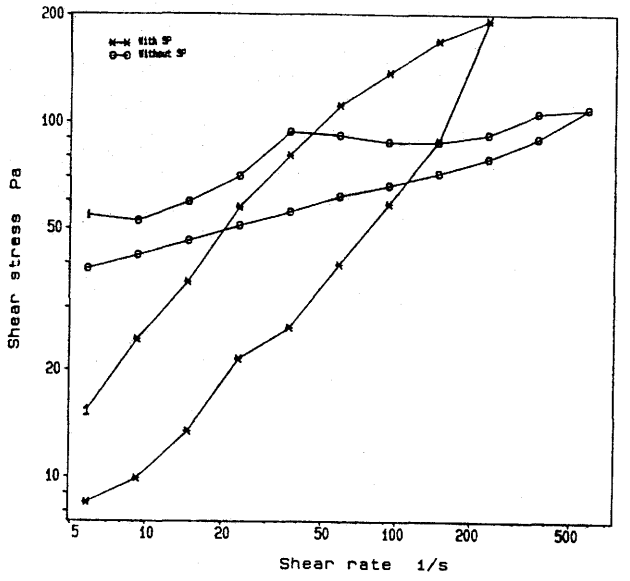

Fig IV:12. Flow curves for cement mixed with 10 % silica fume with and without superplasticizer. The w/c are 0.32 and 0.63 respectively. The difference in behavior between increasing and decreasing the shear rate is due to tixotropic effects.

3.1.3 "Dynamic" flow properties

Experimental set-up

The VOR Rheometer is designed to characterize the materials with respect to traditionally determined flow properties. It has therefore been necessary to use a different arrangement in order to test the influence of vibrations.

In the present tests, a Brookfield viscometer has been used, the arrangement being that the viscometer unit was separated from the sample holder and both the rotation and shear stress measurements made using the bob. (Fig IV:13). In this apparatus an electromagnetic vibrator could be attached to the cup containing the grout. The amplitude of the vibrations was measured by a small accelerometer, fixed to the sample holder.

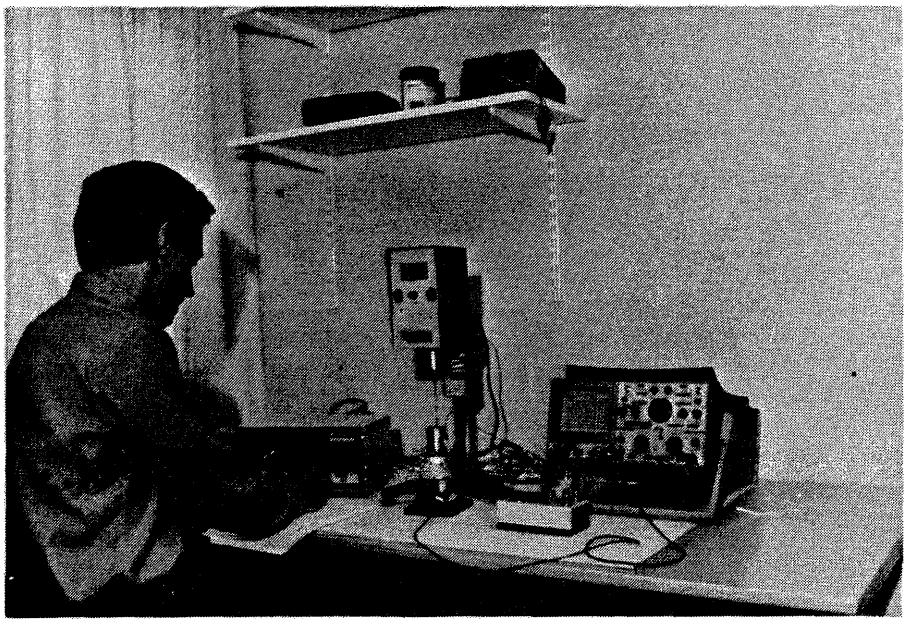

Fig IV:13. Test arrangement for vibration tests. To the left is the sine wave generator. In the mittle is the viscometer and the vibrator. The small piezotron accelerometer is mounted on the side of the cup. To the right is the piezotron coupler and the oscilloscope which is used to measure the voltage from the coupler

Influence of vibrations

The "static" flow test showed that shearing of the grout decreased the viscosity somewhat. It is also concluded that it is possible to break down the microstructure of the grouts by vibrations. The decrease in viscosity, due to the vibrations, depends on the frequency and amplitude of the vibrations as shown in Fig IV:14.

The materials tested had approximatively the same composition as the grouts used in the Stripa field tests.

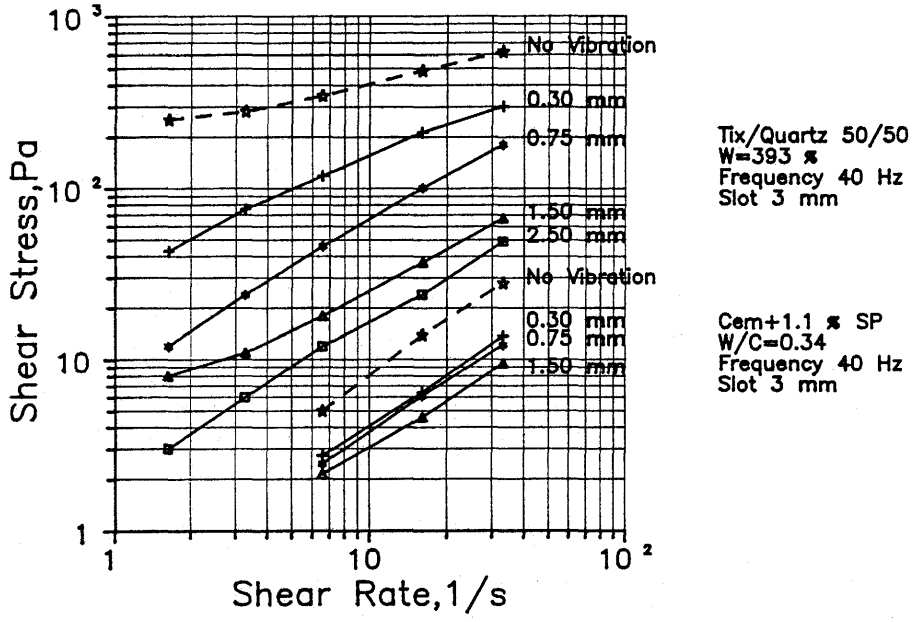

Fig IV:14. Rheological behavior of the materials used in the Stripa field tests.

Besides the decrease in viscosity, the flow curves showed that large vibrations make the grouts behave almost Newtonian, a fact that is very important for the flow modelling.

Influence of the input power

Since an increase in both frequency and amplitude calls for more power input in the system, a major issue has been to find out if there is an optimum in frequency. Therefore, tests have been performed using vibrations with a constant power (Fig IV:15). The conclusion is that the energy input is more important than the frequency, provided that the amplitude is high enough to break down the structure so that the material yields viscous rather than elastic behavior.

Influence of slot width

The input power is not the only factor responsible for the structural breakdown of the grouts during vibration. When the slot width is reduced and the power kept

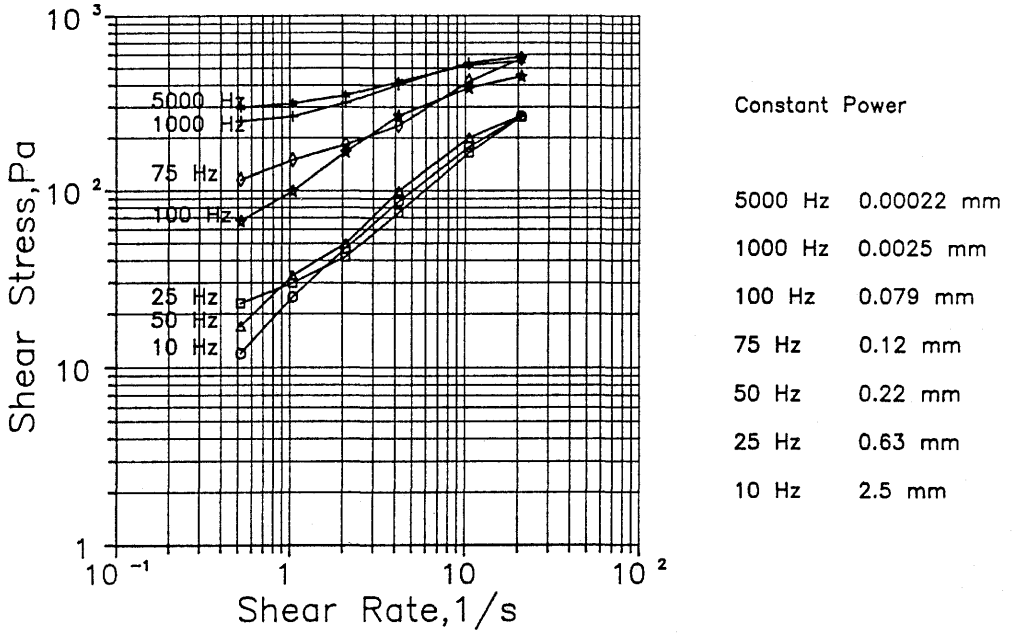

Fig IV:15. Vibration measurements of bentonite at constant power.

constant, the shear resistance decreases. This phenomena is explained by the fact that the shear strain of the vibration increases in narrow slots, and thus breaks the structure down more efficiently. It is therefore important that the influence of the slot width is included in the mathematical modelling.

3.1.4 Material models

The grout flow modelling requires a simple material model which reflects the behavior of the grout properly. It is concluded that the ordinary Newtonian viscosity law is not applicable for these materials. Nor are the Bingham parameters very useful. Instead, the power law seems to be a relevant model and it can be expressed as in Eq. (63):

$$\tau = m \cdot (\dot{\gamma}/\dot{\gamma}_0)^n \qquad (63)$$

where τ = shear resistance (Pa)
m = shear resistance at $\dot{\gamma} = \dot{\gamma}_0$ (Pa)
n = inclination of the $\dot{\gamma}$ - τ relation in a double logarithmic diagram
$\dot{\gamma}_0$ = normalized shear rate (1.0 1/s)
$\dot{\gamma}$ = shear rate (1/s)

If $n = 1.0$ Eq. (63) turns into the ordinary Newtonian viscosity law.

Non-vibrated grout

The parameter *n*, which is a measure of the rate dependence, varies with the material composition. *n* seems to be very low (0.05-0.10) for bentonite while it is about 0.25 for cement. Addition of superplasticizer increases the n value to 0.5-1.0.

The parameter *m*, which is a measure of the consistency, is primarily dependent of the water content but is also influenced by the amount of superplasticizer in the cement. Some typical values of *m* and *n* are shown in Table 1.

Table 1 Values of the parameters *m* and *n* in Eq. (63) for some typical grout compositions without vibrations

Materiel	Equipment	m	n
B/Q 100/0, w=705%, 1.36·w_L	Bohlin	340	0.05
B/Q 50/50, w=328%, 1.29·w_L	"	370	0.06
B/Q 100/0, w=834%, 1.60·w_L	"	290	0.02
B/Q 50/50, w=395%, 1.55·w_L	"	240	0.08
Cem, CSF, 1% SP, W/C=0.40	"	1.0	1.0
Cem, CSF, W/C=0.60	"	27	0.38
C, CSF, 2% SP, W/C=0.30	"	1.3	1
C, CSF, 1.7% SP, W/C=0.32		1.0	1
B/Q 100/0, w=600%, 1.15·w_L	Brookfield	400	0.30
B/Q 50/50, w=294%, 1.15·w_L	"	270	0.43
C, CSF, 1.1% SP, W/C=0.42	"	6.5	0.7
C, CSF, 0.63% SP, W/C=0.41	"	8.5	0.7

Vibrated grout

When the material is vibrated, the properties change dramatically; n increases and m decreases. If the vibrating effect is high enough the structure of the grout is totally broken down and $n = 1.0$, meaning that the grout has become Newtonian. The effect of the vibrations is clearly demonstrated by Fig IV:16.

It is not the total oscillating deformation that affects the flow properties but the magnitude of the oscillating shear strain:

$$\gamma = dE/dD \qquad (64)$$

where E is the oscillation of the cup at the rheological tests while D is the width of the slot between the cup and the bob. In a fracture D is half the fracture aperture since the vibration takes place between the raw rock surface and the center of the fracture. E corresponds to the amplitude of the vibrated deformation in the center of the fracture.

The maximum strain which can be measured is $\gamma = 1.0$, i.e. the same vibration amplitude as slot width. The influence of γ on the viscosity at different grout compositions is summarized in Fig IV:16. The symbols are explained in Table 2.

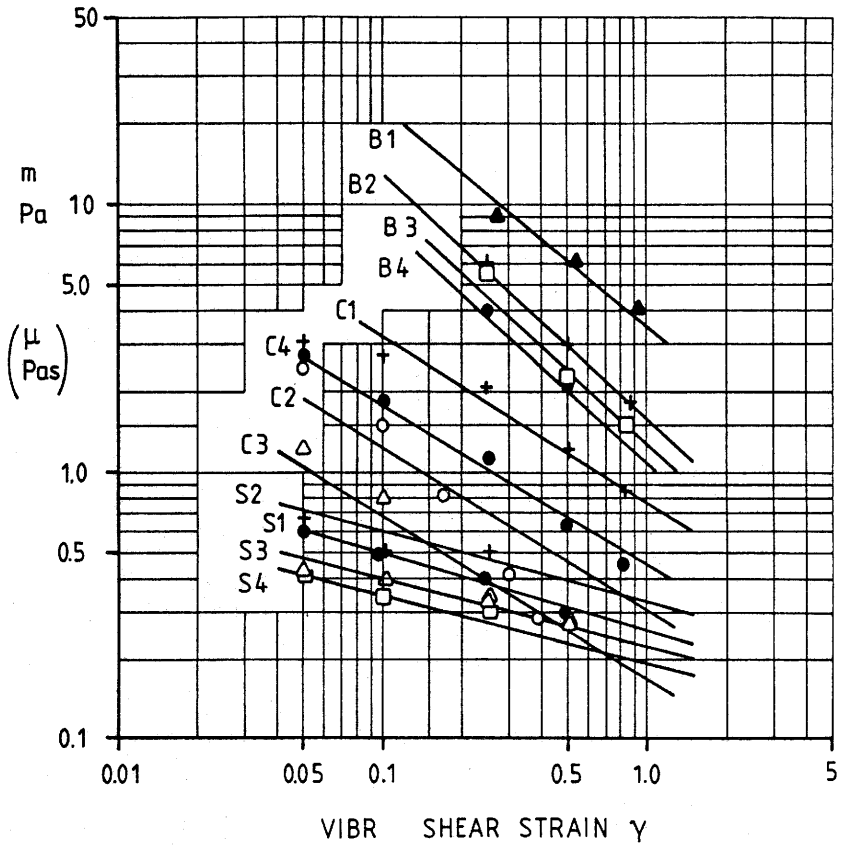

Fig IV:16 The parameter m in Eq. (63) as a function of the vibrating shear strain γ. For these vibrated grouts m = the Newtonian viscosity μ. See Table 2

As can be seen, the relation forms a fairly straight line in a double logarithmic diagram. It can also be seen that the influence of the vibrations is somewhat different for the different grouts. It seems as if the influence is highest for the bentonites and lowest for the Swedish cements. However, the accuracy of the measurements is not very high at low viscosities and further examination is required to certify this difference.

The change in viscosity is not directly included in the flow model but can be taken into account by step-wise calculations. Due to problems with choosing a starting value, the viscosity at the oscillating shear strain $\gamma = 1.0$ has been used in the predictions. This matter is further dealt with in Chapter IV:3.3.4.

Table 2 Data of the materials illustrated in Fig IV:11.

Cement grouts

Type	Silica fume %	Super plast %	w/c	Notation	
Canadian	10.0	0.42	0.41	C1	x
Canadian	10.0	0.63	0.41	C2	O
Canadian	10.0	1.1	0.41	C3	Δ
Canadian	10.0	1.1	0.35	C4	●
Swedish	10.0	1.1	0.42	S1	●
Swedish	0.0	1.1	0.32	S2	x
Swedish	0.0	1.1	0.34	S3	Δ
Swedish	0.0	1.1	0.35	S4	□

Bentonite grouts

Bentonite %	Quartz cont. %	Water ratio %	Ratio w/w_L	Notation	
100	0	630	1.2	B1	Δ
100	0	740	1.4	B2	+
50	50	375	1.5	B3	□
100	0	840	1.6	B4	●

3.2 HARDENING PROCESSES

3.2.1 Clay

Strong mechanical agitation, induced by the flow as well as by the vibrations, break down the continuous clay particle network to discrete thin packs of a few coherent montmorillonite lamellae. As long as flow takes place, these packs move easily along each other, but once the movement ceases, they become rapidly bound

by electrostatic forces, which yields coupling of the edge of a stack to the basal plane of a neighboring one. This yields the wellknown thixotropic strength regain of smectite clays and results in a microstructural pattern of the generalized type shown in Fig IV:17. The thin stacks are fully expanded, i.e. they hold 3 interlamellar hydrates.

Fig IV:17 Microstructure of soft Na montmorillonite gels. Upper: generalized regular pattern of soft aggregates. Lower: Scanning micrograph of freeze-dried specimen with a density of about 1.3 g/cm^3

3.2.2 Cement

As to ordinary cement, the chemical reactions that lead to the formation of a continuous cement gel follow a well known pattern. However, the influence of superplasticizers and silica fume on these reactions is complex and needs further study. The subject is further treated in Chapter IV, par. 4.2.2.

The opportunity has been taken to identify the hydration process by use of "Humid Cell" high voltage electron microscopy. This study is reported in the subsequent text.

3.2.2.1 General

The purpose of the present study was to identify detailed features of the hydration in order to check the validity of current concepts. This was achieved by using high voltage "humid cell" electron microscopy, which allows for direct observation of the involved physico/chemical processes. The instrument was a 3 MV microscope of the Laboratoire d'Optique Electronique Du C.N.R.S, Toulouse, France, which has been used previously for studying the hydration of smectite clay.

The object was to investigate how and to what extent superplasticizers added to cement/silica-fume mixtures affect their hydration and silification for which there are three current concepts:

1 The superplasticizers may form a barrier around the solids, which leads to a decrease in uptake of the free water and a retardation of the hydration process.

2 Adsorption of the superplasticizer on the surface of cement grains and hydrates leads to a modification of the zeta potential and thus particle interaction.

3 Adsorption of superplasticizers on the solids changes the chemical and physical properties of the hydrated crystals.

3.2.2.2 Test program

The material consisted of finely ground sulphate resisting Portland cement (d< 17 microns), silica fume (d< 0.6 μm), and superplasticizer (sodium naphtalene formaldehyde condensate). The cement/silica fume ratio was 9:1, while the content of superplasticizer ranged between 0 and 4 weight percent of the dry weight of solids.

Mixtures of cement/silica fume and superplasticizer in liquid form were inserted in a small cell located in the electron path of the microscope. The cell was evacuated and micrographs taken before humid atmosphere with RH = 100 % was developed in the cell. Radiation damage by heat production was excluded since liquid water was identified and ionization effects of the electron bombardement were eliminated by keeping the objects in the radiation path only for about 1 minute. In total, the main series comprised 9 test, major data being given in Table 3.

3.2.2.3 Test results

General

A number of observations were made in the course of the microscope tests, which had a duration of 0.5 to about 2 hours. Each test commenced with taking micrographs of the dry object, which normally consisted of fairly large particle aggregates of representative composition, and ended by drying the wet object and recording images as well as electron diffractograms. This latter investigation was applied to determine whether new objects formed during the hydration were crystalline or not.

Observations

Viewing the screen of the monitor and comparing the series of micrographs from each test gave the basis of the conclusions given below, in which C denotes cement, SF silica fume, and SP superplasticizer. The resolution power of the microscope was at least 10 Å for dry objects and 50-100 Å for the wet ones, which allows for accurate evaluation of all the consecutive stages that the objects underwent.

Table 3 Test data. C = cement, SF = silica fume, SP = superplasticizer

Test no	Duration of wet test, h	Material	Procedure	Remark
1	0.45	C+SF+SP	Mixed in dry form, exposed to water in the microscope	Exploratory test to identify components. The superplasticizer was in dry form forming 1 weight percent of the (C+SF) mixture
2	0.5	SF	Applided in dry form, exposed to water in the microscope	
3	0.5	C+SF	Applied in dry form, exposed to water in the microscope	
4	0.8	C+SF+SP	Applied in powder form, exposed to water in the microscope	The superplasticizer was in liquid form constituting 2.5 % of the (C+SF) mixture. Expressed in terms of dry weight the percentage is 1 %
5	1.8+15*	C+SF+SP	Applied in powder form, exposed to water in the microscope. Exposed to water and humid air during subsequent night.	The superplasticizer was in liquid form constituting 5.0 % of the (C+SF) mixture. Expressed in terms of dry weight the percentage is 2 %
6	1.3	C+SF+SP	Applied in powder form, exposed to water in the microscope	The superplasticizer was in liquid form constituting 10.0 % of the (C+SF) mixture. Expressed in terms of dry weight the percentage is 4 %
7	2.2+15*	C+SF	Applied in powder form, exposed to water in the microscope. Exposed to water and humid air during subsequent night	
8	1	C+SP	Applied in powder form, exposed to water in the microscope	The superplasticizer was in liquid form constituting 10.0 % of the cement. Expressed in terms of dry weight the percentage is 4%
9	1	C	Applied in powder form, exposed to water in the microscope	

* over night

Test 1 (C + CSF + SP)

Dry mixing of the components probably led to a homogenous distribution of the cement and silica fume particles but a very uneven representation of the superplasticizer.

The aggregates tended to become homogeneous and to expand after 10-20 minutes. Crystals started growing from certain cement grains after about 30 minutes.

Test 2 (SF)

Under the prevailing rather intense flushing of water, the silica fume spheres were slightly attacked, by which some silica was released in dissolved form already after 15 minutes.

Test 3 (C + SF)

After 10 minutes the system of discrete clearly discerned particles began to homogenize, yielding softer particle boundaries. After 20 min, further homogenization was seen and expansion was also evidenced. Electron diffraction of a few representative protuberances after drying the sample showed that they were crystalline.

Test 4 (C + SF + SP)

Reactions were initiated 10 min after wetting in the microscope and 20 min after this event no silica fume grains could be seen in the rather homogeneous gel. After 30 min density variations indicated crystallization of new phases. After storage under humid conditions for some hours some cement grains had got a fibrous character and were covered by a thick amorphous gel.

Test 5 (C + SF + SP)

The w/c ratio had to be raised to about 10 in order to identify hydration processes. The resulting soft material was applied on the grid and immediately dried under vacuum conditions, after which wetting took place in the cell. The superplasticizer initially formed a condensed skin around all the particles by which the hydration

was delayed although the plasticizer formed only a very small fraction of the compound. After 30 min, crystallization became obvious and density changes as well as homogenization clearly indicated significant hydration. Electron diffraction analyses after drying gave evidence of the formation of crystalline protuberances extending from the periphery of the aggregates.

Test 6 (C + SF + SP) (Fig IV:4)

Test 6 was designed so as to introduce so much liquid SP that all the components were coated in excess.

A reaction was noticed after 15 minutes, and relative movement of the cement grains and slight expansion of these grains was noticed after 20 min at the interface between cement and silica fume particles. Silica fume particles did not enter the reaction until 1 hour after the wetting. Electron diffraction analyses gave evidence of the formation of numerous crystalline protuberances along the edges of the aggregates, which had become more or less fibrous.

Test 7 (C + SF)

The purpose was to observe hydration over a longer period of time. After storage under humid conditions over night it was found that only amorphous protuberances had been formed on the surface of the aggregate in contrast to the distinct crystallinity of the initially formed objects in the humid cell. Interaction, i.e. intergrowth of adjacent cement particles was a very obvious effect in contrast to the cases when superplasticizer had been added.

Test 8 (C + SP)

On wetting, a small expansion and some homogenization was observed after 10 min and after 30 min, density changes could be observed. Electron diffraction analyses after drying, showed that the protuberances along the edges of the aggregates were mainly amorphous. This suggests that formation of crystals is enhanced by the precence of silica fume.

Test 9 (C)

In this test both expansion and crystallisation were obvious 10 min after wetting. After 20 min, the hydration had proceeded such far that it was difficult to distinguish between the individual cement grains. Electron diffraction analysis showed crystalline protuberances.

3.2.2.4 Conclusions

We conclude from the observations that:

1. Silica fume grains are attached to cement grains in water. Thus, there is no spontaneous dispersion or separation of the solid particles.

2. Cement reacts with water to yield rapid expansion and crystal growth. The reaction products appeared to be crystalline, presumably calcium sulphoaluminate hydrates

3. Where excess water was available for unlimited hydration, soft amorphous gels were formed at the boundaries of the cement grains, indicating rapid formation of CSH gel.

4. The superplasticizer appeared to retard the initial reactions only moderately, while later hydration phases were delayed. The retardation was found to be rather insignificant at the interface between cement and silica fume, indicating that the latter substance does not interact with the superplasticizer and prevents this agent to reach the cement grains where they are SF-coated.

5. Silica fume grains smaller than 0.05 microns are dissolved relatively rapidly while large grains in stagnant water (pores) persist for hours, and probably much longer than that.

We conclude that the "pellicle concept", i.e. that the cement and silica fume grains are effectively protected from water attack is hardly valid since the difference in reaction rate between the SP-free and the SP-rich mixtures was small. Probably, SP acts as a salt, the negatively charged organic ions being dispersed in the water and causing a delay in cement hydration rate mainly by causing an increased

resistance to the diffusion of water molecules (drag effects) to the strongly hydrophilic cement grains. The reology of the grout is significantly affected also by small amounts of superplasticizer, demonstrating that this substance affects the surface charge of the cement grains. It is suggested that the superplasticizer ions are attached to the oxygen- or OH-dominated surfaces of the cement grains through weak hydrogen bonds and mass forces. Assuming them to be polar or to have reactive end members, they are expected to form a Helmholtz-type cloud with an extension that depends on the concentration. This would lead to an increased rate of hydration of the cement when the concentration of superplasticizer has been reduced by dispersion into the voids of the cement or by removal by percolating water.

A consequence of this is also that the concentration of superplasticizer rapidly drops in the voids of high w/c-cement, while it remains high in closed pores of a dense low w/c-cement. In neither case it is probable that the superplasticizer becomes integrated with the cement gel.

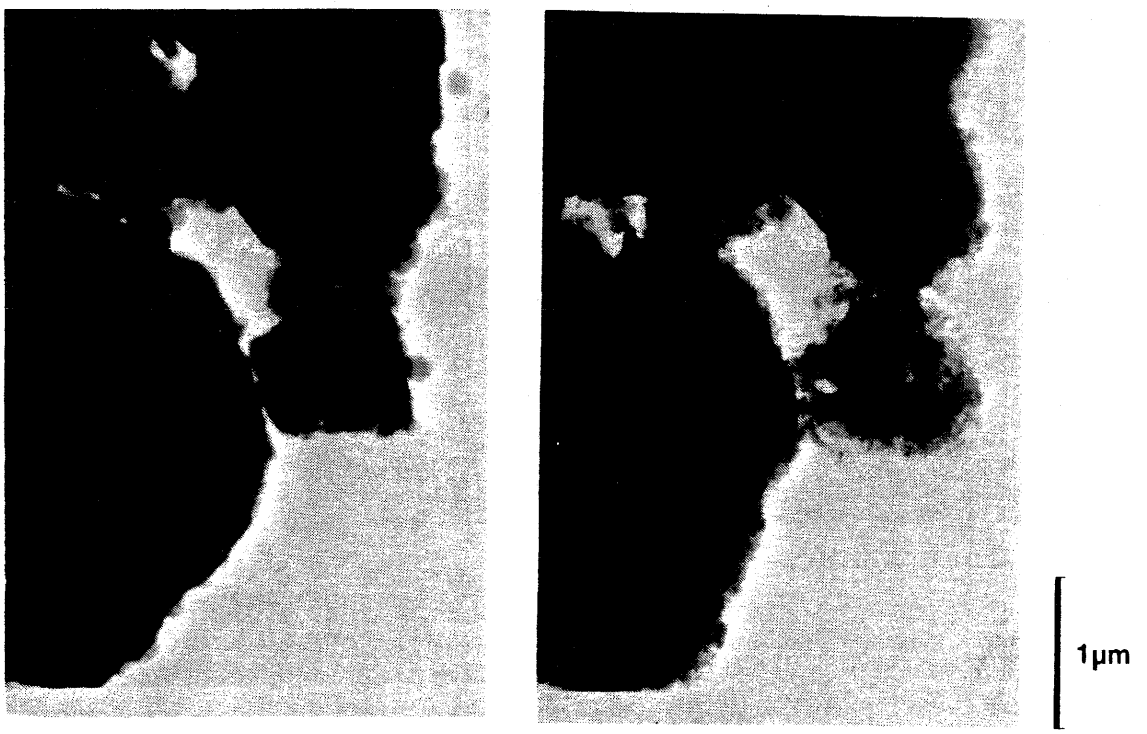

Fig IV:18 Cement, silica fume and superplasticizer before hydration (left) and after 1.3 h hydration (right)

3.3 SLOT INJECTION TESTS

3.3.1 Test device and data acquisition

Equipment

In order to be able to estimate the injectability and actual penetration of different grouts in narrow fractures, a series of laboratory tests has been performed using a specially designed test device.

The device consists of two, very stiff and perfectly plane steel plates. The plates are bolted together, distanced by a copper foil, to form a slot with an aperture of 100 µm, 5 cm width and about 3 m length. The surfaces forming the slot are slightly roughened, and the plates are equipped with glass plugs at regular distances so that the penetration of the advancing grout can be directly viewed. Also, pressure transducers are mounted so that the pressure wave pattern can be recorded at different distances from the injection point.

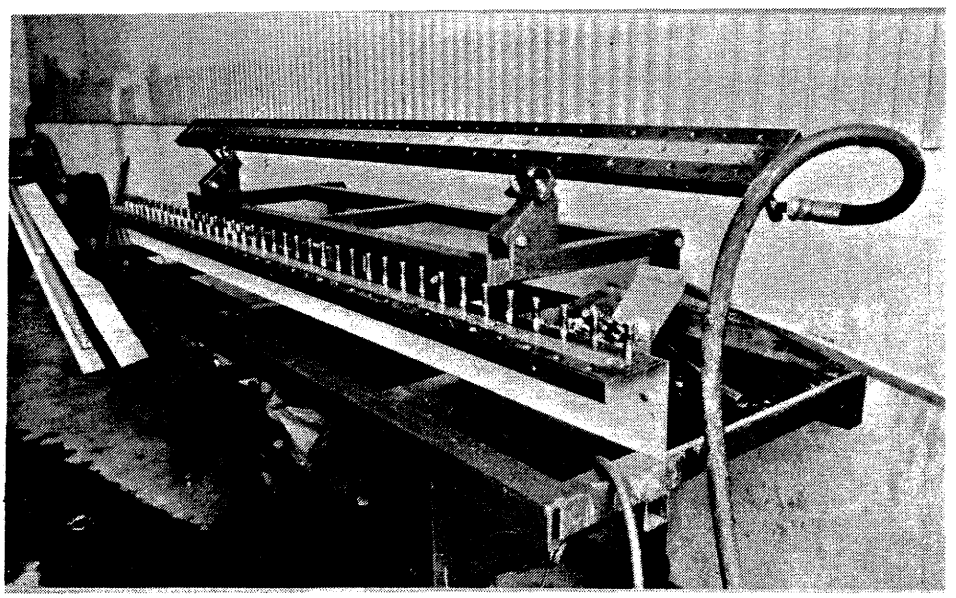

Fig IV:19 The test device

Data Aquisition

The signals from the pressure transducers were collected with a Lab Master (TM) A/D converter together with an IBM-PC compatible computer. The resolution of the converter is 12 bits. Software has been developed which allows for data collection on 5 channels with a sampling frequency of 2300 Hz. The time recordings of

the grout advancement were recorded by use of an ABC-80 computer through a push-button system.

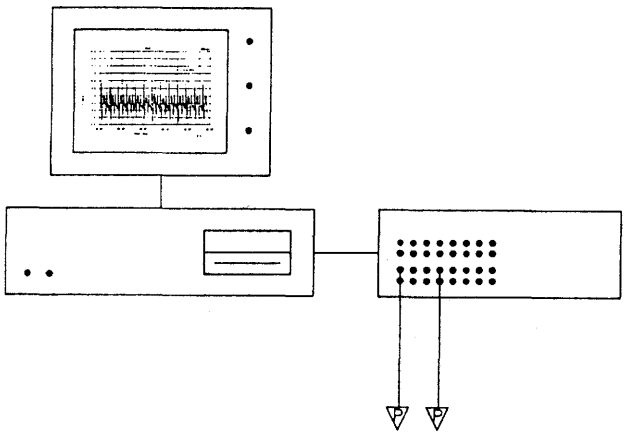

Fig IV:20 The data acquisition system with two pressure transducers (P)

Dynamic injection device

The present version of the equipment used for the injections is a colloidal mixer (A in Fig IV:21), a stirrer (B) and a single acting plunger pump (C) connected to the "dynamic injection device" (DID), which consists of a percussion machine (D) mounted on a sliding frame, hammering on a piston (E) that is attached to a grout cylinder (F). The static backpressure, which can be varied, is produced by a pneumatic cylinder (hidden at G) pushing the sliding frame. From the grout cylinder outlet a 1" steel pipe (H) is connected to the injection point.

Grouting procedure

The mixing of the grout is made in the colloidal mixer (A) (for bentonite grouts at least three days before grouting). When the grout is homogeneous it is pumped over to the stirrer (B) from where it is transferred to the grout cylinder (F). At field grouting, the borehole is filled from the bottom by pumping the grout via the grout cylinder through a hose lowered to the bottom of the hole. During the grout injection a valve (J) between the grout cylinder and the grout pump (refill valve) is closed. If refill of the grout cylinder is required, a valve (K) between the cylinder and the borehole is closed and the refill valve (J) is opened, the pressure from the pump (C) forces the piston (E) backwards and when the cylinder (F) is full the refill valve (J) is closed and the dynamics restarted. The refill procedure takes less than 30 seconds.

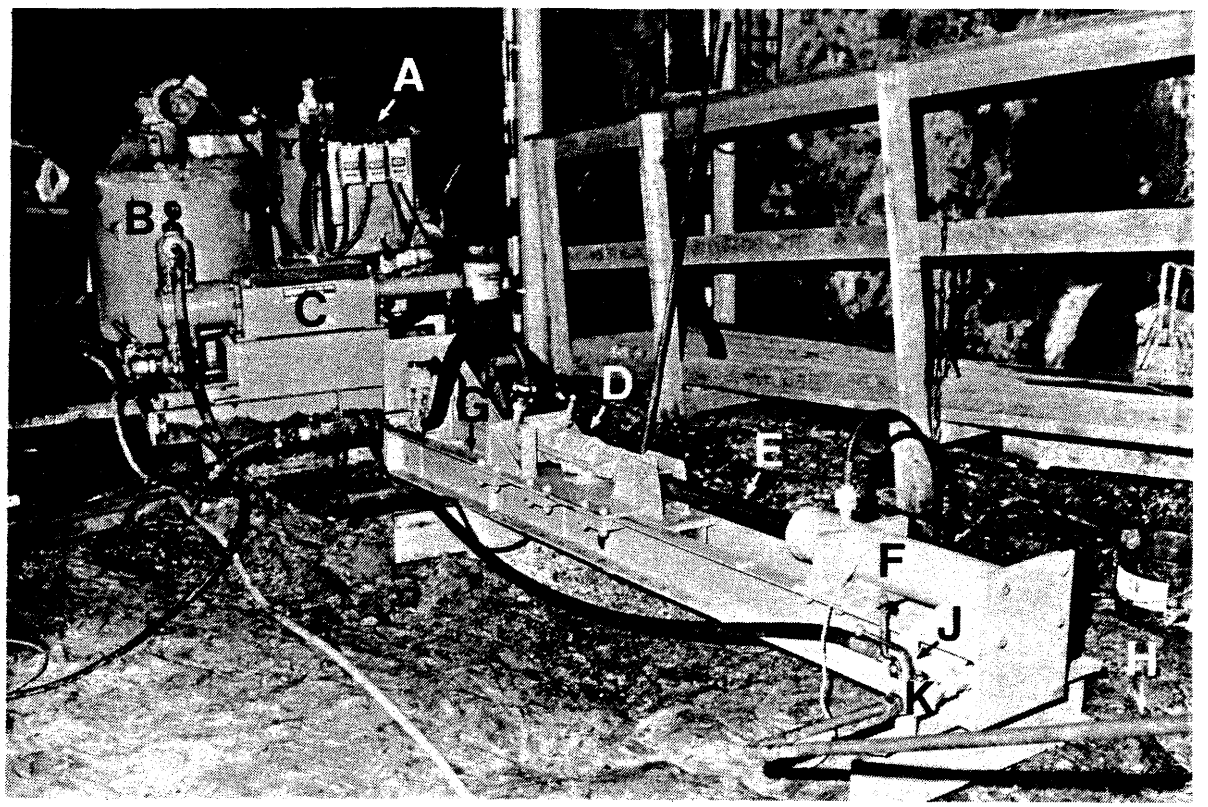

Fig IV:21 The dynamic injection device

3.3.2 Test program

The program comprised tests of different mixes of the two main candidate materials cement and bentonite. The cement materials investigated were finely ground cement with varying proportions of condensed silica fume (CSF) and superplasticizer (SP) added. For the bentonite grouts the sodium bentonite Tixoton was used combined with varying proportions of quartz filler (grain size < 15 µm). The previously performed rheology studies of the materials were used as a basis for the selection of suitable mixtures for the lab injection tests. The mixtures investigated are listed in Table 4. It should be added that microscopy showed that the maximum grain size of the quartz filler was probably about 5 µm.

Comments

The percentages of CSF and SP and the w/c ratio are calculated as parts of the total dry weight of cement and CSF.

The percentages of Tixoton and quartz are calculated as parts of the total dry weight of Tixoton and quartz.

Table 4 The lab injection test program

Test no	Material	Water content
1	100% Tixoton	$2.0 \cdot w_L$
2	"	"
3	"	$1.6 \cdot w_L$
4	"	$1.5 \cdot w_L$
5	"	"
6	"	$1.2 \cdot w_L$
7	"	$1.1 \cdot w_L$
8	75% Tixoton/25% quartz	$1.5 \cdot w_L$
9	"	$1.4 \cdot w_L$
10	50% Tixoton/50% quartz	$1.7 \cdot w_L$
11	"	"
12	"	$1.6 \cdot w_L$
13	"	$1.5 \cdot w_L$
14	"	$1.2 \cdot w_L$
15	"	"
16	25% Tixoton/75% quartz	$2.0 \cdot w_L$
17	"	$1.3 \cdot w_L$
18	Cement + 10% CSF + 0% SP	w/c = 0.50
19	Cement + 10% CSF + 0.42% SP	w/c = 0.37
20	"	w/c = 0.42
21	"	"
22	"	"
23	Cement + 10% CSF + 1.1% SP	w/c = 0.42

w_L denotes the water content of the grout at the liquid limit.

The different grouts were investigated at different pressure situations, the frequency was varied from 25 - 50 Hz, the static back pressure level was varied from 0 - 20 MPa and the peak height ranged from 2 - 10 MPa. The slot aperture was kept constant at 100 µm.

3.3.3 Results

The lab injection equipment has also been used for testing and development of the dynamic injection device, described in Chapter 3.3.1, and it has undergone successive development in the course of project. The variation in design of the different versions has yielded a spectrum of dynamic pressure conditions.

The equipment has been developed in five stages. Typical pressure conditions for the different versions are shown in Table 5.

Table 5. Typical pressure conditions

Version	Static pressure (MPa)	Dynamic amplitude (MPa)	Frequency (Hz)
A	1	3	33
B	20	10	27
C	4	7	40
D	2-3	3-7	40
E	2.5	3.5	48

Note that these are the pressures normally used in the lab tests, the equipment offers the possibility to use lower static pressure levels.

Table 6 lists all the relevant test injections that have been performed in the laboratory. The different versions of the equipment each has one column, A-E as above.

Table 6. Lab injection tests

Test no	Material	Water content	Penetration depth, cm				
			A	B	C	D	E
1	100% Tixoton	$2.0 \cdot w_L$	200				
2	"	"	190				
3	"	$1.6 \cdot w_L$			210		
4	"	$1.5 \cdot w_L$				145	
5	"	"	110				
6	"	$1.2 \cdot w_L$				60	
7	"	$1.1 \cdot w_L$	0				
8	75% Tixoton/25% quartz	$1.5 \cdot w_L$	110				
9	"	$1.4 \cdot w_L$					52
10	50% Tixoton/50% quartz	$1.7 \cdot w_L$			275		
11	"	"			195		
12	"	$1.6 \cdot w_L$				175	
13	"	$1.5 \cdot w_L$				90[1]	
14	"	$1.2 \cdot w_L$		≥280			
15	"	"				44	
16	25% Tixoton/75% quartz	$2.0 \cdot w_L$			≥280		
17	"	$1.3 \cdot w_L$			175		
18	Cem + 10% CSF + 0% SP	w/c = 0.50				45:9[2]	
19	Cem + 10% CSF + 0.42% SP	w/c = 0.37				125:9	
20	"	w/c = 0.42				55[3]:11	
21	"	"				75[4]:10	
22	"	"				120:20	
23	Cem[5] + 10% CSF + 1.1% SP	w/c = 0.42				210:20	

The penetration of the grout in the test slot is given in centimetres in the table. The figure after the colon for the cement grouts denotes, in minutes, the time elapsed between the start of the mixing of the grout and the start of the injection. Further explanations are:

1) 40 m long 15 mm tube attached to the slot
2) Second figure denotes time span between preparation and injection of cement grout
3) Only static injection pressure
4) Injection stopped after 7 seconds
5) Swedish, finely ground cement

The diagrams in Figs IV:22 and IV:23 show the results of an injection test with cement + 10 % CSF + 0.42 % SP, w/c = 0.37 (Test no. 19).

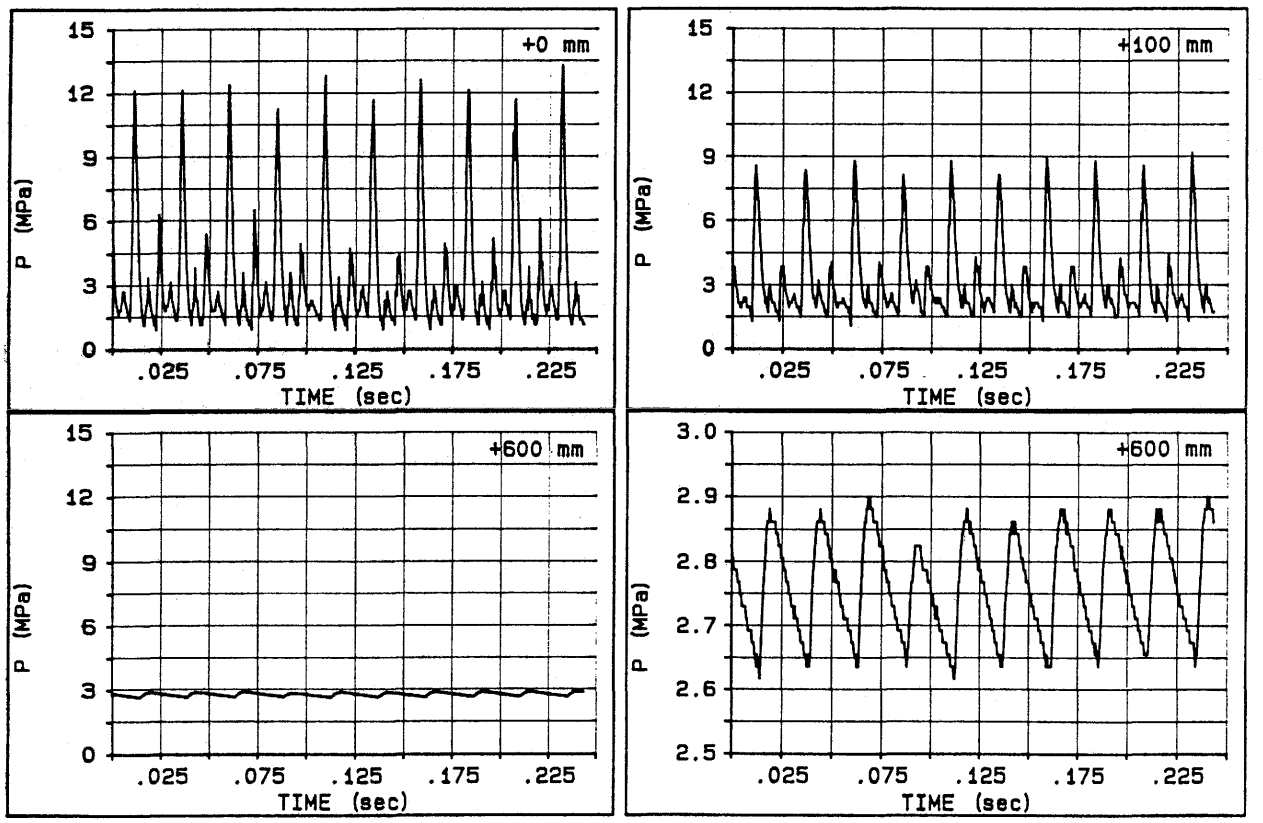

Fig IV:22 Pressure recordings after 20 seconds of injection. Recordings at slot inlet and in the slot at 100 and 600 mm from the inlet

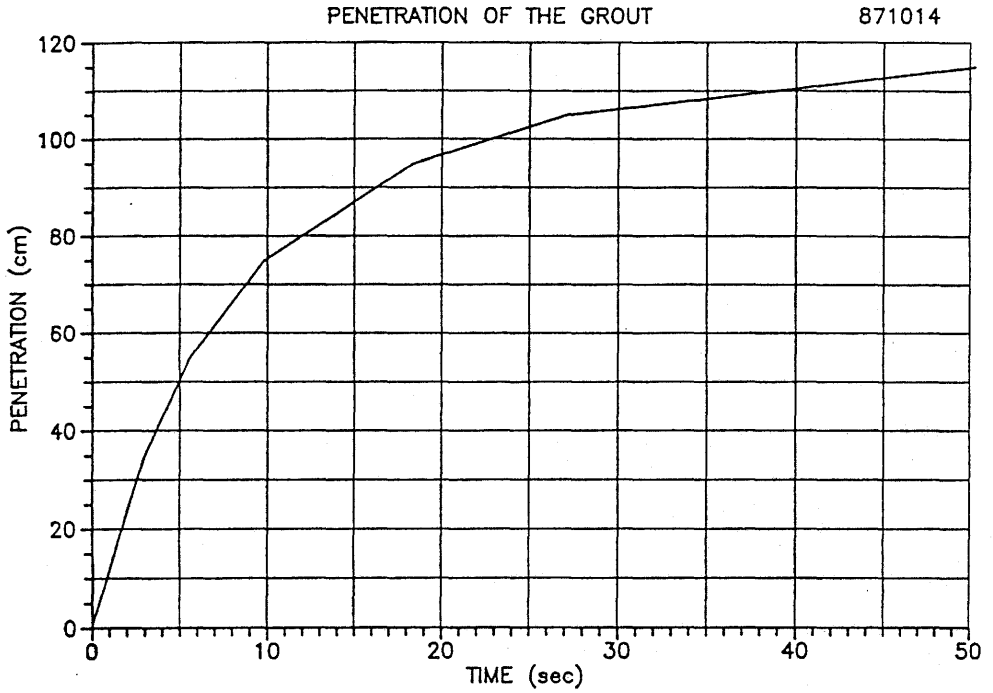

Fig IV:23 The penetration of the grout in the slot vs time

After injection the test slot was opened and samples were taken of the injected grout. A study of the water content of some bentonite grouts sampled from the slot after injection is presented in Table 7.

An interesting observation is that, except for one case, the bentonite gel sampled from the slot was drier than the gel sampled from the grout cylinder. This is probably due to instant drying of the very thin (two layers of each 50 μm) clay gel when the slot is opened, despite the immediate sampling.

Samples from the slot are only taken from the tests in Table 7.

Conclusions:

* The penetration depth of the grouts in a 100 μm wide fracture is considerable for all clay gels with a water content exceeding 1.5 times the liquid limit and for cement grout with more than 0.4 % super plasticizer and a w/c ratio of more than 0.35.

Table 7. Water content of bentonite grouts

Test no	Grout Tix/qu	$w_{cylinder}$ (%)	w_{slot} (%)	Penetration (cm)	Volume grout in slot[1] (cm^3)	Slot volume[2] (cm^3)	Conditions in slot
4	100/0	800 $w_L \cdot 1.5$	705 $w_L \cdot 1.4$	145	7.7	7.8	Dry
6	100/0	650 $w_L \cdot 1.2$	580 $w_L \cdot 1.1$	60	2.7	3.0	"
10	50/50	430 $w_L \cdot 1.7$	483 $w_L \cdot 1.9$	275	-[3]	13.8	Water (badly cleaned)
11	50/50	430 $w_L \cdot 1.7$	407 $w_L \cdot 1.6$	195	-[3]	9.8	Water
13	50/50	375 $w_L \cdot 1.5$	350 $w_L \cdot 1.4$	175	8.2	8.8	Dry
15	50/50	300 $w_L \cdot 1.2$	240 $w_L \cdot 1.0$	44	3.1	2.2	Dry
16	25/75	276 $w_L \cdot 2.0$	193 $w_L \cdot 1.4$	≥280	-[3]	14.0	Water

1) Calculated from the weight of the sample from the slot with an assumed density of 1.1 g/cm^3
2) To the penetration depth
3) Not measured

* The investigation of samples from the slot indicates that no separation takes place, and that there is no dilution of the gel even when there is water in the slot.

* The grouts in the slot were found to be homogeneous, i.e. without visible pores and variations in density.

3.3.4 Model evaluation

The artificial slot has the well-defined geometry necessary for testing the flow models. A lot of calculations have been made in order to compare the flow models with the measured inflow. The equations derived earlier in Chapter III and the flow properties modelled in this chapter, par. 3.1 have been used in these calculations.

However, there are some difficulties in making the calculations due to the change in oscillating shear strain amplitude and the associated change in viscosity during the penetration. A step-wise calculation starting with the properties of non-vibrated grout would seem possible. New values of the grout parameters based on the amplitude of the vibrations would then be used in the next step of calculation. However, it turns out that the amplitude of the vibrations is very high in the beginning of the test. The magnitude of this amplitude is entirely dependent on whether e.g. 1 cm or 10 cm is chosen as the first step, meaning that if the first step is too short, the viscosity will be too low and thus the penetration calculated in the next step too long. If the first step is too long the opposite will occur. Thus the initial step will be a determinant of the calculated penetration, which is of course unacceptable.

One way to overcome this difficulty is to assume an average shear strain amplitude and use the flow parameters, belonging to that amplitude, in the calculation. The penetration depth is then limited by either the calculated rate or the calculated strain amplitude. The calculation is made for different penetration depths and the flow is assumed to stop when the rate is too low (< 1 mm/s) or the amplitude falls below the assumed average value.

A suitable value for the oscillating shear strain amplitude is $\gamma = 1.0$. This value has been chosen both on experimental and theoretical grounds. Fig IV:24 shows an example of calculated and measured penetration. As can be seen from this diagram the agreement is acceptable although the calculated inflow is slower than the measured in the beginning of the test and faster at the end. The calculated dynamic shear strain amplitude γ is also shown. γ is very large in the beginning of the test but $\gamma = 100$ corresponding to an oscillating deformation of 5 mm after 8 seconds is not unrealistic and implies a lower viscosity, which is in fact confirmed by the fast penetration in the beginning of the test. γ is decreasing very

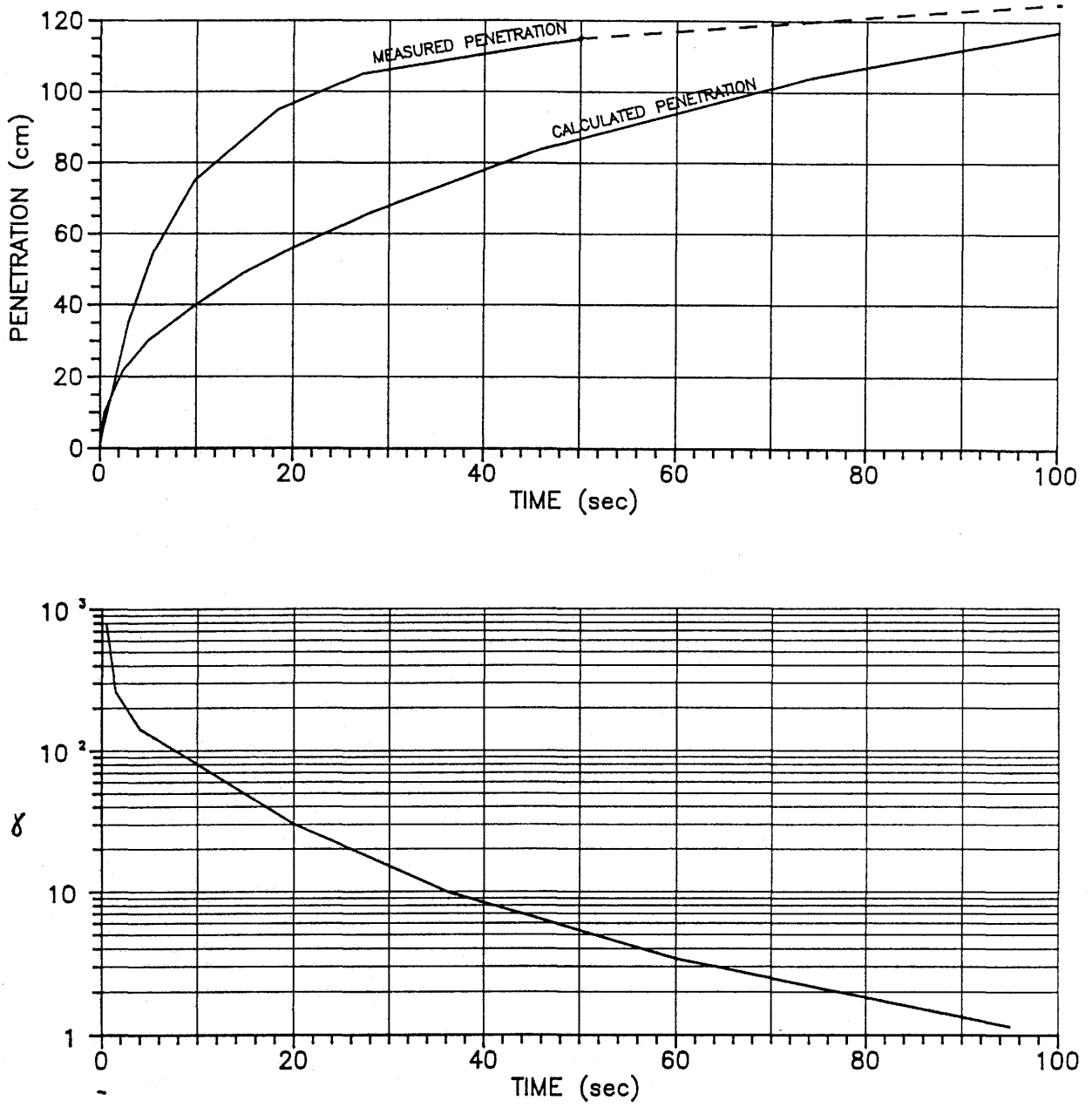

Fig IV:24. Calculated and measured penetration as a function of time. The calculated shear strain amplitude γ is also shown.

fast and after 100 s the amplitude falls below $\gamma = 1.0$, meaning that the penetration stops at 120 cm, which is close to what was measured.

This example suggests that the proposed method is useful for predicting the penetration depth. To see if this conclusion holds for the other slot tests the penetration has been calculated for the different grouts used and then compared to the

measured penetration. Table 8 shows the results from such a comparison. Only the tests made with one of the recent grouting equipments are studied.

Table 8. Comparison between the calculated and measured penetrations at the slot injection tests.

Test no	Material	Consistency	Penetration, cm		Remark
			Calc	Meas	
19	C.c 10% CSF 0.42% SP	w/c=0.37	90	125	
20	C.c 10% CSF 0.42%	w/c=0.42	45	55	Stat
22	C.c 10% CSF 0.42%	w/c=0.42	120	120	
23	S.c 10% CSF 1.1%	w/c=0.42	180	210	
4	100% Bentonite	$1.5 \cdot w_L$	70	145	
6	100% Bentonite	$1.2 \cdot w_L$	35	60	
12	50% Bent 50% quartz	$1.6 \cdot w_L$	70	175	
13	50% Bent 50% quartz	$1.5 \cdot w_L$	65	90	
15	50% Bent 50% quartz	$1.2 \cdot w_L$	35	44	

All calculated penetrations are found to be smaller than the measured ones. The calculated values at the cement injections are very close to the measured values with an average relation of 85% while the difference, i.e. 55%, is more obvious but still not very significant for the bentonite. The scatter of this relation is quite small, proving that the flow model and calculation technique are relevant.

It seems as if the assumed average $\gamma = 1$ results in a slight underestimation of the penetration especially for bentonite. The influence of a change in γ is consistently greater for bentonite than for cement according to the measurements accounted for in par. 3.1.

A sensitivity analysis intended to illustrate the influence of the viscosity on the penetration depth at different fracture apertures has been made using this method. The following basic data were used:

Ev = $2.1 \cdot 10^9$ Pa (grout)
Er = $5.0 \cdot 10^9$ Pa (rock)
$h1$ = $2.0 \cdot 10^6$ Pa (static pressure)
w = 251 1/s (40 Hz frequency)
ρv = 1100 kg/m^3 (grout density)
h_o = $5 \cdot 10^6$ Pa (oscillating pressure amplitude)
n = 1
m = 0.1-100 Pa (or viscosity Pas)
d = 10-500 µ (fracture aperture)

The results from this analysis are shown in Fig IV:25.

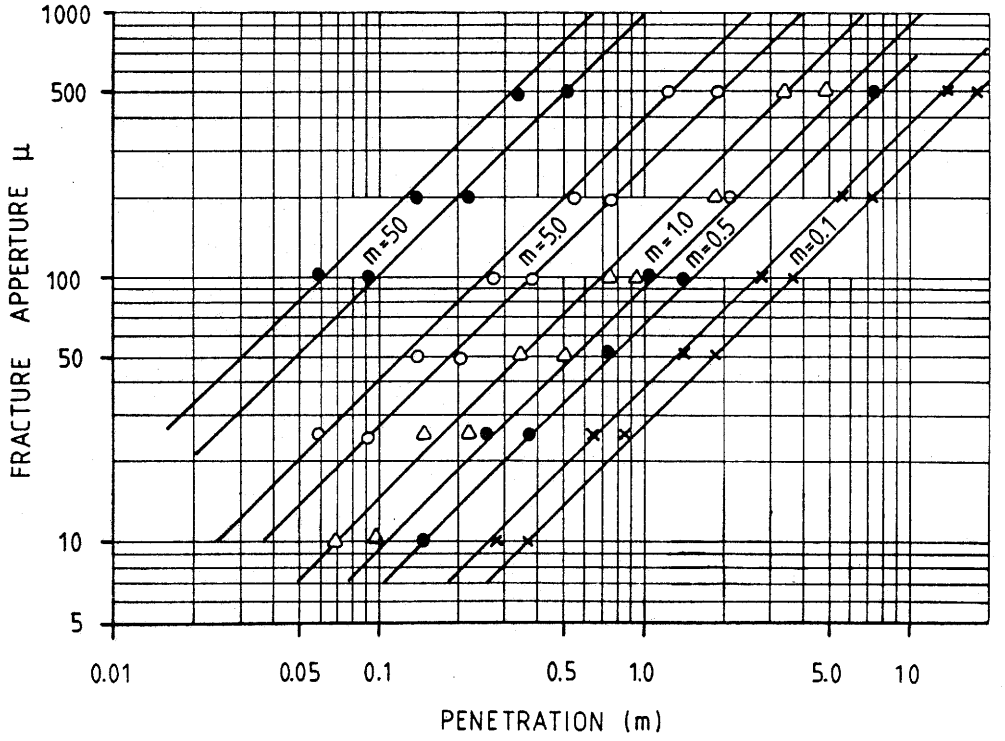

Fig IV:25. Influence of m-value (viscosity) and fracture aperture on the penetration.

The influence of a change in water ratio or superplasticizer content can be studied by taking the different values of m at $\gamma = 1.0$ in Fig IV:16 and use them in Fig IV:25. E.g. a decrease in water ratio of bentonite from $1.6 \cdot w_L$ (w = 840%) to $1.2 \cdot w_L$ (w = 630%) means an increase in m from 1.1 to 3.5, resulting in a decreased penetration from 34 cm to 18 cm in a fracture with the aperture 50 µm

or from 62 cm to 33 cm if the probable previous underestimation in penetration power is taken into account.

4 LONGEVITY

4.1 CLAYS

4.1.1 Current views

The crystal structure of smectite consists of two layers of tetrahedra - principally Si with minor Al - sandwiched to the top and bottom of a layer of octahedrally coordinated cations, usually Al but with some Mg and Fe. The structure is apt to undergo alteration on environmental changes in the form of heat-induced replacement of a significant fraction of the tetrahedral silica by aluminum, and possibly by loss of octahedral aluminum. This yields a very significant charge change, which is a first step in possible mineral transformations (beidellitization, illitization) and altered hydration properties of the material. The release of silica may be closely related to a transfer from a "low temperature" form of montmorillonite, in sodium or lithium state, to a "high temperature" version. This matter is a key question that needs much attention.

Solid/solid transition

For the particular case of pH ranging from about 7 to 10, a great number of investigators have suggested a solid solution-type, heat-induced conversion mechanism in which illite forms from smectite through tetrahedral substitution and interlamellar uptake of potassium. A general expression of the reaction has the following form:

$$Montmorillonite + Al^{3+} + K^{+} \rightarrow Illite + Si^{4+}$$

This conversion scheme implies that a charge change is produced through replacement of tetrahedral silica by aluminum originating either from octahedral lattice positions or from external sources, and that no actual dissolution takes place, except that silica is liberated. The mineral so formed is beidellite, the charge change being balanced by adsorbed cations. If potassium ions are available they become fixed in conjunction with interlamellar collapse yielding illite.

In terms of Maegdefrau's general formula, the mineral created by the replacement of tetrahedral silica by aluminum and interlamellar uptake of monovalent cations to balance the charge change, would be:

$$M^{I}_{y}\, Si_{(8-y)}\, Al_{y}\, O_{20}(OH)_4\, (M^{III}, M^{II})_4$$

where y is in the range of 1-2, M^{I} represents monovalent cations, M^{II} magnesium and divalent iron and M^{III} aluminum or trivalent iron. Electrostatic forces, hydrogen bonds and mass forces keep the layers together. If K^+ is available in sufficient concentration, illite will ultimately be formed, while absence of potassium means that the smectite is preserved in beidellite form. It exhibits similar expansion properties as montmorillonite on hydration/dehydration, and does not collapse permanently with other cations than K^+ in the interlamellar space. It is possible, however, that certain conditions, like high pressure and temperature, may yield collapse of sodium-saturated beidellite to non-expanding 10 Å-minerals of paragonite-type such as brammalite ("sodium-illite").

By applying thermodynamics to montmorillonite in polyelectrolyte solutions, Tardy and Touret recently demonstrated that different cations are taken up in interlamellar positions at different degrees of water saturation. Assuming that "dry" conditions are equivalent with heavy compaction, they concluded that potassium is preferred to sodium in very dense smectite clay while the opposite is valid for "soft" conditions. This finding is of extreme importance and if it can be validated it means that illitization would not be a problem for clay grouts.

Dissolution/neoformation

In 1985 Pollastro suggested a model according to which illite is formed by partial dissolution of smectite components of expandable I/S aggregates and precipitation of dissolved species on low-expandable aggregates. The same year Nadeau et al suggested a somewhat similar alteration mechanism for the conversion of smectite to illite and their idea is supported, in a general sense, by other studies, such as the comprehensive investigation of the Shinzan area in Japan by Inoue et al and by Güven's electron microscopy investigations which indicated that heat-exposed smectite has two major forms: a flakey or mossy appearance representing interstratified I/S, and lath-shaped minerals representing illite that has grown in the pores. The latter objects are supposed to be formed by precipitation of components dissolved from the smectite, in which the potassium content is successively

altered. In principle, the creation of both I/S alteration products and neoformed "illite" can be explained by Boles and Franks' illitization reaction in which implies that some of the smectite is consumed through "cannibalization":

$$3.93\,K + 1.57\,KNaCa_2Mg_4Fe_4Al_{14}Si_{38}O_{100}(OH)_{20}, 10\,H_2O \rightarrow$$
$$5.5Mg_2Fe_{1.5}Al_{22}Si_{35}O_{100}(OH)_{20} + 1.57\,Na^+ + 3.14\,Ca^{2+} +$$
$$4.28\,Mg^{2+} + 4.78\,Fe^{3+} + 3.14\,Ca^{2+} + 4.28\,Mg^{2+} +$$
$$4.78\,Fe^{3+} + 24.66\,Si^{4+} + 57\,O^{2-} + 11.40\,OH^- + 15.7\,H_2O$$

This reaction requires that potassium is available for transformation of montmorillonite to illite and it implies that the first-mentioned mineral is extremely stable provided that the potassium content remains very low. The fact that beidellite forms from montmorillonite on heating demonstrates, however, that one of the major reaction steps in the transformation of this mineral to illite takes place also in the absence of potassium and therefore that the dissolution/reformation process and K-uptake may follow quite different paths.

Reaction rates

It is usually assumed that the crystal lattice reorganization of smectites yielding illitization is a true Arrhenius-type kinetic process. This philosophy was also applied by Pytte, who made a comprehensive field study and related it to conventional rate expressions in order to evaluate the activation energy of the illitization. His empirical syntheses based on geological data from illite/smectite suites of Cretaceous and Tertiary age (Pierre shale, Colorado, and Dulce siltstone, New Mexico, respectively) led to the conclusion that kinetic factors control the dissolution reaction progress. XRD plots of I/S clay samples taken at different distances from the interface between clay-bearing strata and diabase intrusives were compared with I/S-distributions derived by use of the following rate law:

$$-dS/dt = (Ae^{-U/RT(t)})(\{K+\}/\{Na+\})^m S^n$$

where S equals the mole fraction of smectite in I/S assemblages, R is the gas constant, T the absolute temperature, t is time, and m and n indicating different order equations. Using back-calculated temperature histories good agreement was obtained with the XRD data by setting m equal to unity and n equal to 3,4 or 5. The activation energy was found to be in the range of 27 to 33 Kcal/mole, which is higher than the values derived by Eberl and Hower on the basis of hydrother-

mal tests (19.6 Kcal/mole) but on the same order of magnitude as the activation energy obtained by Roberson and Lahanne. Fig IV:26, which illustrates the illitization rate for the activation energy 27 Kcal/mole, leads to the conclusion that a temperature of 60°C would not yield a noticeable illite content in 100 000 years in a closed system with K-bearing minerals, while 130°C would convert most of the smectite to illite in about 1000 years. At 150°C significant illitization would be expected in 10 to 50 years and at 225°C one would find 30-50 percent of the smectite to be illite in a few months. Such transformation rates would be compatible, in principle, with the reaction model implying dissolution of the smectite and neoformation of illite, while it is not clear whether the charge change solid reaction that produces beidellitization exhibits the same kinetic pattern or if it is an Arrhenius-type reaction at all. It may well be that the I/S distributions observed by Pytte may result from different contents of beidellite at different distances from the hot diabase intrusions, the exchange of tetrahedral silica by octahedral aluminum that produces this mineral form being a very rapid process. Such a scenario would actually be supported by the results obtained by Howard and Roy, who derived the activation energy value 3.5 Kcal/mole for K-saturated collapse of hydrothermally pre-treated montmorillonite. The clay exposed to heat had been saturated with solutions with Na as dominant cation (total cation content 197 - 260 ppm), the water content being 2500 %, the water pressure 30 MPa and the temperature 150 and 250°C in different experiments. The very low activation energy arrived at does not indicate crystalline reorganization involving disruption of Si-O and Al-O bonds but merely breakage of hydrogen bonds, which may actually be involved in the conversion of montmorillonite to beidellite as shown later in this chapter. In this context it is worth mentioning that their experiments at 250°C produced only half as much silica as available, while 150°C gave congruent dissolution of the montmorillonite, indicating that beidellite had been formed in the temperature range 150-250°C.

As concerns the simple solid-solid transformation one concludes that once the charge change leading to beidellitization has taken place, the transformation to illite may simply be a matter of time, and the actual rate of alteration being determined by the rate of dissolution of K-bearing minerals in the clay, or by the rate of transport of dissolved potassium to the clay through percolating groundwater or through diffusion. It is realized that both can be very much retarded in nearfield canister embedment as illustrated by examples given by Duwayne M. Anderson. Thus, applying a cation exchange capacity of 70 meq/100 g clay, a potassium concentration of the groundwater of 20 ppm, a hydraulic conductivity of the clay of

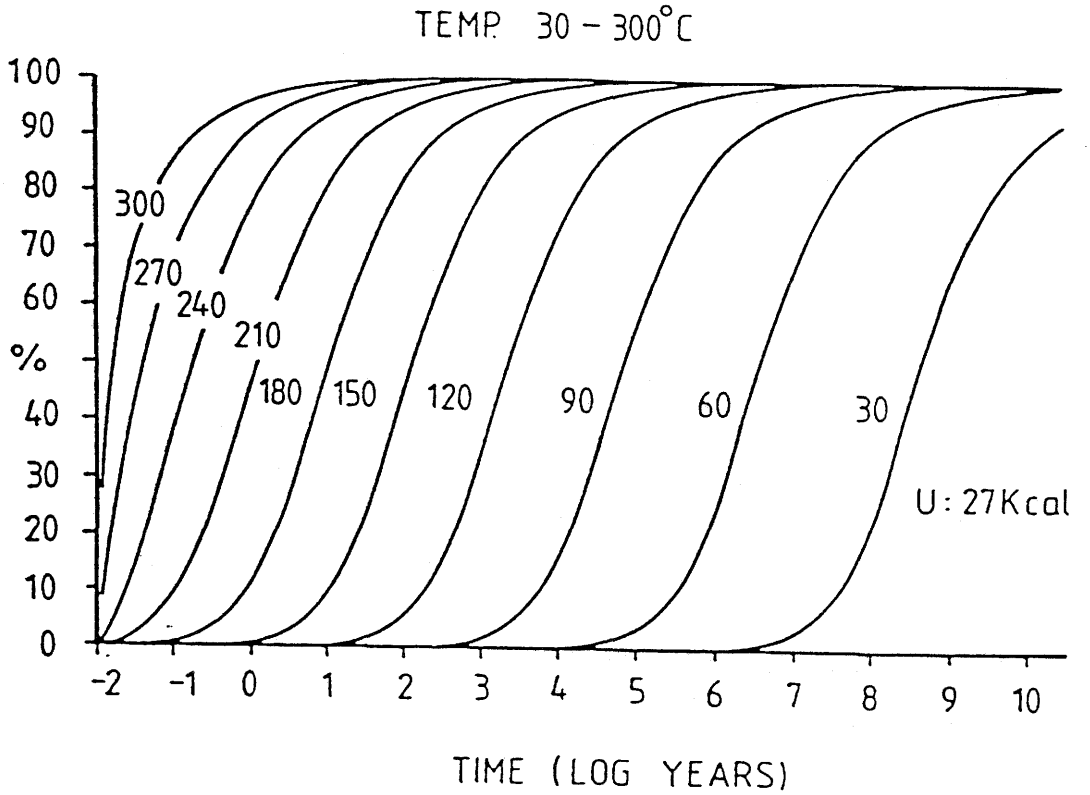

Fig IV:26. Illitization rates at different temperatures (after Pytte)

10^{-8} m/s, and a thickness of percolated, dense Na smectite of 1.0 m, complete conversion to illite would take about 1 million years provided that the hydraulic gradient is 0.01. Although calculations of this sort are not altogether conservative because of the fact that potassium-bearing water will flow 10 to 100 times faster through a small number of continuous passages from which lateral diffusion takes place, it indicates that the smectite content - in beidellite form - would remain high for very long periods of time.

Silica release and precipitation

As to mineral transformation at medium pH, one concludes that the reactions leading to partial or complete transformation of smectite to hydrous mica will affect the character of the particle network, particularly the microstructure and the rheological properties. From a practical point of view the two major types of reactions, i.e. the simple solid/solid transition with internal crystal reorganization and potassium uptake, and the dissolution/neoformation, are expected to yield different physical properties with respect to hydraulic conductivity and swelling ability. Thus, if the total volume is kept constant, the first-mentioned

alteration would lead to collapse of the interlamellar space and to a very significant increase in pore size and content of "external water" by which the hydraulic conductivity would be significantly increased, and the swelling pressure strongly reduced. The second type of reaction with neoformation of illite in the pores may partly reduce the effect of smectite dissolution so that the hydraulic conductivity is only slightly enhanced and the swelling pressure moderately reduced.

It is not clear, however, what effect the released silica will have or what the detailed mechanisms are in the release process. It has been assumed by the senior author that the release of silica takes place in conjunction with heat-induced collapse of apical tetrahedrons of the "low temperature" montmorillonite (Edelman/Favejee) crystal structure and that the dissolved silica may be precipitated in the form of an amorphous hydrated silica gel at the edges of montmorillonite stacks (Fig IV:27). The Ordovician Kinnekulle bentonite was suggested as a possible example since electron microscopy has shown that this clay has a high frequency of precipitation "nodules", which were taken to be silica compounds resulting from heat-induced release and precipitation of silica originating from the montmorillonite lattices, since earlier investigations using optical microscopy have indicated the presence of minute quartz rims on bentonite grains.

Conodont analyses and back-calculation of the heat flow from a basalt intrusion have shown that the temperature averaged at 110°C at minimum and 160°C at maximum for 1000-2000 years, which would indicate that release and precipitation of silica takes place at temperatures around 150°C. The central portion of this I/S- rich 2 m thick Kinnekulle clay bed is less illiticized than its upper part as documented by a higher potassium content and a lower swelling ability of the latter. Since the entire bed must have been exposed to practically the same temperature, the different degree of illitization is related either to slower (heat-aided) diffusion to the central part from external K-rich sources or to different initial contents of K-bearing minerals.

The precipitation of silica, which must be strongly dependent of the concentration of dissolved silica in the porewater of the bentonite clay may be very significant. Thus, about 25 % of all silica will be released solely on transformation of montmorillonite to beidellite and since this corresponds to at least 10 % of all solid matter it should affect the rheological properties substantially if the precipitates serve as cement. Actually, precipitation of only 1-3 % solid substance in cementitious form

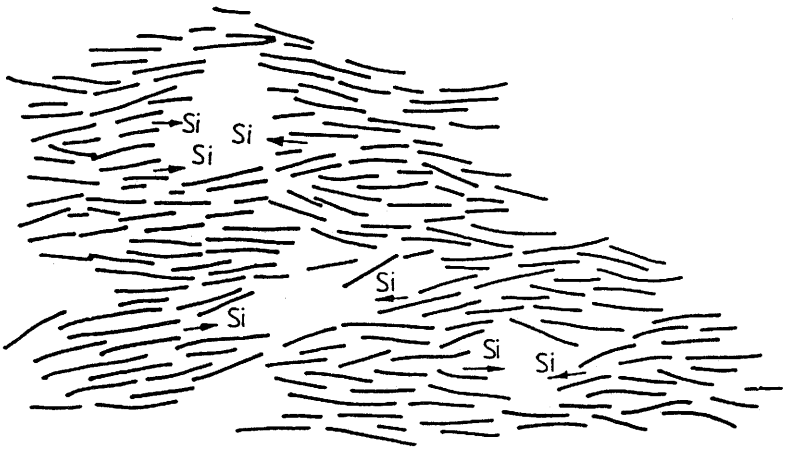

Fig IV:27. Schematic smectite flake arrangement in natural bentonites. Arrows indicate assumed Si migration at heating

is known to have a strong effect on the mechanical properties of most soils and we find this to be true also for the Kinnekulle clay.

Further information on silica precipitation has been offered by the large scale BMT field heating experiment, in the Stripa mine. It was conducted a few years ago, one purpose being to investigate whether the chemistry and physical properties of dense, almost completely water saturated Na bentonite would be altered in one year at 125°C under low water pressure conditions (300-700 kPa). The water had sodium as major cation and the ion strength was very low. The analyses comprised XRD and chemical analyses as well as electron microscopy and determination of two characteristic physical properties, i.e. the swelling pressure and the hydraulic conductivity. It was found from this comprehensive study that the only alterations that could be identified were a very slightly reduced swelling capability as observed by use of XRD technique and traces of precipitations at the edges of certain montmorillonite aggregates. Probably these effects were caused by vapor attack in the non-saturated bentonite close to the clay-embedded heaters, which were located in large-diameter boreholes.

Provided that there actually is a heat-induced transition between the two structural states and that they are real, heating to the critical temperature would

bring the silica atoms in an unstable condition by which they would be released and free to move in the interlamellar space. The resulting gradient in concentration of liberated silica would logically cause it to migrate towards the edges of the montmorillonite stacks, where it may become precipitated. The migration of silica would logically take place in connection with collapse of the structure from the 12.5 Å state to the dehydrated 10 Å state (left in Fig IV:3), meaning firstly that a compressive force is required to yield contraction of the stacks, and secondly that the migration of silica would be associated with expulsion of water formed from the OH:s. The contraction, which should be rapid as concluded from the corresponding quick collapse of the stacks on freezing, is expected to be perfectly reversible as long as no cementation of the flakes has taken place. Hence, we conclude that the beidellitization process, yielding free silica, may be associated with a contraction of the stacks of montmorillonite flakes, and if this is so, the rheological properties and perviousness should be altered.

A primary reason why interlamellar dehydration and collapse of the stacks would take place on heating under constant volume conditions is that the attraction forces that hold the flakes together dominate over the compressive resistance produced by the remaining hydrates. It is quite obvious from the larger "thickness" of the third hydrate than of the second, that the mechanical strength of the latter is significantly higher, the strongest hydrate layer naturally being the first one. Successively higher temperatures are therefore required to make the contraction proceed and considerable, thermally induced disturbance is therefore logically required to yield complete dehydration, which is known to require an effective pressure of about 200 MPa at room temperature. In very general terms the stability of sandwiched thin water films and solids, like those represented by phyllosilicate flakes with interlamellar water, can be explained in terms of mass forces and entropy effects. Applying Frenkel's theory one finds that sandwiched systems consisting of very thin silicate flakes separated by equally thin (~10 Å) water films should collapse to form thick solid particles. This is actually confirmed by the fact that stacks of non-charged phyllosilicate minerals like pyrophyllite do not contain any water films. The reason why interlamellar water films that are only a few molecules thick still exist at room temperature in hydrophilic clays is the entropy component, the main contribution of which is in the region of small film thicknesses. The general conclusion from this is that colloidal particles may remain attached to each other through extremely thin films of a dispersive medium provided that there is an ordering influence induced by the solid substance, of which montmorillonite gels are typical examples. Applying Frenkel's views, it is clear

that a sufficient increase in temperature inducing thermal motions would yield instability of the water films. Thus, heating to certain critical temperature levels is expected to lead to stepwise contraction of previously expanded montmorillonite stacks.

We conclude from this, that further research on the longevity of smectites must be based on a deepened understanding of the nature of water/lattice couplings. The matter is further treated in Chapter IV, par. 8.

Preliminary conclusions

Current hydrothermal tests, partly conducted in a parallel SKB research project, have resulted in the following preliminary model of hydrothermal effects on water saturated Na montmorillonite clay.

The effects of heating, i.e. the temperature-related contraction of previously expanded montmorillonite stacks and dispersed particle network branches, and the release of silica associated with transfer from montmorillonite to beidellite, are schematically illustrated in the form of tentative scenarios in Figs IV:28 and IV:29 for potassium-poor porewater. The various contraction stages are related to temperatures that are not yet safely established, while the last dehydration phase leading to collapse to 10 Å and release of silica, is documented to take place in the temperature range of 150-200°C. This latter stage is assumed to yield transfer from montmorillonite to beidellite. It is assumed that rehydration yielding the initial 2-3 hydrates in interlamellar positions takes place on cooling except for some permanent closure in material heated to 150-200°C. The original microstructure is, however, never recovered.

The detailed mechanisms involved in uptake of potassium and conversion to illite have not yet been revealed. It is estimated that they are very much related to the heat-induced contraction and silica precipitation. Further research is needed and if it confirms Tardy's and Touret's conclusion that Na is preferred to K in soft montmorillonite gels, the problem of the longevity of montmorillonite would be reduced to the simple one concerning microstructural changes on heating.

At a relatively low degree of water saturation the silica release at about 200°C is expected to yield precipitation of cementing compounds at any porewater composition, simply because the solubility of silica will be exceeded. Since larger voids

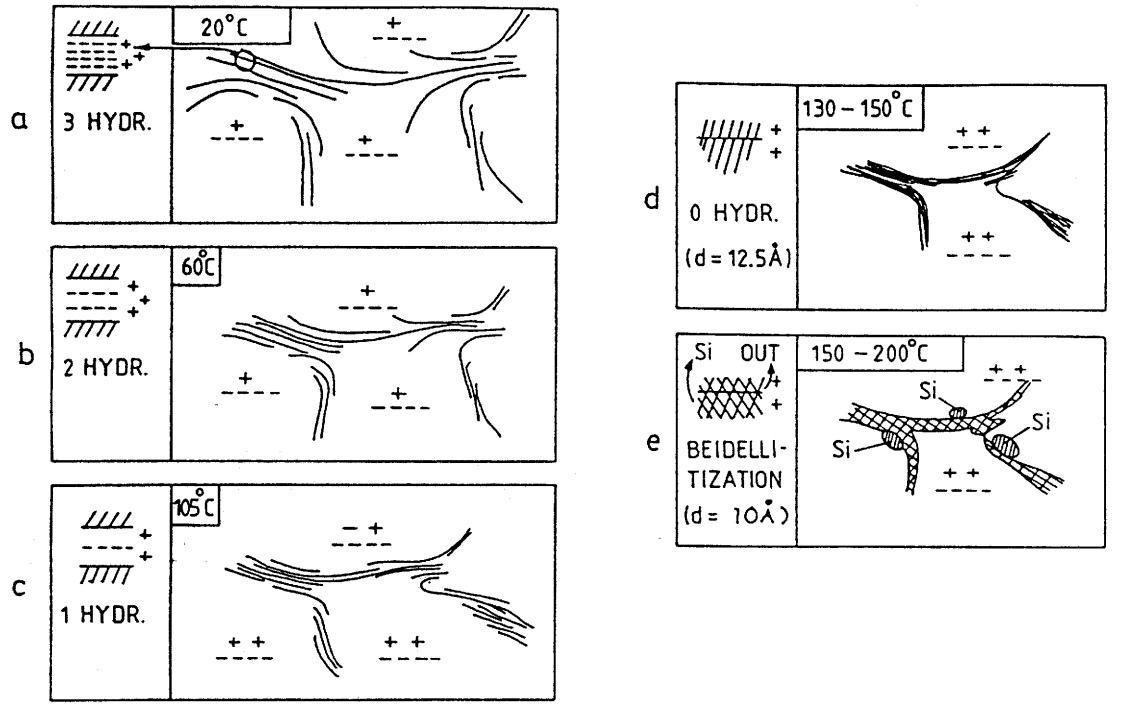

Fig IV:28. Schematic tentative model of microstructural changes and silica release at low bulk density

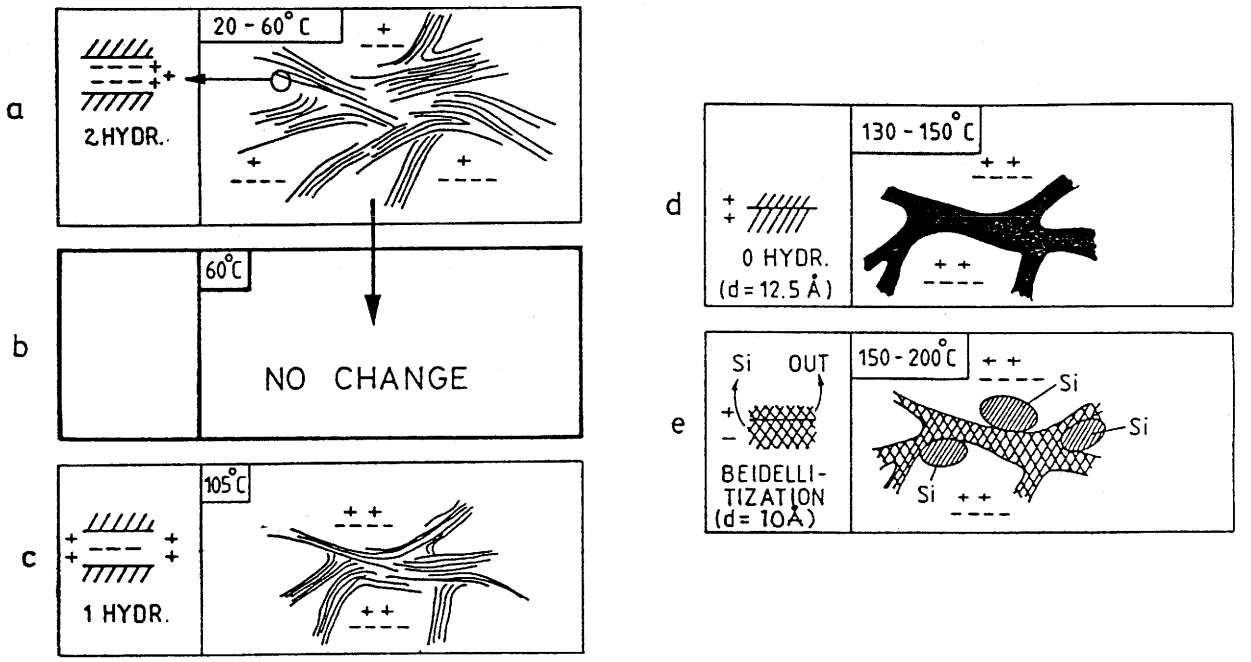

Fig IV:29. Schematic tentative model of microstructural changes and silica release at high bulk density

contain vapor, the precipitates are formed in the clay complexes, yielding more effective cementation than in water saturated clay. This may offer an explanation of the "Couture effect", i.e. the empirical finding that vapor-treated montmorillonite rapidly looses a significant part of its expandability already at about 150°C.

A preliminary, practical conclusion of all this can be put in the following condensed form:

* Beidellitization may require higher temperatures than about 150°C

* Illitization can be predicted if the rate of potassium uptake can be foreseen. Complete illitization may require more than 1 M years at temperatures lower than 150°C depending on the flow and diffusion patterns in the grouted rock

* The major practical effect of hydrothermal treatment at temperatures ranging between 70 and 150°C is a non-reversible microstructural reorganization

* The major practical effect of "short-term", i.e. a few thousand years of hydrothermal treatment at higher temperatures than 150°C is silica cementation

4.1.2 Thermomechanical treatise, "cone-in-cone"

Five long-term percolation studies have been completed using "cone-in-cone" probes to test different sealing material functions on expansion and heating. Four of the tests were made with soft smectite gels and the fifth one with cement.

Probe construction and gel preparation

The gels (Table 9) were carefully mixed and richly applied on the inner cones (Fig IV:30). These were slowly inserted in the outer cones under rotation by which the excessive gel mass was pressed out through the evacuation holes. When the slots were 0.3 mm wide, the probes were closed. 10 ml burettes with rubber policemen were connected to the outlet ends while the inlets were exposed to a constant excess water pressure of 50 kPa. For gel saturation and percolation de-aired distilled water was used .

Table 9. Thermo-mechanical test data

Probe	Tixoton (%)	Quartz (%)	Initial ρ_m (g/cm^3)	Expanded ρ_m (g/cm^3)	Hydralic gradient
1	50	50	1.19	1.14	70
2	100	0	1.10	1.07	70
3	50	50	1.14	1.11	70
4	100	0	1.07	1.05	70

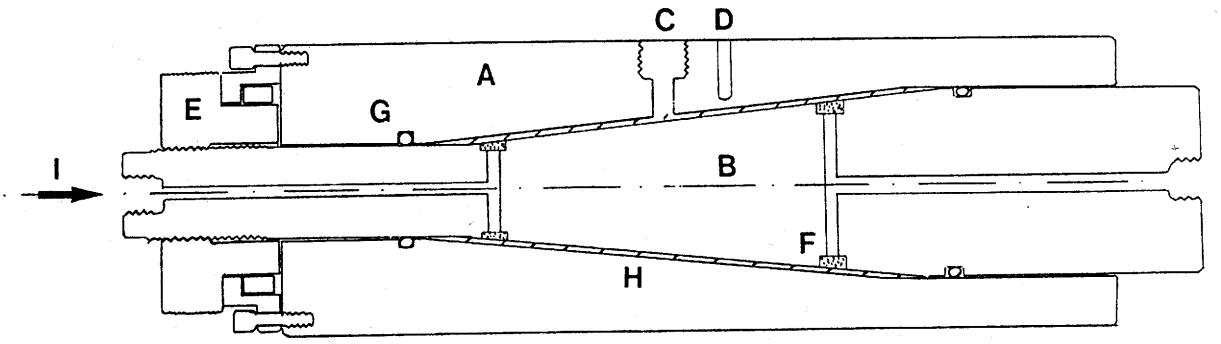

Fig IV:30. Cone-in-Cone apparatus
A Outer cone, goldcoated brass
B Inner cone. goldcoated brass
C O-ring
D Thermocouple
E Slot expansion mechanism
F Filter (bronze)
G Evacuation hole
H Sealing material
I Water inlet

Test method

The permeability tests were running for 45 days and had three stages (Fig IV:31). In the initial stage (I) the slot width was 0.3 mm and the temperature 20°C. After 8 days the water flow was approximately constant through all probes, and the

second stage was entered by imposing an expansion of the slots by 30% to 0.4 mm aperture (II). This was made by a quick axial displacement of the inner cones, still under constant water pressure. The gels were allowed to recover for 30 days before the heat was turned on (III). During two days the temperature was raised in steps to 90°C and was held constant at this level to the end of the tests. The gels were dried, still in the probes, after the tests and examined by use of optical microscopy and SEM.

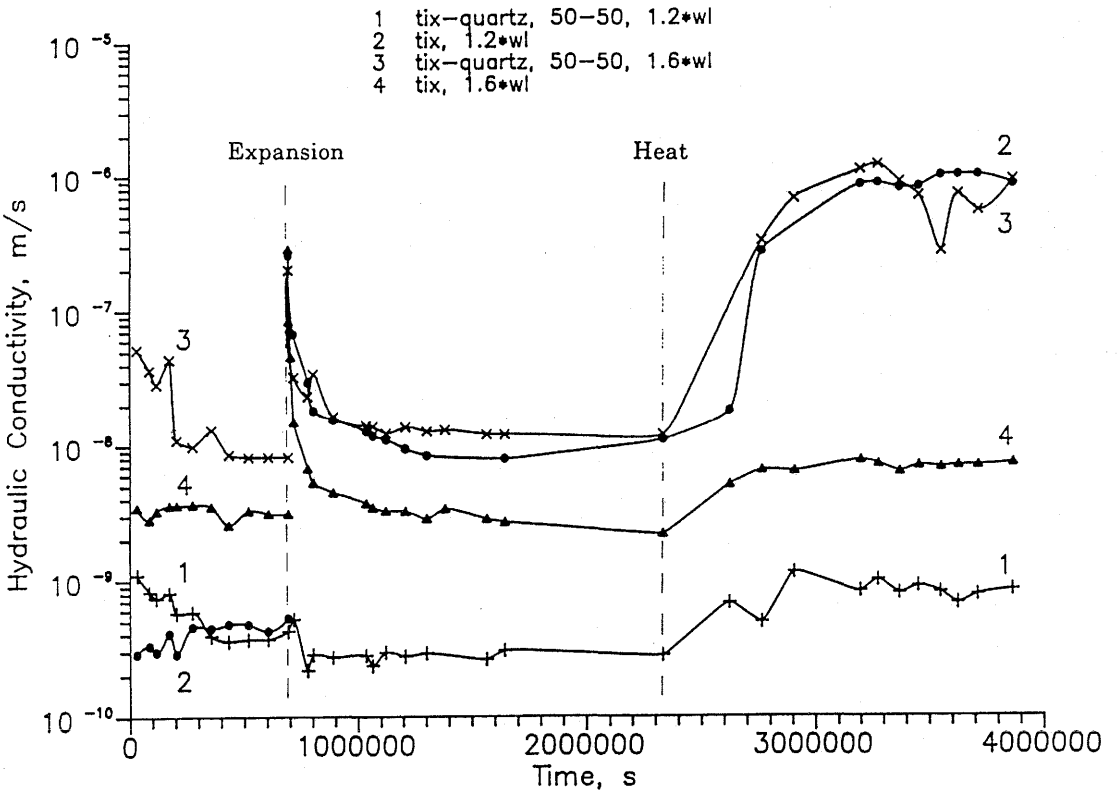

Fig IV:31. Hydraulic conductivity as a function of time

Results

As expected, the hydraulic conductivities during period I were about 10^{-8} m/s for the two gels (3 and 4) with a water ratio corresponding to $1.6 x w_L$, and 10^{-9} m/s for the $1.2 x w_L$ gels (1 and 2). The dropping permeabilities in the first days of gels no 1 and 3 containing quartz, are probably due to a reorganization of the smectite-quartz system (Fig IV:32).

Fig IV: 32. Smectite-quartz gel with reorganized quartz particles. Magnification 600 times

On expansion of the slots to 0.4 mm a large permeability increase took place in probe no 2, 3 and 4, due either to piping or more likely to a gap between the gels and the cones surfaces. The subsequent drop in permeability demonstrates that the self-sealing ability is considerable, even though there must be a low swelling capacity of these soft gels. In probe no 1 the gel was obviously stretched without loosing contact with the cone surfaces. The expanded volume implied that water was sucked up from both ends which explains the apparent drop in permeability.

The sealing function of gel no 2 was far from the initial even after recovery. At examination after the test one major piping channel was found (Fig IV:33). It was probably produced in conjunction with the expansion and it was never completely closed again.

Fig IV:33. Piping channel in smectite gel no 2. Magnification 34 times

A few days after the expansion the flow reached a steady state for all probes and no significant changes were observed for the remaining part of period II. When the heat was turned on, there was a permeability increase by about five times for gels no 1 and 4. This can be explained by the change in water viscosity and by heat-induced contraction of the montmorillonite stacks (Fig IV:34). The insignificant increase in permeability of gels no 2 and 3 is concluded to be due to the formation of major channels.

It appears from these tests that the density of the injected gel is the major determinant of the hydraulic conductivity of the undisturbed gels, while the bond strength becomes most important when the slot is rapidly expanded by as much as 30 percent.

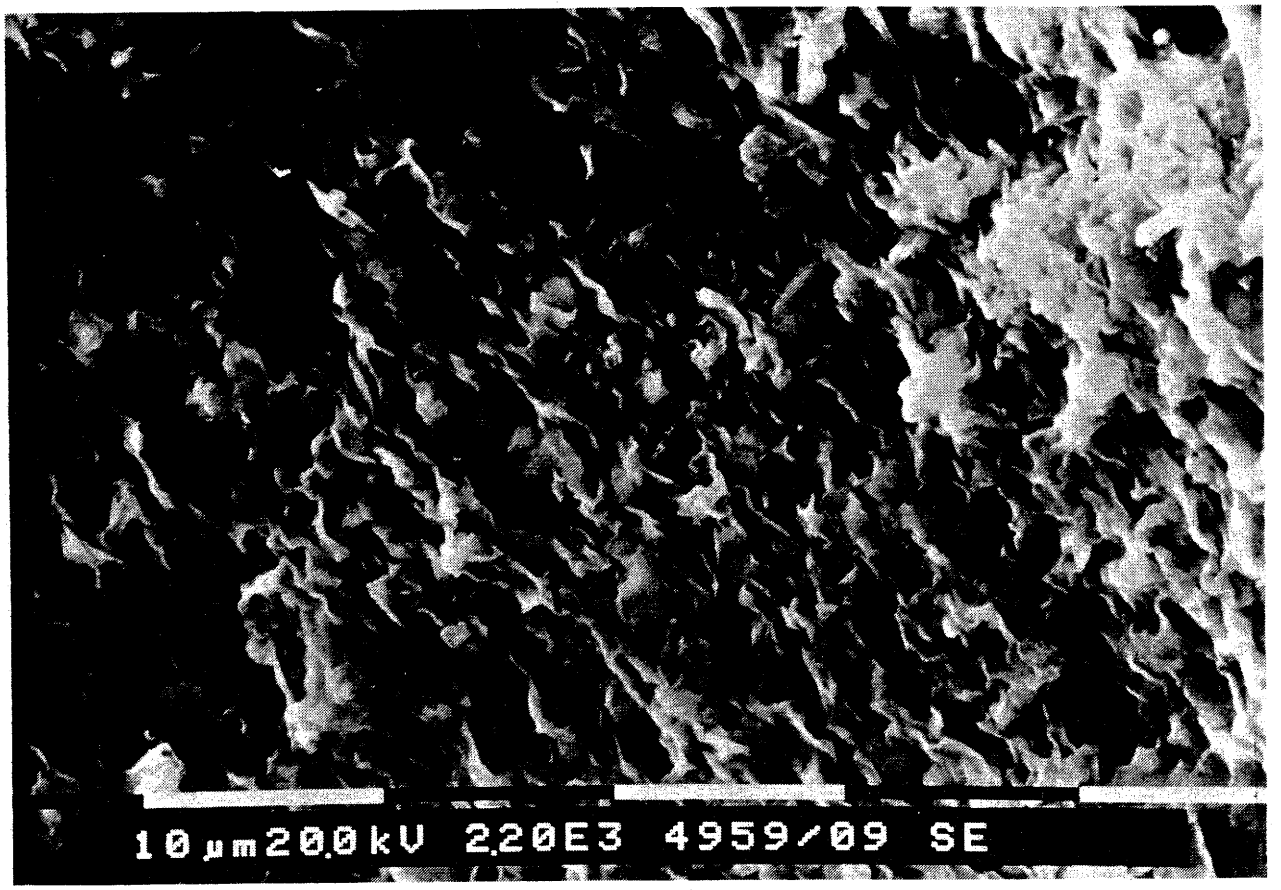

Fig IV: 34. Smectite network. Magnification 2200 times

Results - Cement cone-in-cone test

The grout consisted of 90 % Canadian cement and 10 % silica fume. w/c was 0.41, and 0.4 % superplasticizer was added to the de-aired distilled water. The grout was applied in the same way as the smectite gels. Hydration without water pressure was allowed for two weeks.

In this test the initial slot width was 1.0 mm. Very low permeability and still ongoing hydration made it impossible to evaluate the hydraulic conductivity for the initial phase with any accuracy.

To produce expansion the cone apparatus was placed in a press for displacing the inner cone so that the slot became expanded by 10 %. Constant water pressure (50 kPa) was applied on the inlet side and the flow-through continuously measured. After 20 days the temperature was step-wise raised from 20°C to 90°C during 2

days and the flow recorded for another 5 days (cf. Fig IV:35). After the test the cement sample was examined by use of optical microscopy and SEM.

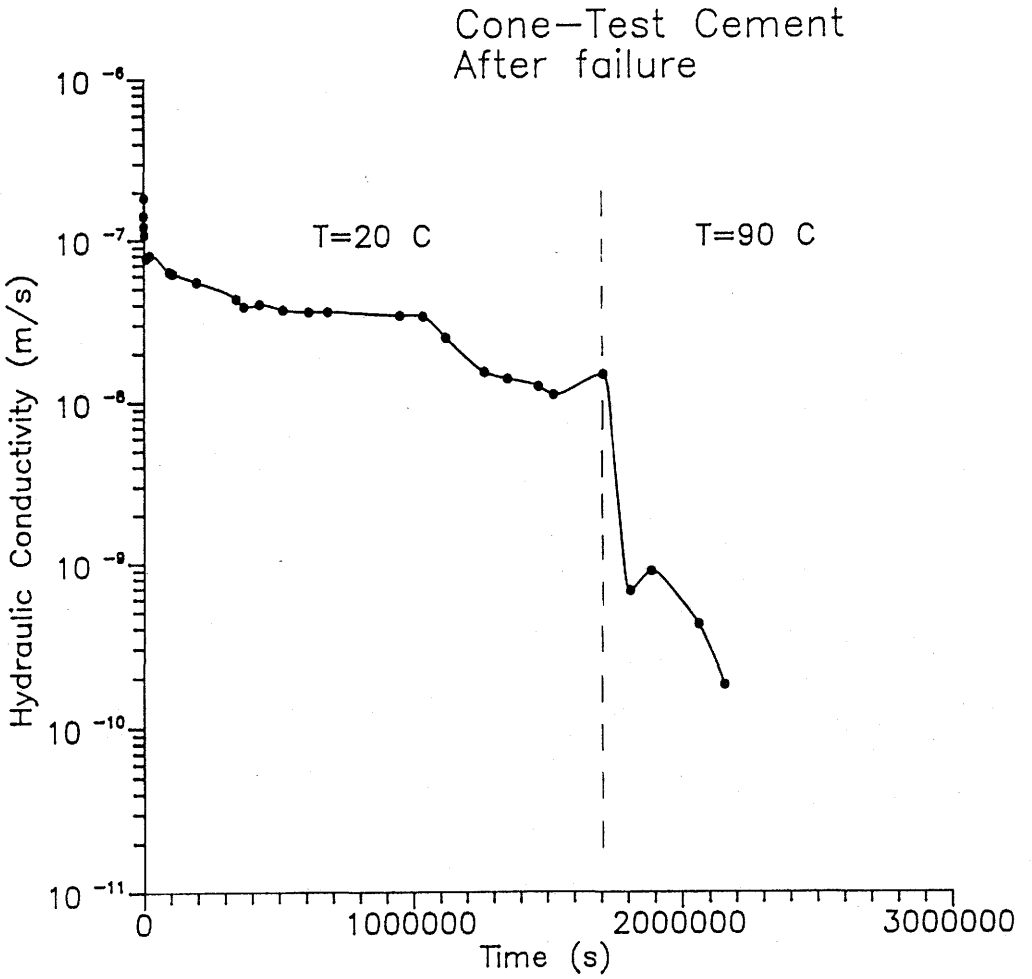

Fig IV:35. Change in hydraulic conductivity of the cement grout as a function of time and temperature

Results

The expansion of the slot created a gap between the inner cone and the cement sample. Micro-fractures at the inner cement surface indicated damage of the cement structure (Fig IV:36). The permeability was naturally high after the expansion ($2 \cdot 10^{-7}$ m/s) but decreased rapidly to $8 \cdot 10^{-8}$ m/s, probably due to reorganization of dispersed material. The drastic reduction in permeability when the probe was heated clearly shows that chemical reactions were initiated.

The SEM study showed that a porous precipitation had been formed in the gap caused by the expansion. This "superstructure" was mainly found at the water inlet side and the thickness corresponded to the 0.1 mm expansion (Fig IV:37). It is obvious that the self-sealing ability of this cement compund is mainly caused by

Fig IV:36. Fractures in the cement structure

such precipitations and that the hydration potential is considerable even at w/c ~0.4.

Preliminary conclusion, recommendations

The "cone-in-cone" equipment turned out to be of great value for conducting experiments of this sort, from which we conclude the hydraulic conductivity of clay grouts confined in fractures is not expected to exceed 10^{-5} to 10^{-6} m/s on moderate changes in aperture. Further investigations of both clay grouts and cement is strongly recommended.

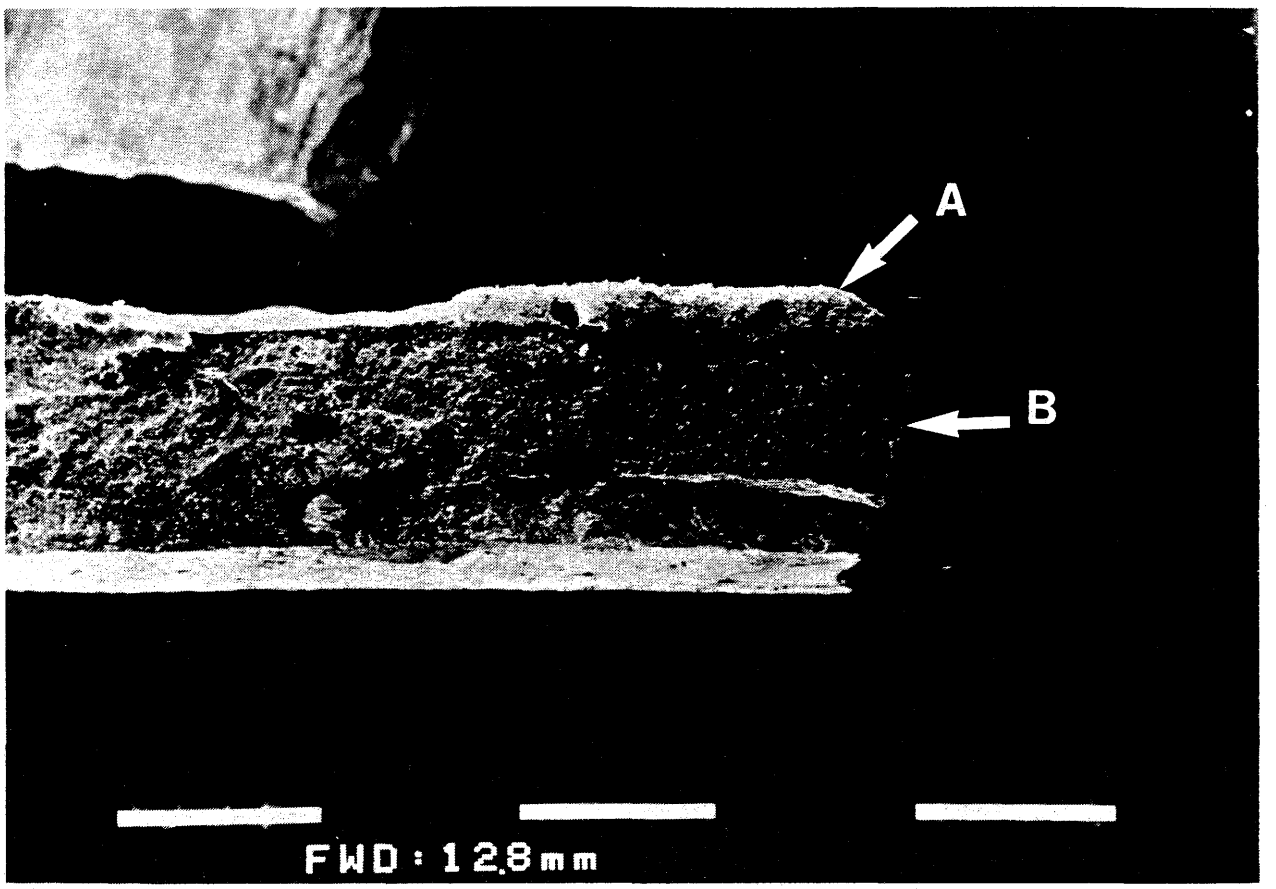

Fig IV:37. Precipitation (A) on the original cement surface (B). The precipitate filled the slot of the cone-in-cone apparatus completely

4.2 CEMENT

4.2.1 Current Views

Cement grouts are generated by mixing water with portland cement, often with additives to modify the properties. Portland cements are composed of:

tricalcium silicate	$3CaO{\cdot}SiO_2$	(alite) $3CaO{\cdot}SiO_2$
dicalcium silicate	$2CaO{\cdot}SiO_2$	(belite) $2CaO{\cdot}SiO_2$
tricalcium aluminate	$3CaO{\cdot}A1_2O_3$	$3CaO{\cdot}Al_2O_3$
tricalcium aluminaferrite	$4CaO{\cdot}A1_2O_3{\cdot}Fe_2O_3$	$4CaO\ Al_2O_3{\cdot}Fe_2O_3$
calcium oxide	CaO	
Calcium hydroxide	$Ca(OH)_2$	(portlandite) $Ca(OH)_2$
Calcium sulphate	$CaSO_4$	$CaSO_4$
Additives	various, depending on purpose	

The relative proportions of the different compounds varies with cement type. The compounds are hydrophyllic, i.e., they react readily with water. These reactions are exothermic and result in the formation of hydrated phases, mostly crypto-crystalline and amorphous hydrated calcium silicates (CSH). As the hydration reactions approach completion, a hardened, interconnected network composed predominantly of CSH results. The physical characteristics of the hardened cement product depend in part on: (1) the rise in temperature due to the heat generated by the hydration reactions; (2) the degree of hydration; and (3) the degree of interconnection of the CSH network. These factors also affect the chemical stability of the hardened product and the permeability of the hardened material, which is a function of the material's macro/micro porosity and the degree of micro-cracking/thermal strain induced during curing. Thus practically, the permeabilities, strength, and chemical stability of the final product may be adjusted by changing the details of the mix design, specifically, the proportions of

initial non-hydrated cement phases, the water/cement ratio (w/c), and the presence or absence of additives.

The reference grout mix design used for the Stripa Project includes amorphous silica in the form of silica fume as an additive. At the high pH's imposed by cement hydration silica fume reacts readily with the cement phases to form calcium silicate hydrates (CSH). The resulting hardened grout is generally more leach resistant in natural groundwater than a grout without silica fume added. Moreover, an excess of residual silica in the hardened grout may improve the long-term leach resistance of the grout. This would be the case if groundwater is saturated with respect to amorphous silica, which is more soluble than quartz. Groundwater associated with granite is usually saturated with respect to quartz. Thus, although there is no potential for dissolving additional SiO_2 from grout, silica fume in grout may not be chemically compatible with the host environment and some may dissolve. The calcium content of the groundwater may be chemically controlled to a certain extent also, e.g, by $CaCO_3$. Therefore, the potential for dissolution of CSH may be small. Hence, by design, the reference formulation has been optimized to resist leaching.

A concern related to the compatibility of the grout and the groundwater is the compatibility of the grout with the host rock. Of specific concern is the chemical behaviour at the grout-rock interface. Because water flow through grouted fractures is expected to occur primarily at the grout-rock interface, a chemical bond between the grout and the rock is advantageous. Since rock contains quartz and the cement grout is designed to react with available SiO_2, it is likely that some interfacial bonding is possible. Moreover, it is possible that such bonding can develop with time through some of the same mechanisms that cause mineralization in fractures where flow is restricted naturally (e.g., nucleation/growth and precipitation of supersaturated components). By designing the grout appropriately interfacial bonding can be enhanced. The degree of success that will be obtained by the mix nevertheless needs to be detailed. These details are needed to extend the results of short-term experiments to geologically significant durations. It should be noted that the effects of long-term leaching cannot be predicted accurately but can be bracketed. This is because the exact hydrologic nature of the system is unknown. In a fully open system (i.e., a freely flowing system) ultimately all the material will be dissolved and removed, even though this may require millions of years. In a totally closed system (i.e., static system), the material dissolves until the solubility limit of its phases is reached, secondary

phases may be precipitated, and chemical degradation ceases. In a totally closed system only a very small percentage of the material would be dissolved. Consequently, in order to predict the rate at which cement grout performance deteriorates, it is important to know the leach rate of the material. If this factor is known, then the degradation of the system can be predicted as a function of water flow rate.

The reference grout design incorporates materials such silica fume, sulfate resisting portland cement and superplasticizer which are expected to enhance longevity. However, mechanisms such as sulfate attack, $Ca(OH)_2$ leaching, carbonation and dissolution/alteration of CSH and CAH phases could still impact on long term grout performance.

Sulphate Attack

Attack on cement by sulphates can take place where the sulphate reacts with the $Ca(OH)_2$ and calcium aluminate hydrate. The mechanism of the sulphate attack on cement seems to proceed through a front of ettringite penetration.

$$C_3AH_6 + CS + 6H = C_3A{\cdot}CSH_{12}$$
monosulphate (65)

$$C_3A{\cdot}CSH_{12} + 2CS + 2\,O(H) = C_3A{\cdot}3(CS)\,H_{32} \quad (66)$$
ettringite

The calcium sulphate is a necessary intermediary in the reaction. Most groundwaters considered in various studies are approximately saturated with respect to gypsum (e.g., Canadian groundwater)and therefore the above attack on the hydrated aluminates is potentially serious. The most resistant cements are those with a low C_3A content and low permeability.

The reaction of cement with $MgSO_4$ is more aggressive than that of $CaSO_4$.This is mainly due to the low solubility of Mg(OH)2, which has a pH 10.5 for the solid $Mg(OH)_2/H_2O$ equilibrium. When the aqueous phases contains both Mg and SO_4 ions not only do the sulphate reactions considered above take place, but there is an additional attack of the CSH by the Mg ions. This destroys the CSH gel and precipites $Mg(OH)_2$. The sulphate attack can be reduced by the use of cement low in C_3A. This has been used in the reference grout.

$$CSH + Mg^2 = Ca^{2+} + Mg(OH)_2 + SiO_2 \quad (67)$$

$Ca(OH)_2$ Leaching

Calcium hydroxide (portlandite) leaching may be one of the processes likely to dominate cement grout degradation. When grout is exposed to water $Ca(OH)_2$ is leached. The free $Ca(OH)_2$ is first removed and then Ca is preferentially lost from CSH gel. The loss of Ca will result in a loss of cement strength. In dense grout the rate at which these processes proceed will depend on the rate of diffusion of Ca ions through the grout and/or of the water penetration through it. Pozzolanic silica fume and low w/c ratios as used in the reference grout should minimize $Ca(OH)_2$ leaching.

Carbonation

Carbonation describes the chemical and physical effects caused by reaction of carbon dioxide CO_2 or carbonate ions (CO_3^{2-} ,HCO_3^-) with components or the composite matrix of cementitious systems. Carbonation of cement will occur under many environmental conditions.

The literature contains abundant references to the effects of carbonation, particularly with reference to its effect on cement durability. However the mechanism of carbonation is far from being resolved. This is mainly because of the multitude of physical and chemical factors which may control the rate at which carbonation occurs and the nature of the carbonation products. Among the relevant factors are: w/c ratio, porosity, permeability of the matrix, the composition or constituents of the cement including the nature of additives, temperature and pressure of CO_2 during carbonation.

Cement paste subjected to carbonation loses water and behaves, dimensionally as though it has been dried to a much lower r.h. than that to which it is actually exposed. Carbonation shrinkage is irreversible and it is belived that CO_2 reacts with both calcium hydroxide and CSH. The latter reaction occurs with with concommitant loss of water following the equation:

$$C_m \cdot S \cdot H_m + xCO_2 \rightarrow x\,CaCO_3 + C_{n-x} \cdot S_{m-y} \cdot H_{m-y} + y\,H_2O \quad (68)$$

The decrease in C/S ratio in the CSH phase during this reaction is eventually brought to a halt by the limits of homogeneity of this phase, subsequent to which free silica begins to separate from the CSH. Thus, carbonation can be viewed as promoting changes in the CSH that occur in the presence of reactive SiO_2. Either spontaneous or previously induced carbonation of a cement matrix may protect it to some extent against acid attack. Limestone aggregate in concrete behaves similarly; it preferentially reacts with acid, thus sacrificially protecting the cement matrix. The benefit of carbonation may extend to sulphate waters, especially if the attack is produced under conditions of total immersion.

Persistance of CSH and CAH Phases

Portland cement grout is composed of phases which are thermodynamically metastable. Hydrated calcium silicates (CSH) phases such as hillebrandite, afwillite, foshagite, xonotlite, and tobormorite are all likely or possible principal grout phases. In addition hydrated calcium aluminates and calcium alumino-ferrites are possible as potential minor phases. The exact combination of phases that will be present in a given grout after curing is a function of the cement type employed, the overall chemistry of the grout, including additives, the w/c of the mix and the amount of heat produced by cement hydration. In addition, not all cement phases hydrate. For example, only the beta phase of C_2S hydrates appreciably. Thus, the cured grout is likely to contain residual unhydrated phases, as well as CSH and other hydrated products. These phases and the degree to which they fill space and interlock control the properties of the grout have been measured through performance tests described in preceding sections. However, the measured properties may only be considered initial properties that are subject to change with time as the metastable phases that comprise the grout revert toward a phase assemblage that reflects thermodynamic equilibrium. This condition is a minimum free energy state, and changes toward it can be considered to occur spontaneously without any external, physical, or chemical driving force being supplied. When these phase changes occur, the volumes occupied by the new phases will not necessarily be the same as those occupied by the materials they replace. These volume changes will give rise to variations in internal stresses and will probably lead to increased porosity. If porosity of the grout increases, it is likely that it will be largely connected porosity (e.g., microcracks) that will lead to increased permeability. This increased permeability will not necessarily lead to unacceptable performance by cement grout. For example, it is quite possible that cement grout can be engineered with a factor of safety

sufficient to accommodate the effects of metastable-stable phase transitions (i.e., a Ki (initial) of 10^{-14} m/s versus a performance based need of 10^{-9} m/sec). In addition, if the changes driven by equilibrium considerations occur sufficiently slowly, then it is possible that their effects will be negligible over the time frame of interest. For example, many millions of years may be required for phase changes and increased permeability to occur (diamond is not thermodynamically stable at the earth's surface; yet diamonds millions of years old can be found).

In summary the issues that relate to cement phase stability and its affect on grout performance are:

- What is the approximate initial phase composition of a given cement grout and what is the associated stable assemblage? Answering this question will provide the starting point for assessing if the changes are of potential consequence to cement grout performance.

- What is the volume change/stress induced by the alteration of metastable phases to stable phases? Answering this question will permit calculating and distributing the measured porosity, and modeling the expected permeability increases that might occur if all transitions were to occur simultaneously.

- Is the increased permeability that might arise still low enough to warrant acceptable performance by the cement grout? Answering this question may obviate the next issue, and may remove concern about the thermodynamically metastable phases comprising cement grout.

- Do the changes occur at such a slow rate that they are insignificant to cement grout performance in a repository application? The relevance of the question is similar to that above.

The remainder of this section presents preliminary results from the laboratory and theoretical investigation addressing these issues.

4.2.2 Cement Grout Longevity-Laboratory Studies

The laboratory studies were directed to determine the following the mechanistic function of Na-sulphonated naphthalene formaldehyde condensate superplasti-

cizer (Na-SNF) in fresh cement pastes: the form and place of the residence of the superplasticizer in hardened pastes; the influence of the superplasticizer on the cement leaching processes: and, the general leaching properties of selected cement based grouts. The majority of the tests were carried out on the reference grout (Table 10). For comparison, a smaller number of tests were carried out on MC-500. This is a slag-cement product, specially formulated and sized to serve as an alternate to chemical grouts it is gaining increasing use in engineering practice. To facilitate comparisons, the grouts were generally mixed at equiviscous water contents. These tended to be higher for MC-500 than for the reference grout.

Table 10. The composition and selected properties of the reference cement grout

Mix	
Cement	90% Type 50, 10% Silica Fume to be mixed by dry mass. Cement reground to Blaine Fineness of 600 m^2/kg.
w/c	0.4 to 0.6, to be kept as low as possible
Superplasticizer	Disal, Na-sulphonated naphthalene formaldehyde. Content to be kept as low as possible, >1.5%
Properties	
Viscosity	As desired with w/c and Disal content
Setting time	Initial: varies with T, 10 - 16 h Final : varies with T, 12 - 20 h
Strength	Varies with w/c, t and T, 20 - HPa at 28 days
k	Less than 10^{-12} m/s

4.2.2.1 Superplasticized Adsorption In Unset Grouts

A systematic investigation of the adsorption of Ne-SNF superplasticized in unset grout paste was undertaken. The rate of adsorption of the superplasticized has been determined as a function of: superplasticized content, water/cement ratio and silica fume content.

Material and Methods

The pore water present in mixtures of Type 50 (sulphate resistant portland cement - SRPC), silica fume, Na-SNF and water was extracted using the specially designed and fabricated device shown in Fig IV:38. Mixtures containing zero and 10 per cent silica fume and 0.5 to 1.5 per cent Na-SNF with w/c ranging from 0.3 to 0.6 were investigated. The pore water was extracted from unset grout pastes at different times after mixing. The organic contents of the pore water were quantitatively analysed using calibrated UV-spectrophotometry.

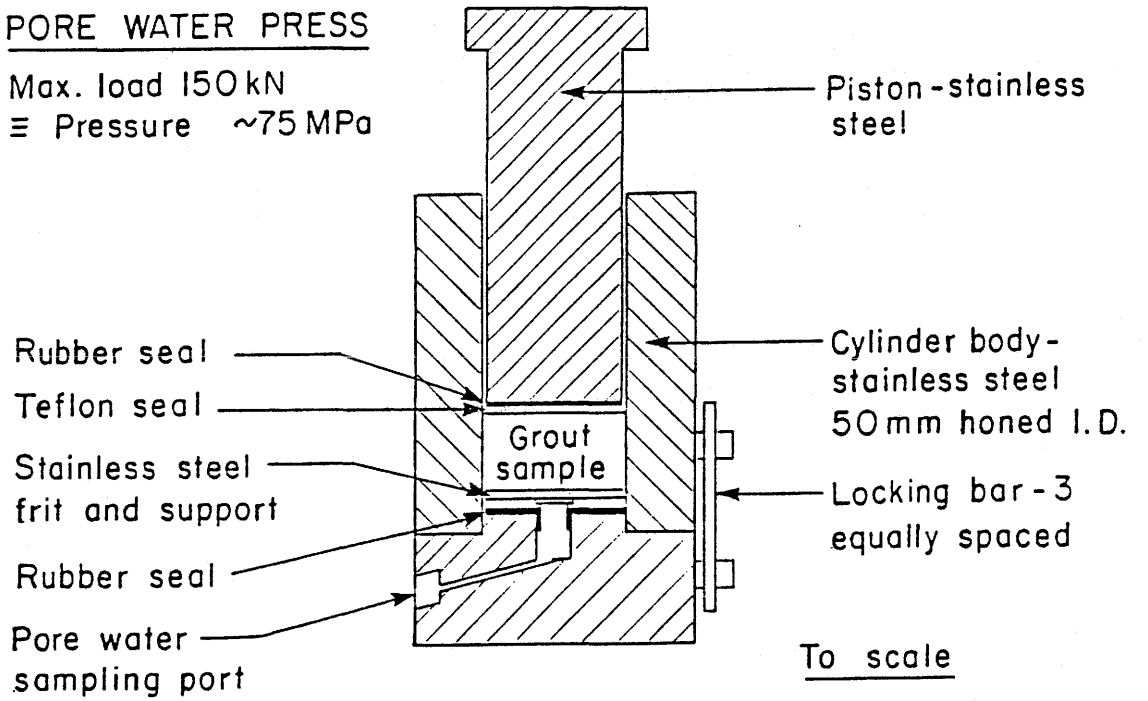

Fig IV:38. Pore Water Extractor

Results

The data from these tests, shown in Fig IV:39, indicate the following:

(a) Adding 10% silica fume increases the quantity of Na-SNF adsorbed. This is probably related to the increased specific surface area of the grout. Silica fume has a specific surface are of approximately 20,000 m^2/kg, which is 20 to 30 times greater than that of the cement. The increases in the quantities of Na-SNF adsorbed caused by admixing silica fume are less than proportional to the corresponding increase in specific surface area.

(b) Increasing the quantity of Na-SNF will increase the quantity adsorbed before the grout finally sets and begins to harden. The grout adsorbs less than the total quantity added. There is always Na-SNF in the free, extractable pore water.

(c) At Na-SNF contents greater than 0.5%, increasing the w/c from 0.3 to 0.6 tends to increase the quantity of Na-SNF absorbed. In this respect it is noted that, for clarity, the data for 1% superplasticizer are not shown on the Figure for w/c = 0.3. These were similar to those for Na-SNF% = 1.5.

(d) The quantity of Na-SNF adsorbed tends to increase with time after mixing except for Na-SNF% = 0.5, where w/c also has little effect. Time has greater influence on adsorption at lower w/c.

From observation a) it can be suggested that the cement preferentially adsorbs the Na-SNF. Observation b) indicates that, in hardened grouts, the capillary pore space could contain readily leachable Na-SNF; the quantity of leachable super-lasticizer should decrease with increasing degree of cement hydration. From c) and d) it can be suggested that the distribution of Na-SNF in the grout, and it's availability for adsorption on, and/or reac- tion with, the grout improves with w/c. It is recalled that a w/c < 0.3 is required to theoretically stoichiometrically satisfy the hydration reactions. However, the data indicate that merely mixing the materials in appropriate proportions is not sufficient to complete the cement hydration. Subsequent migration of the water and the superplasticizer completes the hydration processes. The phases present in the systems depend on the inti-macy of the mix, which, in turn, depends on w/c. Therefore, thermodynamic

studies in mixtures with low w/c, such as those that are of interest to this study, are unlikely to conclusive regarding grout longevity.

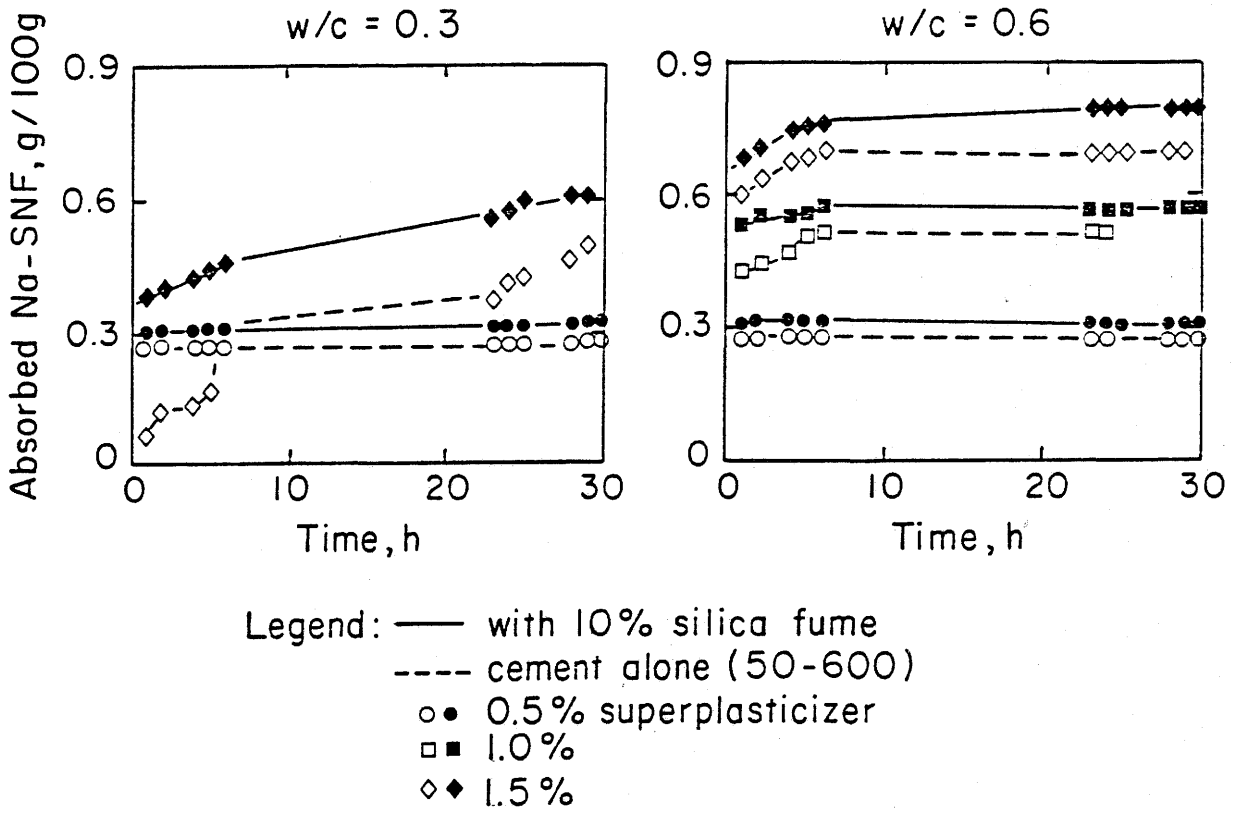

Fig IV:39. Influence of w/c, Superplasticizer Content, Silica Fume Addition and Time on the Quantity of Na-SNF Absorbed by Fresh Grout

4.2.2.2 Superplasticizer Adsorption in and Leaching from Hardened Grouts

Studies were undertaken to identify the cement phases on which the Na-SNF is adsorbed and to determined, the effect of temperature, surface area to volume ratio and groundwater composition on the superplasticizer leach rate.

Adsorption Studies in Hardened Cement

Presently nothing is known on the form in which superplasticizer molecules are present in the hardened Portland cement paste. Are they trapped in silicate

hydrate or aluminate hydrates? These studies were intended to begin to clarify this issue.

Test Method

The studies required the preparation of a labelled superplasticizer, the introduction of this material to the grout and, after hardening, microscopic examination of type grout. Preliminary examinations indicated that development of special techniques was required to permit success in this study. These have been developed and the phases on which the Na-SNF resides in hardened pastes have been broadly identified.

Na-SNF superplasticizer was labelled with ^{35}S. A special batch of superplasticizer containing this beta ray emitter was prepared by introducing sulphuric acid containing the isotope during the sulphonation step of the superplasticizer preparation. This is shown diagrammatically in Fig IV:40. Reference grout mixtures containing up to 3% of the marked superplasticizer were prepared and cured for 7 days at 10°C. Electron-microautoradiography combined with SEM and EDX were used to identify the cement phases containing the labelled material.

High resolution silver emulsions (KODAK NTE) were applied directly to gold coated, SEM grout specimens containing the ^{35}S. After 700 h exposure, the emulsions were developed "in-situ". After development, the beta exposed silver grains remained on the surface of the SEM specimen. Unexposed silver was removed. The specimen was then examined by SEM and EDX to locate the silver grains which indirectly identified the Na-SNF locations.

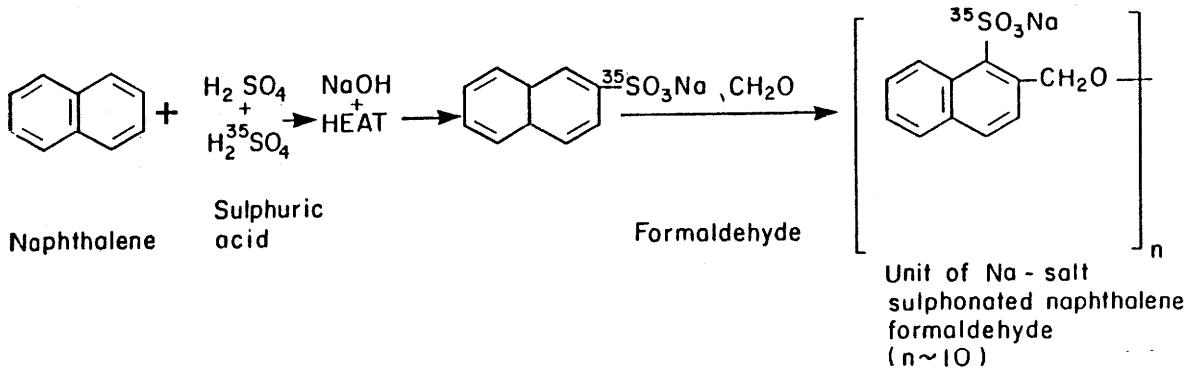

Fig IV:40. Preparation of the Labelled Superplasticizer

Results

Typical scanning electron micrographs and associated EDX analyses for a specimen containing 3% Na-SNF mixed at a w/c of 0.2 are presented in Fig IV:41. The bright spots indicate the silver grains. The analyses indicate that the silver resides on phases rich in Calcium (spectra b_2) and phases containing Al, Ca, Sl and Fe (spectra d). No silver grains could be detected on the Sl rich areas (spectra g_1). The following mechanisms of adsorption can now be suggested: the super-platicizer is directly incorporated into the Calcium rich phases of C-S-H through association with the hydration water; and, the SO_3^- in each monomer of the superplasticizer reacts directly with the C-A-H phases. These suggestions require further investigation.

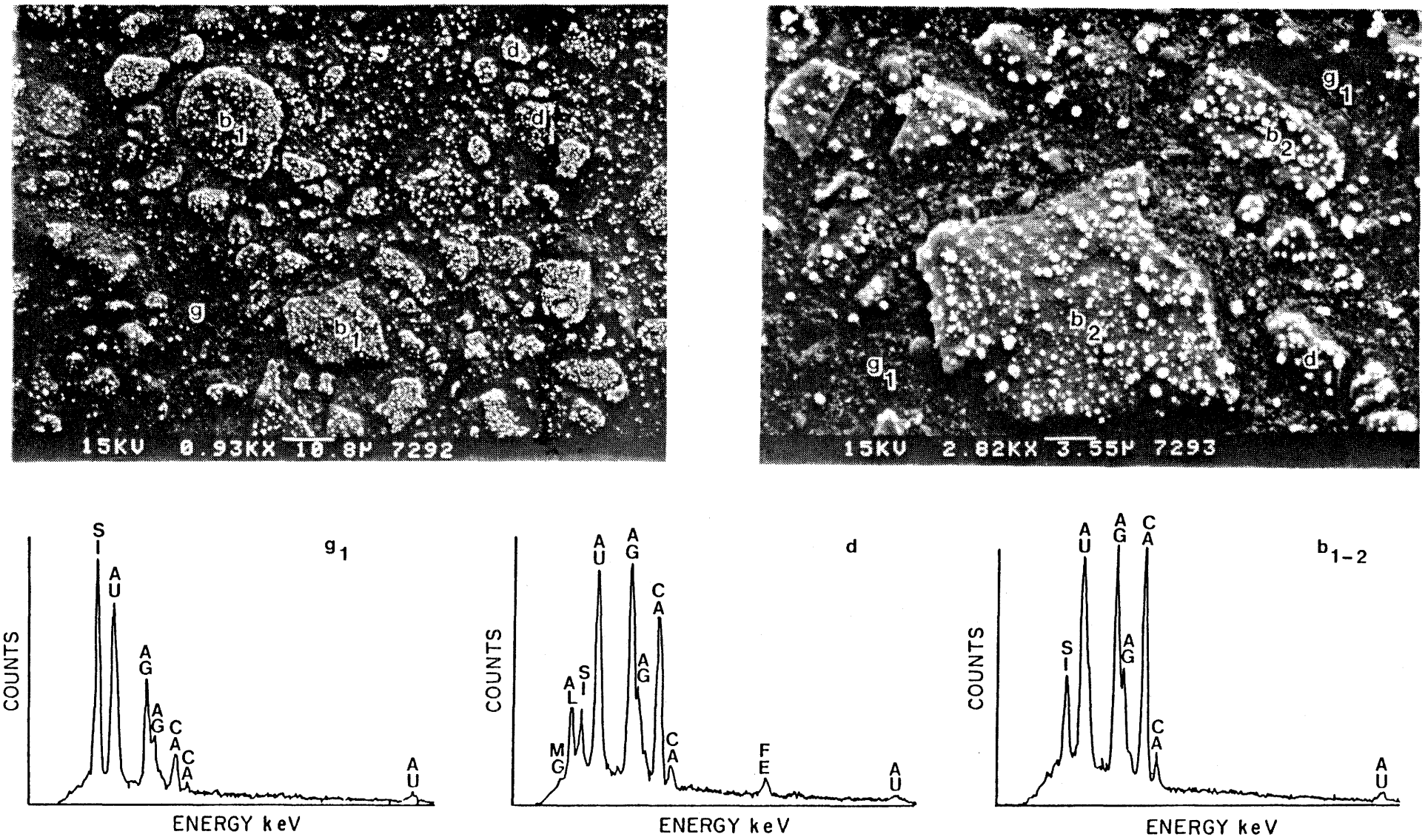

Fig IV:41 Electron Micrographs and EDX Spectra of Polished Surfaces of the Reference Grout at w/c = 0.2, with 10 % Silica Fume and 3 % ^{35}S Labelled Na-SNF

Superplasticizer Leaching Studiese

Hardened grouts containing the labelled superplasticizer prepared as described above were subjected to static leach tests. The test series were statistically designed to investigate the effect of temperature, surface areas to volume ratio and water salinity on superplasticizer leach rate.

Test Method

The experiments were designed on the basis of the Box-Behnken approach. The temperature (x_1), ionic strength of the groundwater (x_2) and the surface area to volume ratio (x_3) were selected as the independent variables.

The dependent variable was superplasticizer leach rate. The ranges of the independent variables were:

temperature (x_1)	$25°C < (x_1) < 85°$
ionic strength (x_2)	10^{-4} M $< (x_2) <$ 1.5 M
SA/V (x_3)	$0.05 < (x_3) < 0.2$

The leachants used in these experiments included: Granitic Groundwater (GGW), standard Canadian Shield Saline Solution (SCSSS) and Whiteshell Nuclear-1 (WN-1). The chemical composition of the groundwaters is presented in Table 11. The release of superplasticizer into solution was determined by monitoring the release of ^{35}S into solution by using the Liquid Scintillation Counting technique.*

Results

Preliminary analyses from these tests have concentrated on the effect of leachant volume to surface area ratio and temperature on the release of superplasticizer. Results from tests carried out with WN-1 groundwater have been examined first

---

* Packard 2000 CA/LL Liquid Scintilation Counter

Table 11. Nominal composition of groundwaters in mg/L

	GGW(*)	WN-1(*)	SCSSS(*)
Na	8.3	1,910	5,050
K	3.5	14	50
Mg	3.9	61	200
Ca	13.0	2,130	15,000
Sr	-	24	20
Fe	-	0.56	-
Si	-	-	15
HCO_3	n.d.	68	10
Cl	5.0	6,460	34,260
SO_4	8.6	1,040	790
NO_3	0.62	33.0	50
F	0.19	-	-
pH	6.5±0.5	7.0±0.5	7.0±0.5
TDS [kg·L-1]	1.0x10-4	1.3x10-2	7.0x10-2
I	1.4x10-3	0.27	1.37

(*) GGW: Granite Groundwater
WN-1: Brine based on preliminary analysis from drillhole WN-1 at Whiteshell Nuclear Research Establishment

SCSSS: Standard Canadian Shield Saline Solution based on known incidence of saline waters in the Shield

since this groundwater is commonly found in natural fractures in granitic rock at a depth of ~500m. Fig IV:42 presents the cumulated fraction release (CFR) of ^{35}S from the reference grout mixed at low w/c (0.2 and 0.4) with 3% Na-SNF super plasticizer. The data clearly show that the superplasticizer can be leached from

the grouts, however, the cumulated release quantities are very small ($\sim 10^{-7} kg/m^2$). These findings tend to confirm those from the adsorption studies on unset pastes. The small quantities of Na-SNF released in solutions are probably derived from the capillary pore space of the hardened grout. Moreover, it is likely that the cement contains many occluded pores from which the Na-SNF cannot be released.

The quantities of released superplasticizer are significantly increased by the increase in temperature. It can reasonably be assumed that by increasing temperature the leachability of grout have increased (from the evidence of the static leach tests data, see Section 4.2.5). Hence, the increase in leachability of the grout will result in an increase in the number of pores which are accessible to leaching solution. Unexpectedly higher releases of superplasticizer were obtained in the leach tests carried out with the reference grout mixed at low w/c (0.2) than these from leach tests carried out with the grout mixed at higher w/c (0.4). This may suggest that in the cements with low water content, the adsorption sites available for superplasticizers are limited due to a poor mixing (poor distribution of superplasticizer in cement).

4.2.2.3 General Leaching Studies

Static and dynamic leaching tests were carried out

The static leach tests were conducted on MC-500, the reference grout and a sulphate resisting portland cement. The Box-Benkhen statistical design approach was used for each of the test series: the influence of temperature, groundwater salinity and clay type on the rate of leaching of important elements from each of the cements was investigated.

Dynamic leaching of the grouts was investigated through chemical analysis of the leachates emanating from specimens during tests to determine their hydraulic conductivities.

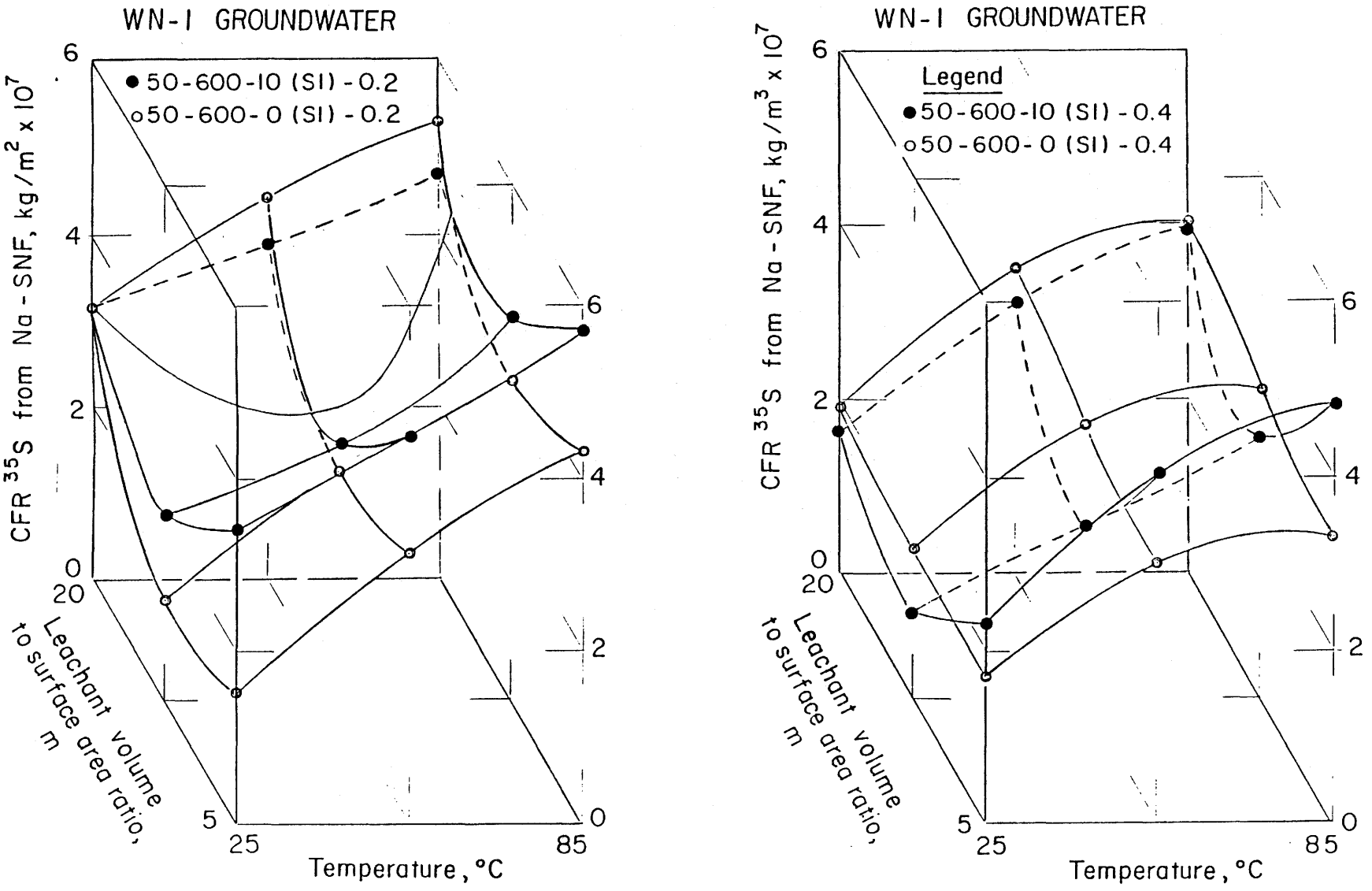

Fig IV:42 Cumulated Fraction Release of ^{35}S from Reference Grout

Hydraulic Conductivity and Dynamic Leaching

Material and Methods

The hydraulic conductivities of intact granite rock, hardened MC-500 and SRPC-based grouts and grouted fractured granite rock were determined in radial flow hydraulic conductivity cells at hydraulic gradients of up to 8000. The hollow cylindrical specimens were 100 mm long with an annular thickness of 25 mm. Flow was radially outwards. These tests, which used distilled deionized water as the leachant, were carried out at approximately 25°C. The influence of granite on the leaching processes were investigated.

Results

The hydraulic conductivity of the granite was measured to be approximately 10^{-12} m/s. The hydraulic conductivity (k) of the grouts tended to decrease with time, w/c and silica fume content and for the reference grout was less than 10^{-14} m/s after 28 days. Fig IV:43 shows the k-t relationships for MC-500-0-1.1, 50-450-0-0.4 and for fractured rock grouted with these materials. The grouted fracture was approximately 1 mm thick (rock to cement volume ratio of approximately 100). The data show that successful injection of either of the two grouts will reduce the k for fractured granite to that of the intact rock.

The pH of the leachate from the grout specimens varied from 11.5 to 11.9 for both the MC-500 and the reference grout. The leachant from SRPC grout alone was higher (12.4). The leachate from the granite maintained a pH of 7.2. From tests on fractured rock grouted with MC-500 and the reference grout, Fig IV:44 shows the variations in leachate pH with grouted fracture aperture. With apertures less than approximately 0.5 mm (rock to grout volume ratios greater than approximately 200) the leachate pH is similar to that of the leachate from the intact rock specimens. With grouted apertures wider than 1 mm, pH is increased to that of the leachate from the grout specimens.

Ion concentrations in the leachates from intact granite, the reference grout and grouted granite specimens are presented in Table 12. The following observations can be made from the data: for grouts alone the silica fume does not significantly change the quantities of Ca^{2+} released from the grout, the quantities of released Ca^{2+} are significantly decreased by the presence of granite; the quantities of Na

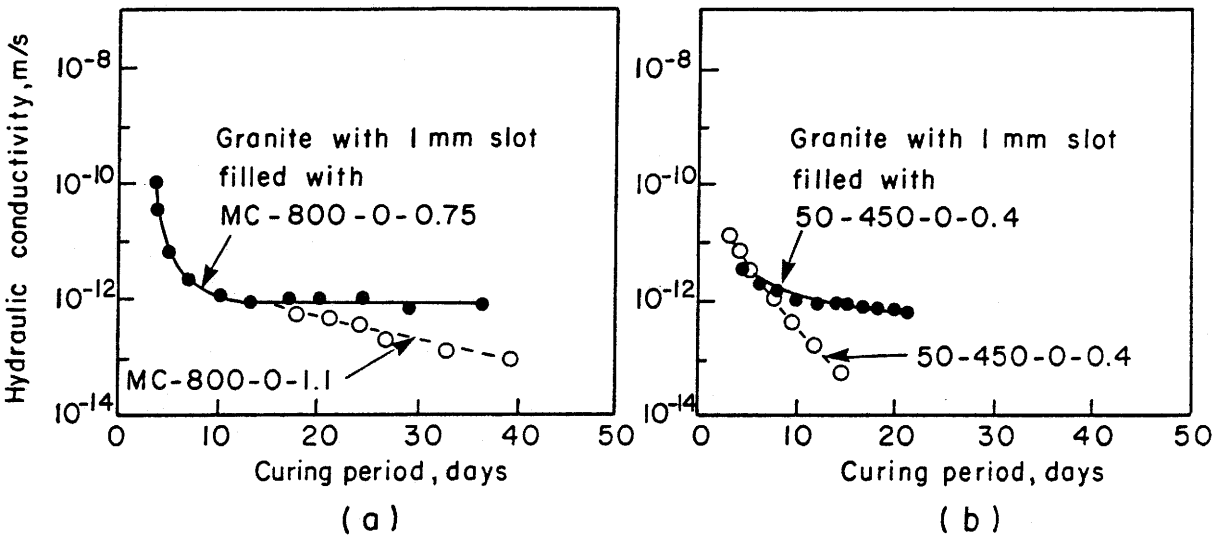

Fig IV:43 Hydraulic Conductivity - Time Relationships for Granite with Cement Filled Slots Compared with Those for Cement Along: a) MC-500; b) Sulphate Resisting Portland Cement

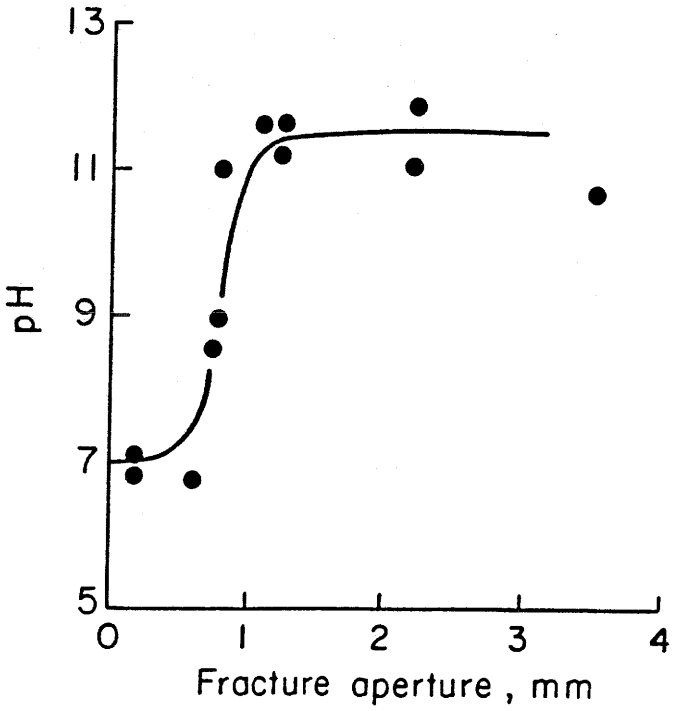

Fig IV:44 Influence of Grouted Fracture Aperture on pH of Leachate from Grouted Specimens

and SO_4^{2-} released are significantly increased when superplasticizer is included in the grout; and, the total quantities of released ions are significantly less than those naturally present in brackish or saline granitic groundwaters. The observations confirm that some of the superplasticizer remains free for extraction from the grouts by permeating groundwaters. Moreover, coupled with the pH data, the leachate analyses suggest that, globally, the granite will buffer the effects of cement grouts on the groundwater. The cement grouts may cause local perturbations in the ionic concentrations and pH of the groundwater. The perturbations are likely to be small in comparison to the natural variations in the groundwater.

Table 12. Ionic concentrations in leachates from permeater tests

Specimen	Ion Conc. in Leachate (mg/L)						pH
	Ca	Na	Mg	K	Si	SO_2	
Granite	10	5	0.1	5	2	8	7.2
Grout alone:							
50-350-10-4	400	400	0.01	800	6	20	11.5
50-350-10S-4	500	2000	0.1	2000	10	90	11.9
Grouted granite							
50-350-0-.4	200	40	0.1	50	7	20	11.2
50-350-10S-.4	20	700	0.5	10	10	90	15.5

Leachant - Distilled deionized water

Static Leach Tests

Materials and Methods

The leach rates of the reference grout were determined "under static conditions". For comparison, a smaller number of leach tests were carried out on MC-500.

The corrosion performance of grouts is being determined by measuring the leach rates of Ca^2, K^2, Si^{4+}, Al^{3+}, Na^+, Mg^{2+} and SO_4^{2-} with time from specimens of hardened grout pastes. The tests are conducted by immersing grout specimens in groundwater held within autoclaves from which aliquots can periodically be

removed for analysis. At each sampling, the autoclave is recharged with the original groundwater used. Hence the tests are not strictly static. The test conditions are probably more severe than truly static ones. The ultimate purpose is to define leach rate for each cement type as a function of temperature (x_1), groundwater ionic strength (x_2) and clay type present (x_3). The range of values tested for the independent variables are:

Temperature (x_1)	25°C < (x_1)	< 150°C
Water ionic strength (x_2)	10^{-4}M < (x_2)	< 1.4 M
C.E.C. of clay (x_3)	No clay < (x_3)	< 800 meg/kg

Preliminary analyses from the tests have concentrated on the effects of temperature and groundwater ionic strength on leach rates. Results from tests carried out with illicit clay in the groundwater have been examined first since these clays are commonly found in natural fractures in granite.

Results

Fig IV:45 presents the cumulated fractional release (CFR) of silicon from MC-500 and the reference grout mix at low w/c (0.4 to 0.5). The CFR of Si from each of the cements are similar and increase with groundwater ionic strength. Similar functional relationships are observed at high w/c (0.6 to 0.7). However, the CFR was approximately 10 times lower at the higher w/c. This is contrary to expectations since increasing w/c should increase capillary porosity and hence, increase the cement surface area available for reaction with the groundwater. It is speculated that the result may be linked to improved mixing and higher degrees of cement hydration at the higher w/c. Further analyses are required to explain the data.

Fig IV:46 presents the CFR for Ca from MC-500 and the reference grout at low (0.4 to 0.5) and the high (0.6 to 0.7) w/c. Over the range of w/c investigated, for the reference grout the CFR for Ca is virtually stable, tending to marginally increase with temperature when leached with waters of high ionic concentration and salinity. For MC-500 the CFR for Ca exhibits a marked increase with increasing temperature. This is particularly pronounced when the material is leached with waters of high ionic concentrations and salinity. Moreover, in the most extreme conditions (highest temperature and groundwater strength), the MC-500

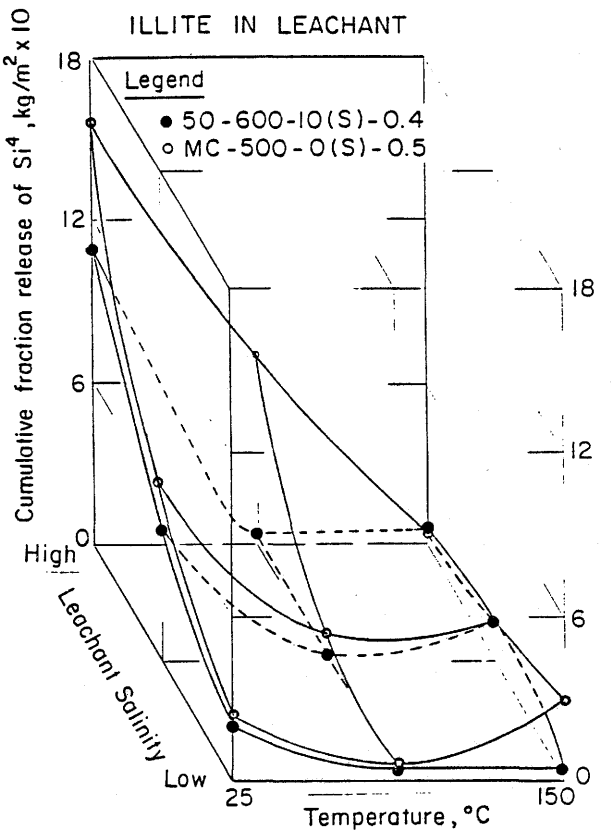

Fig IV:45 Release of Si from the reference grout and MC-500

releases Ca at approximately 6 times the rate of the reference grout. Results from SRPC grout alone (not shown) indicate released Ca quantities that are similar in magnitude and functional dependence to those the reference grout. This preliminary analysis suggests that longevity of the MC-500 may be less than that of the reference grout. It is noted that neither for the reference grout nor for the MC-500 does w/c significantly influence Ca release.

The CFR data presented in Figs IV:45 and IV:46 are the values of CFR at a time of 56 days. An analysis of the CFR-time release curves generated from the tests indicated that at this time after starting the tests the CFR for most ions became virtually constant. However, in attaining this constant value, depending on the test conditions, CFR could increment positively and negatively with the time step (i.e. material could be either dissolved into the solution or precipitated from it). Further analysis of the individual CFR-time relationships and coupling of these relationships is required to clarify the mechanisms controlling grout longevity.

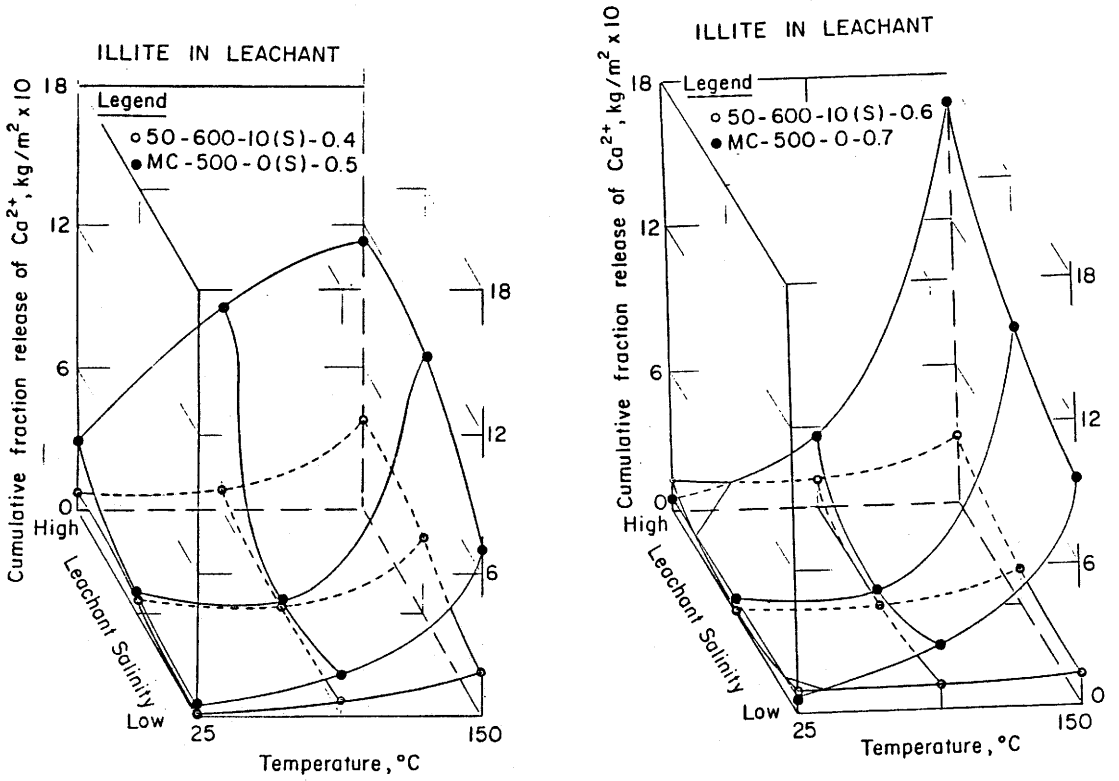

Fig IV:46 Release of Ca from the reference grout and MC-500

4.2.2.4 Conclusions

Based on the available preliminary data and analyses, the following conclusions are tentatively drawn:

- By influencing the degree of homogeneity of the grout the w/c influences the proportion of superplasticizer adsorbed and may influence grout longevity. The most durable grout may not necessarily have the lowest possible water content.

- Due to mixing effects and diffusion processes in the grout, thermodynamic studies are unlikely to be absolutely conclusive regarding grout longevity.

- The microautoradiographic method using ^{35}S labelled material is appropriate for identifying the cement phases which preferentially adsorb Na-SNF superplasticizer.

- In hardened grouts, the major portion of the superplasticizer is directly incorporated into the calcium rich phases of C-S-H through association with the hydration water: the superplasticizer is also involved with reaction with the C-A-H phases. Some of the superplasticizer remains in capillary pores.

- Superplasticizer can be leached in small quantities from the hardened grout. The released quantities are probably derived from the capillary porosity of the hardened grout.

- Successful injection of either MC-500 or the reference grout will reduce the hydraulic conductivity of fractured granite to that of the intact rock.

- The granite is likely to buffer the effects of cement grouts in the groundwater. Local perturbations in the ionic concentrations and pH of the groundwater associated with the presence of the grout are likely to be less than the natural variations.

- The reference grout is probably more durable than MC-500

4.2.3 Thermodynamic analysis and modeling

4.2.3.1 Purpose of the Investigation

The primary purpose of this investigation was to assess the usefulness of geochemical principles and computer modelling techniques in predicting longterm performance of cement grout. More specifically, the techniques were used to better understand the possible kinds of alteration of the seal material, including alteration due to interaction with ground water, and the effects of the alteration on the hydrologic properties of the seal. A secondary purpose of this investigation was to begin consideration of the role of reaction kinetics in favoring or inhibiting cement alteration, which is critical to the assessment of seal longevity.

4.2.3.2 Approaches to the Investigation

The question of the geochemical stability of cement grouts was addressed using two distinctly different approaches. These two approaches were designed so that mechanisms with potential for causing decreased performance can be compared and prioritized and so that potential changes in performance can be qualitatively determined. The two mechanisms of chief concerns are: (1) solid-solid cement phase transitions to denser products that the original cured assemblage with resulting increase in porosity/permeability, and (2) dissolution of portland cement phases with concomitant increase in porosity/permeability. An assumption common to both is that with time, progressive dehydration of the hydrated cement phases will result in recrystallization of CSH gel to more thermodynamically stable forms.

Approach 1

In the first approach, solid-solid reactions were written assuming a closed ("isochemical") system to test the feasibility of a "hand calculation" approach to investigating the simplified, six component portland cement system (CaO, SO_3, Al_2O_3, H_2O, SiO_2, and O_2. The results also aid in estimating the ultimate effect on performance of an approach to thermodynamic equilibrium by cement phases.

In this analysis, water released from the starting phases was assumed to become free (pore) water and not become incorporated into the solid reaction products.

This assumption is highly conservative and, since the primary phases are hydrous (i.e., increased porosity) and most of the reaction products are not, results in negative volume changes for solid-solid reactions. In addition, the absence of Fe, Mg, Na, and K in this idealized system adds to the conservatism by precluding the presence in the reaction products of many clays and zeolites. Clays and zeolites have large molar volumes and if they were generated as reaction products, the calculated results would have lower final porosities and permeabilities.

Tobermorite, ettringite, and hydrogarnet were assumed to be the primary phases in hydrated cement. Tobermorite is thought to be an important constituent in CSH gel of hydrated portland cement. X-ray diffraction patters of CSH gel often show weak tobermorite reflections, indicating its presence in crypto-crystalline form. In addition, tobermorite crystals in close association with the CSH gel have been observed in SEM photomicrographs (Taylor, 1964). Sarkar, et al. (1982), in a derivation based on thermodynamic considerations, suggest that excess silica added to cement, as in pozzolanic portland cement, reacts with $Ca(OH)_2$ to form additional tobermorite during hydration. Therefore, the assumption that tobermorite is an abundant phase in hydrated cement is reasonable. Ettringite is commonly formed during hydration of C_3A. Using the three phases described above, a normative model of a generic Type V portland cement was constructed. Components were partitioned into the assumed phases in the following manner:

- 33 tobermorite
- 1 ettringite
- 2 hydrogarnet

The result is a simplified thermodynamic model of cryptocrystalline portland cement. Theoretical reactions were then calculated and constrained by the phases/ proportions in the model. Results were analyzed to identify plausible phase assemblages and consequent porosity increases using tabulated thermodynamic data. Specifically, on the basis of tabulated thermodynamic data, approximately 30 additional phases appear to be possible and reasonable products of cement alteration in the simplified system. All of the possible reactions involving these solid phases were determined, for an assumed temperature of 25°C. The changes in Gibbs free energy of the reactions (ΔG_r), and the changes in volume of the solid phases taking part in the reactions (ΔV_r), were calculated from the thermodynamic data. ΔG_r is a measure of how favoured, on a thermodynamic basis, a reaction is: the more negative the ΔG_r, the more favoured the reaction. The reactions with

the most negative ΔG_r were noted and evaluated, using best geochemical judgment, as to the likelihood of their occurring. The ΔV_r of these reactions was used for estimating changes in porosity and hydraulic conductivity in a grout for reactions of this sort. Results of these calculations are presented in Section 4.2.3.3 of this report.

In summary: Approach 1 is intended to delineate the maximum increase in porosity/permeability that would arise from thermodynamically driven changes in the mineralogic make-up of portland cement. In this approach, it is assumed that a cryptocrystalline solid (cement gel) approximates the thermodynamic behavior of a calculated macrocrystalline solid phase assemblage. The approach is highly conservative because:

- Time is not a factor, i.e., in spite of the observed persistence of CSH gel, in this analysis it is assumed to alter very quickly.
- Minor elements that would stabilize zeolites and clays are not included in the analysis.
- Water is allowed to leave but not enter the otherwise closed chemical system.
- All porosity is assumed to be connected.

Approach 2

The second approach, which simulates the effects of dissolution of the cement grout, required the use of a computer code. The model assumed equilibration between natural Canadian Shield ground waters and an idealized grout. The code is able to handle many more components than would be feasible with a "hand calculation" analysis.

The computer code PHREEQE (Parkhurst, et al., 1980; Fleming and Plummer, 1983) is a solubility/speciation/reaction path program developed by the U.S. Geological Survey, which can be run on a personal computer and has several capabilities: the concentrations of actual species in solution can be determined; the activities and activity coefficients of the dissolved species can be calculated; the state of saturation of the solution with respect to a range of solid phases can be

calculated; and the successive compositions of a solution, as a mineral reacts with the solution, can be predicted.

In this investigation, these capabilities were used to look at the potential for ground water to dissolve the model grout, with two possible consequences: (1) the composition of the ground water changes due to adding the dissolved grout material, resulting in the precipitation of secondary phases, or (2) the ground water transports the dissolved grout material away and out of the seal.

The first consequence is reasonable for a very sluggish hydrogeologic regime where ground water enters and saturates the seal material and remains for a significant period of time. This can be considered a "closed system" analysis. The second consequence is reasonable as a bounding condition in a hydrogeologic regime where there are relatively high gradients, and ground water could be expected to enter and saturate the seal and then flow out, driven by the gradient at the seal. This can be considered an "open system" analysis.

The "closed system" analysis will result in favourable performances because the increased permeability that might arise due to grout dissolution will be offset by secondary phases precipitating and filling porosity. The "open system" analysis will result in a pessimistic prediction because any grout material dissolved is removed and contributes to increased porosity/permeability of the system. Taken together, the open and closed systems analyses bracket expected performance of the grout.

In order to produce data for the evaluation of these scenarios, the PHREEQE code performs various calculations on the ground water and the idealized grout. In the case of the "closed system" discussed above, the code must perform the following steps:

- Using the ground water chemical composition, calculate the aqueous species present for use in setting up chemical reactions.

- Calculate the phases with which the ground water is saturated, to assess the potential for precipitation of phases and/or to ascertain equilibrium relations between possible host rock minerals and the ground water.

- React (equilibrate) the ground water aqueous species with the grout, and calculate the amount of grout dissolved, if applicable.

- Calculate the new ground water chemical composition resulting from the addition of dissolved grout constituents.

- Calculate the phases with which the new, altered ground water is saturated in order to assess the potential for the precipitation of secondary phases.

In the case of the "open system", only the first three steps are performed, since the water is assumed to leave the grout after dissolving part of it.

Seven different ground water compositions: two fresh (YK-65 and YK-62), two brackish (T-83 and YK-73), and three salines (S-154, T-86, and T-87) were employed in the model to represent the widest range of ground water chemistry possible (Frape, et al., 1984). Concentrated brine compositions were not used because PHREEQE is limited to solutions with ionic strengths lower than about 1.0 M. For purposes of this initial study the grout was assumed to be a single CSH phase. This limitation was driven by the model, i.e., PHREEQE calculates the equilibration of an aqueous solution with a single solid phase. Tobermorite was selected as the phase to model portland cement grout because tobermorite is most representative of the CSH phases in the gel of hydrated portland cements, and because CSH solubility is likely controlled near tobermorite solubilities (tobermorite in individual in x-ray diffraction scans of well-crystallized grouts).

Having selected the phase upon which to base the dissolution model, two different scenarios depicting the dynamics of ground water interaction with a grout-sealed fracture were evaluated. In the "closed system" analysis, the ground water was assumed to come into contact with the grout seal, permeate the grout, and react with the grout until equilibrium was achieved. The resulting altered ground water remains within the grout with no flow through the seal, and secondary phases are formed. This is a reasonable bounding scenario because of the slow travel times anticipated for ground water in grout.

In the "open system" analysis, ground water was assumed to seep through the seal. The ground water permeates the seal, becomes saturated with tobermorite, equilibrates with the grout, and flows out of the seal transporting the aqueous

phases dissolved from the reacted grout. As the altered ground water exits the seal, unaltered ground water enters the seal and the process is repeated. As the ground water flows through and reacts with the grout in this manner, porosity and hydraulic conductivity increase. As with Approach 1, Approach 2 is highly conservative because all ground water is assumed to be completely saturated with tobermorite, and all porosity was assumed to be interconnected. A non-conservative but reasonable assumption was also made, and that was that the porosity was uniformly distributed throughout the grout.

The "closed system" analysis was performed, using PHREEQE, in the following manner. First, saturation indices* were calculated, for each ground water, to identify the solid phases with which the solution was saturated (i.e., buffered). This yielded information on the chemical nature of the ground water as well as a check on the quality of the chemical analysis. After calculating the saturation indices (SI), each ground water was equilibrated with the tobermorite grout. In each case, the number of moles of tobermorite dissolved in one kilogram of each ground water was calculated, and the resulting altered ground water composition was determined, including changes in pH and ionic strength. Finally, possible and reasonable secondary mineral assemblages resulting from the reaction of the ground water with tobermorite were tabulated, and each was equilibrated with the ground water composition resulting from reaction with tobermorite. (This resulting ground water is hereafter referred to as "altered ground water"). Net volume changes calculated from dissolution of the tobermorite and formation of each assemblage were determined, as well as ground water compositional changes resulting from the formation of the secondary mineral assemblages.

In the "open system" analysis, each ground water was equilibrated with the tobermorite grout. Again, in each case the number of moles of tobermorite dissolved in one kilogram of water was calculated. The altered ground water was assumed to flow out of the seal carrying with it the dissolved grout constituents. A number of flow limiting conditions (e.g., hydraulic gradient, conductivity, etc.) were assumed so that the volume of water contacting the grout over long time periods could be bracketed. This is important because the amount of grout removed - hence change in grout porosity/permeability with time - is a direct function of the

---

* The saturation index (SI) is defined as log (IAP/K_{sp}), where IAP is the ion activity product and K_{sp} is the solubility product of the phase in question.

amount of water that contacts and dissolves the grout. The decrease in volume of the remaining grout due to dissolution was assumed to occur uniformly throughout the grout, resulting in a general increase in the uniformly distributed and interconnected porosity.

A direct relationship between changes in permeability resulting from changes in porosity was developed by analyzing data from the literature on concrete experimentation (Powers, et al., 1954; Butler, 1981; Hooton and Mukherjee, 1982). Specifically, data exist which relate the water/cement ratio of the initial mix and measured porosity of the hydrated paste. Other data relate water/cement ratio with the measured permeability (or hydraulic conductivity) of the paste. By correlating the two sets of data by their common factor, water/cement ratio, the relationship between porosity and permeability was derived:

$$\Delta K = K_0 \cdot 10^{(11.14 \cdot \Delta n)} - K_0 \qquad (69)$$

where

ΔK = Change in hydraulic conductivity of the concrete
K_0 = Initial hydraulic conductivity of the concrete
Δn = change in porosity of the concrete

Because the data were taken from experiments performed over a period of thirty years by different workers in different laboratories, and the cements they used varied as to type, there is a variation in the data. However, plots of porosity with water/cement ratio and permeability with water/cement ratio show that the slopes, i.e., changes in porosity and permeability versus changes in water/cement ratio are strikingly consistent. Therefore, the relationship derived relates changes in porosity to changes in permeability. This eliminates many, though not all, of the inconsistencies among the data. In order to quantify the variation in the data, the standard deviations of the slopes of each data set - porosity change versus water/cement ratio change - were calculated and propagated through the derivation of the permeability change versus porosity change relationship.

In the "closed system" analysis, and using the values for volume changes generated by the computer code PHREEQE, changes in porosity were calculated for each secondary mineral assemblage modeled. The changes in hydraulic conductivity with porosity were calculated using the above equation, assuming a value for

initial hydraulic conductivity of the grout of 1 x 10^{-12} meters/second. In addition, the initial porosity was assumed to be 30 percent, which is typical for pastes with water/cement ratios of interest, i.e., approximately 0.4 (Powers, et al., 1954; Butler, 1981; Hooton and Mukherjee, 1982), and porosity changes calculated from volume changes varied from that value.

The hydraulic gradient used for the "open system" analysis was calculated from the length of the concrete/grout seal, which was conservatively assumed to be 0.5 m (the minimal seal length expected to be encountered), and a time sequence of hydraulic heads. The head was assumed to be 1,000 meters initially. This derives from the assumed depth of the repository, and stems from the assumption that the porosity outside the repository is saturated while that inside the repository is unsaturated for the first 1,000 years after closure (pore pressure equals 0). After 1,000 years, it is assumed that the repository horizon becomes resaturated with ground water and the ambient gradient is restored. For this period, i.e., for the next one million years or more, the head was conservatively assumed to be one meter/meter. Changes in hydraulic conductivity were calculated for the incrementally dissolving grout, using an initial porosity of 30 percent and initial hydraulic conductivity of 10^{-12} meters/second. The initial conductivity value was established in a companion study by M. Gray through direct measurement.

This approach is considered conservative for several reasons. First, all porosity in the grout was assumed interconnected. Second, the tendency of the reference grouts to "heal" themselves during laboratory hydraulic conductivity measurements over time, i.e., the hydraulic conductivity has been observed to decrease over successive measurements, has been ignored. Third, in these analyses, a hydraulic conductivity of 10^{-12} meters/second or more was assumed for the unaltered grout; in practice, lower conductivities (i.e., 10^{-13} meters/second or less) appear achievable.

4.2.3.3 Results

Results of Approach 1

The "hand calculation" generation of possible reactions in the simplified cement system yielded variable results. Table 13 presents the phases which were incorporated into the suite of reactions written. For the sake of thoroughness, many phases which can be considered part of the simplified cement system based on

their chemical compositions were used in this analysis, although many of them are not stable except at temperatures and pressures higher than those encountered in hydrating cement or grout undergoing alteration under repository conditions. Table 14 lists the ten reactions with the most negative ΔG_r. The total range of ΔG_r over the ten reactions is less than 0.1 percent of ΔG_r, indicating that on a thermodynamic basis all of the reactions are more or less equally favored.

Table 13. Summary of reactant and product phases incorporated into the suite of reactions considered in a simplified cement system

REACTANTS

Tobermorite ($Ca_5Si_6O_{17} \cdot 5.5\ H_2O$)
Hydrogarnet ($Ca_3Al_2O_6 \cdot 6\ H_2O$)
Ettringite ($Ca_6Al_2(SO_4)_3(OH)_{12} \cdot 26\ H_2O$)

PRODUCTS

Al-PHASES	SO_3-PHASES	Ca-PHASES	OTHER PHASES
Corundum (Al_2O_3)	Anhydrite ($CaSO_4$)	Lime (CaO)	Quartz (SiO_2)
Gibbsite ($Al(OH)_3$)	Gypsum ($CaSO_4 \cdot 2H_2O$)	Portlandite ($Ca(OH)_2$)	H_2O
Andalusite (Al_2SiO_5)	SO_2 (gas)	Larnite (Ca_2SiO_4)	O_2
Gehlenite ($Ca_2Al_2SiO_7$)	SO_3 (gas)	Ca-Olivine (Ca_2SiO_4)	
Grossular ($Ca_3Al_2Si_3O_{12}$)		Wollastonite ($CaSiO_3$)	
Ca-Al Pyroxene ($CaAl_2SiO_6$)		Gyrolite ($Ca_4Si_6O_{15}(OH)_2 \cdot 3H_2O$)	
Anorthite ($CaAl_2Si_2O_8$)		Xonotlite ($Ca_6Si_6O_{17}(OH)_2$)	
Pyrophyllite ($Al_2Si_4O_{10}(OH)_2$)			
Diaspore (AlO(OH))			
Leonhardite ($Ca_2Al_4Si_8O_{24} \cdot 7H_2O$)			
Kaolinite ($Al_2Si_2O_5(OH)_4$)			

Reactions listed in Table 14 involving the products grossular, pyrophyllite, anorthite and andalusite (Reactions 2, 5, 7 and 10) are considered extremely unlikely, since those minerals have igneous and metamorphic origins, i.e., although they can be considered possible grout alteration products on a thermodynamic basis, they will not occur because of insufficient energy in the system. The rest of the reactions appear reasonable. Note that all ten reactions contain wollastonite as a product. There are several phases observed in portland cement pastes which have crystal structures related to wollastonite, namely xonotlite, foshagite, nekoite, okenite, and hillebrandite (Taylor, 1964). Whereas the thermodynamic properties of wollastonite are well known, those of the other phases are imperfectly known. Therefore, it is considered a reasonable approximation to include wollastonite as a reaction product of grout alteration.

Table 14. Results of solid state reactions - ten reactions with the lowest gibbs free energy of reaction and the corresponding volume changes

Reactants: 33 Tobermorite + 2 Hydrogarnet + Ettringite

Products:	ΔG_R (KJ)	ΔV_{solids}^{*} (cm^3)	ΔV (%)	Unlikely to Occur Due to Kinetic Constraints
1) 1.5 Leonhardite + 3 Gypsum + 171 Wollastonite	-332364	-3486.9	-30.4	
2) 3 Grossular + 3 Gypsum + 165 Wollastonite	-332310	-3752.7	-32.7	X
3) 3 Kaolinite + 3 Gypsum + 174 Wollastonite	-332252	-3607.2	-31.4	
4) 6 Diaspore + 3 Gypsum + 174 Wollastonite	-332235	-3662.7	-31.9	
5) 3 Pyrophyllite + 3 Gypsum + 174 Wollastonite	-332225	-3658.5	-31.9	X
6) 6 Gibbisite + 3 Gypsum + 174 Wollastonite	-332210	-3577.5	-31.2	
7) 3 Anorthite + 3 Gypsum + 171 Wollastonite	-332206	-3654.9	-31.8	X
8) 15 Gyrolite + 1.5 Leonhardite + 3 Gypsum + 141 Wollastonite	-332201	6909.6	60.2	
9) 15 Gyrolite + 1.5 Leonhardite + 3 Anhydrite + 141 Wollastonite	-332198	6823.2	59.4	
10) 3 Andalusite + 3 Gypsum + 174 Wollastonite	-332165	-3683.1	-32.1	X

*Assumes product water is unbound or pore water.

Overall volume changes resulting from reactions "likely" in Table 14 vary widely, from -32 percent to +60 percent. Thus, the solid-solid equilibrium approach combined with the simplified chemistry assumed for cement is insufficient for realistically specifying the long-term conductivity of a grouted fracture. The possible range in volume changes calculated from thereactions is large enough to predict increases or decreases in porosity (hence permeability), or no change at all. However, the approach is useful for setting an upper limit on long-term conductivity. For example, a negative volume change for a process where grout is dissolved and secondary phases are precipitated implies that porosity of the grout increases, as does hydraulic conductivity. According to the ΔV-hydraulic conductivity relationship presented and described in the previous section, the maximum volume decrease of 32 percent corresponds to an upper bound hydraulic conductivity of approximately 5×10^{-6} meters/second, based on an initial porosity of 30 percent and an initial hydraulic conductivity of 10^{-12} meters/ second. This is approximately equivalent to the hydraulic conductivity of a sandstone or an unconsolidated silty sand. Thus, permeability of a grouted zone could be predicted to increase or decrease. However, a useful upper bound on conductivity of a

grouted fracture has been produced. That upper bound value is on the order of 10^{-6} meters/second.

Results of Approach 2

The use of the PHREEQE computer code to calculate SI suggests that the ground waters are highly undersaturated with respect to certain phases which may occur in portland cement grouts, e.g., tobermorite, ettringite, and hydrogarnet, suggesting that on a thermodynamic basis these phases will dissolve.

In addition, the ground waters appear to be saturated with respect to carbonates (e.g., calcite, dolomite*), quartz, and plagioclase (e.g., anorthite*), suggesting that the ground waters are in thermodynamic equilibrium with granitic rocks and common secondary minerals (see for example, Figs IV:47 and IV:48). In the "closed system" approach, results of the modeling also indicate that the altered ground waters resulting from the reaction with tobermorite become saturated with respect to several other phases. On this basis, these phases are possible or likely candidates for inclusion in secondary mineral assemblages forming as a consequence of the reaction of ground water with tobermorite. Phases include amorphous silica, gyrolite, wollastonite, pseudowollastonite, and monticellite. (As with certain phases discussed previously, the stabilities of monticellite and pseudowollastonite are misleading. While favoured thermodynamically, they are found in rocks that are formed at much higher temperature-pressure conditions than those to be encountered by repository seals).

Table 15 lists the 47 possible secondary assemblages used in the "closed system" analysis. Through the use of PHREEQE, each assemblage was equilibrated with each of the altered ground waters resulting from reaction with the tobermorite grout. The following stable assemblages result in primarily positive volume changes and decreased hydraulic conductivity:

---

* Note that PHREEQE is not able to assess solid solution; thus, calcite-dolomite and anorthite reflect the Ca-Mg components of calcite and the Ca-component of plagioclase, respectively.

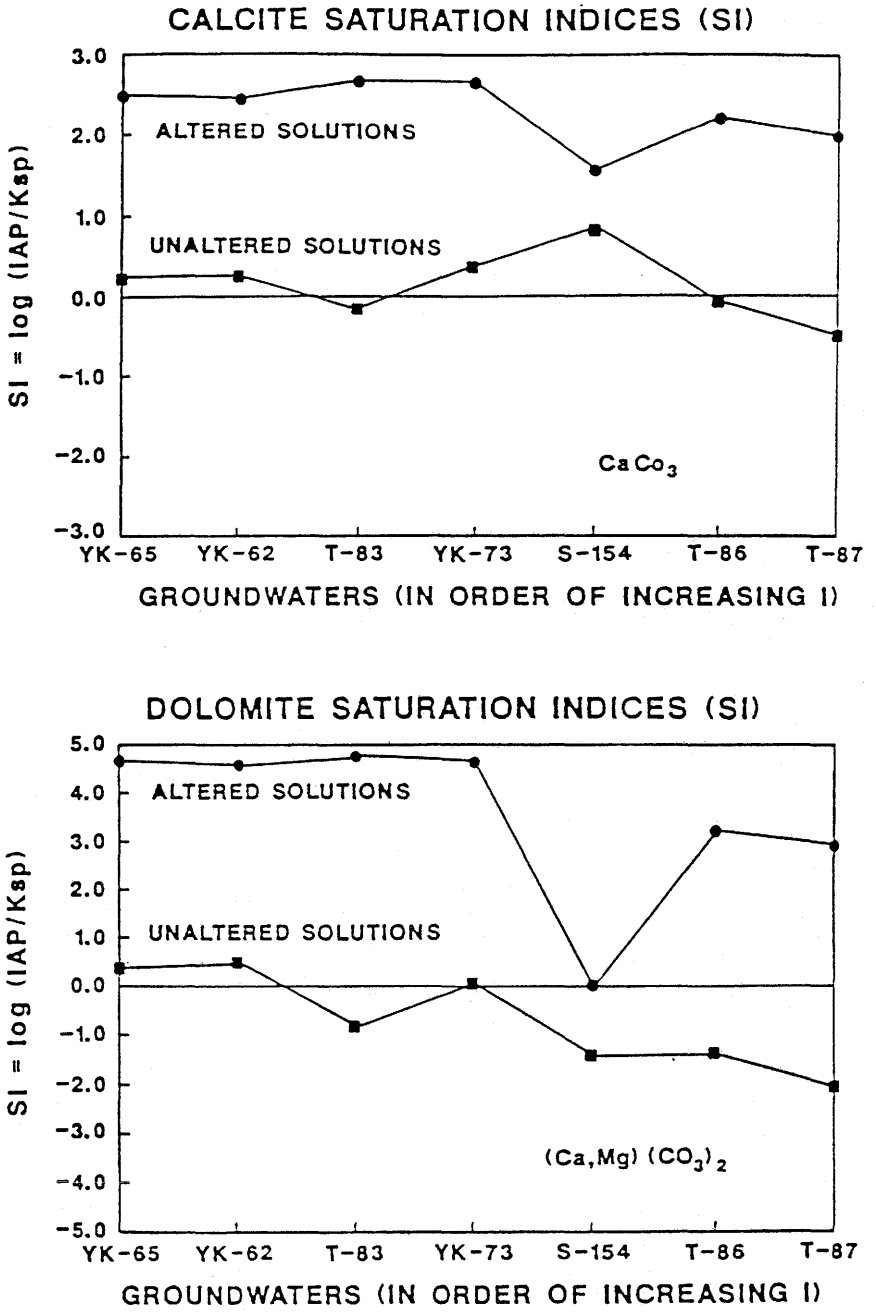

Fig IV:47. Calcite And Dolomite Saturation Indices (SI) Calculated For Seven Ground Water Samples. Fresh ground waters are represented by YK-65 and YK-62, brackish ground waters by T-83 and YK-73, and saline ground waters by S-154, T-86, and T-87

(1) Silica phases + calcite
(2) Silica phases + dolomite
(3) Silica phases + dolomite + pseudowollastonite
(4) Silica phases + dolomite + wollastonite
(4) Silica phases + dolomite + monticellite

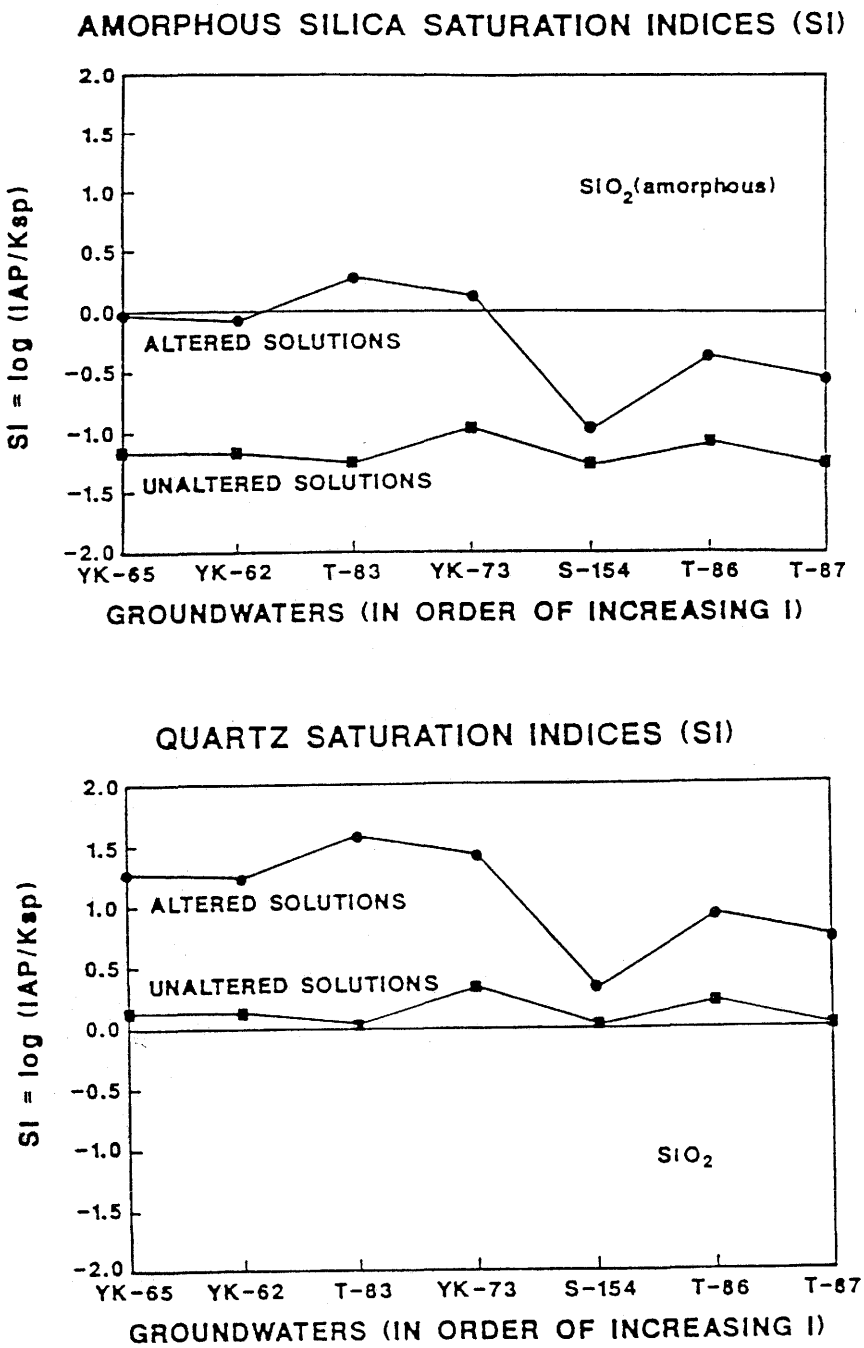

Fig IV:48 Amorphous Silica And Quartz Saturation Indices (SI) Calculated For Seven Ground Water Samples. Fresh ground waters are represented by YK-65 and YK-62, brackish ground waters by T-83 and YK-73, and saline ground waters by S-154, T-86, and T-87

Of these, the assemblages containing amorphous silica result in slightly less positive or slightly negative volume changes. Assemblages (3), (4), and (5) result in negative volume changes and increased hydraulic conductivity. Again, those assemblages with amorphous silica show slightly more negative volume changes.

Table 15. Secondary phase assemblages used in the "closed system" analysis

Calcite+Quartz	Dolomite+Wollastonite+Quartz	Wollastonite
Calcite+Cristobalite	Dolomite+Wollastonite+Cristobalite	Wollastonite+Quartz
Calcite+Chalcedony	Dolomite+Wollastonite+Chalcedony	Wollastonite+Cristobalite
Calcite+SiO_2(A,G)	Dolomite+Wollastonite+SiO_2(A,G)	Wollastonite+Chalcedony
Calcite+SiO_2(A,P)	Dolomite+Wollastonite+SiO_2(A,P)	Wollastonite+SiO_2(A,G)
Dolomite+Quartz	Dolomite+Monticellite+Quartz	Wollastonite+SiO_2(A,P)
Dolomite+Cristobalite	Dolomite+Monticellite+Cristobalite	Monticellite
Dolomite+Chalcedony	Dolomite+Monticellite+Chalcedony	Monticellite+Quartz
Dolomite+SiO_2(A,G)	Dolomite+Monticellite+SiO_2(A,G)	Monticellite+Cristobalite
Dolomite+SiO_2(A,P)	Dolomite+Monticellite+SiO_2(A,P)	Monticellite+Chalcedony
Dolomite+P-Wollastonite+Quartz	P-Wollastonite	Monticellite+SiO_2(A,G)
Dolomite+P-Wollastonite+Cristobalite	P-Wollastonite+Quartz	Monticellite+SiO_2(A,P)
Dolomite+P-Wollastonite+Chalcedony	P-Wollastonite+Cristobalite	Anorthite
Dolomite+P-Wollastonite+SiO_2(A,G)	P-Wollastonite+Chalcedony	Wairakite
Dolomite+P-Wollastonite+SiO_2(A,P)	P-Wollastonite+SiO_2(A,G)	Gyrolite
	P-Wollastonite+SiO_2(A,P)	Gyrolite+Calcite

Figure IV:49 presents examples of these calculated volume changes. The upper graph displays volume changes from reaction of one kilogram of ground water with tobermorite accompanied by precipitation of secondary calcite + quartz, calcite + cristobalite, calcite + chalcedony, calcite + amorphous silica, and calcite + gyrolite for fresh, brackish, and saline. Volume changes are, for the most part, very slightly positive. The lower graph shows that volume changes for tobermorite altering to secondary wollastonite + silica phases are slightly negative.

The relationship between change in volume due to reaction and change in hydraulic conductivity is:

$$\Delta K = K_o \cdot 10^{(11.14 \frac{-\Delta V}{V})} - K_o \qquad (70)$$

K_0 = assumed initial hydraulic conductivity
ΔK = calculated change in hydraulic conductivity
V = original tobermorite volume
ΔV = net volume change from dissolution of tobermorite and formation of secondary mineral assemblage

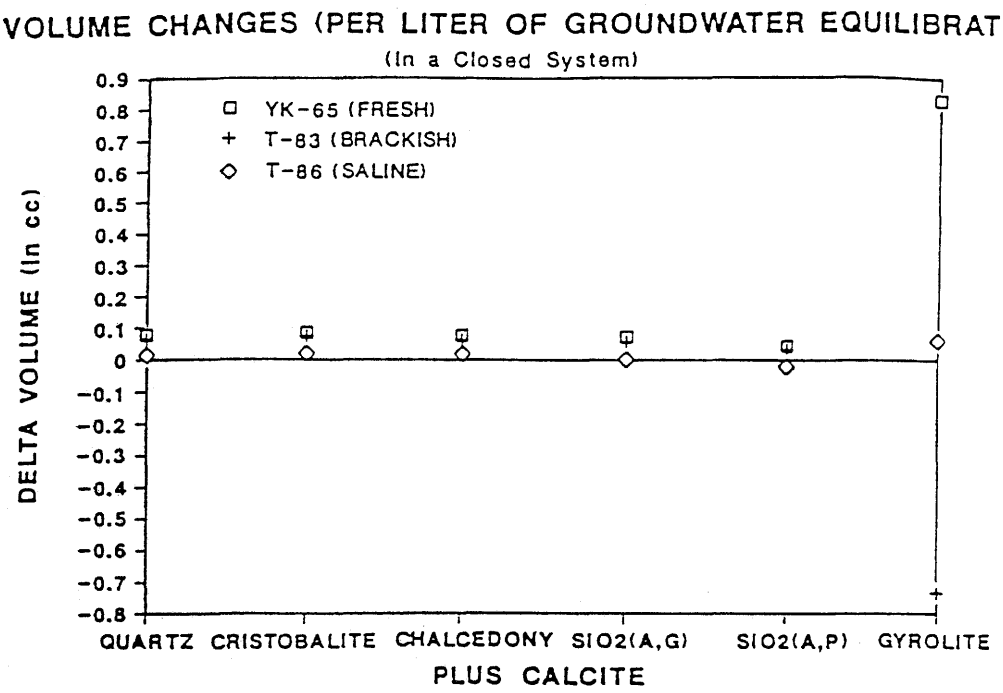

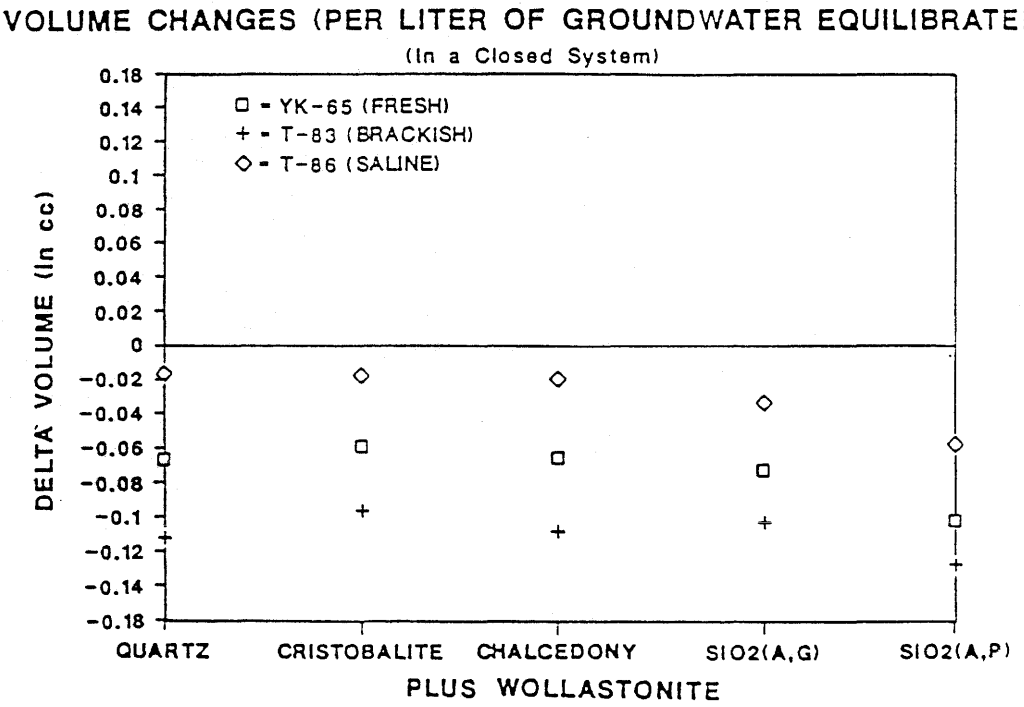

Fig IV:49. Calculated Volume Changes Resulting From Reaction Of Ground Waters With Tobermorites And Formation Of Secondary Phases For Ten Secondary Mineral Assemblages (Closed System)

Hydraulic conductivity as a function of volume change is shown graphically in Fig IV:50. Changes in hydraulic conductivity calculated from volume changes in Fig IV:49 are presented in Fig IV:51. As expected, slightly positive volume changes result in slightly lower hydraulic conductivities (indicated in the upper graph),

whereas slightly negative volume changes result in slightly higher hydraulic conductivities (lower graph).

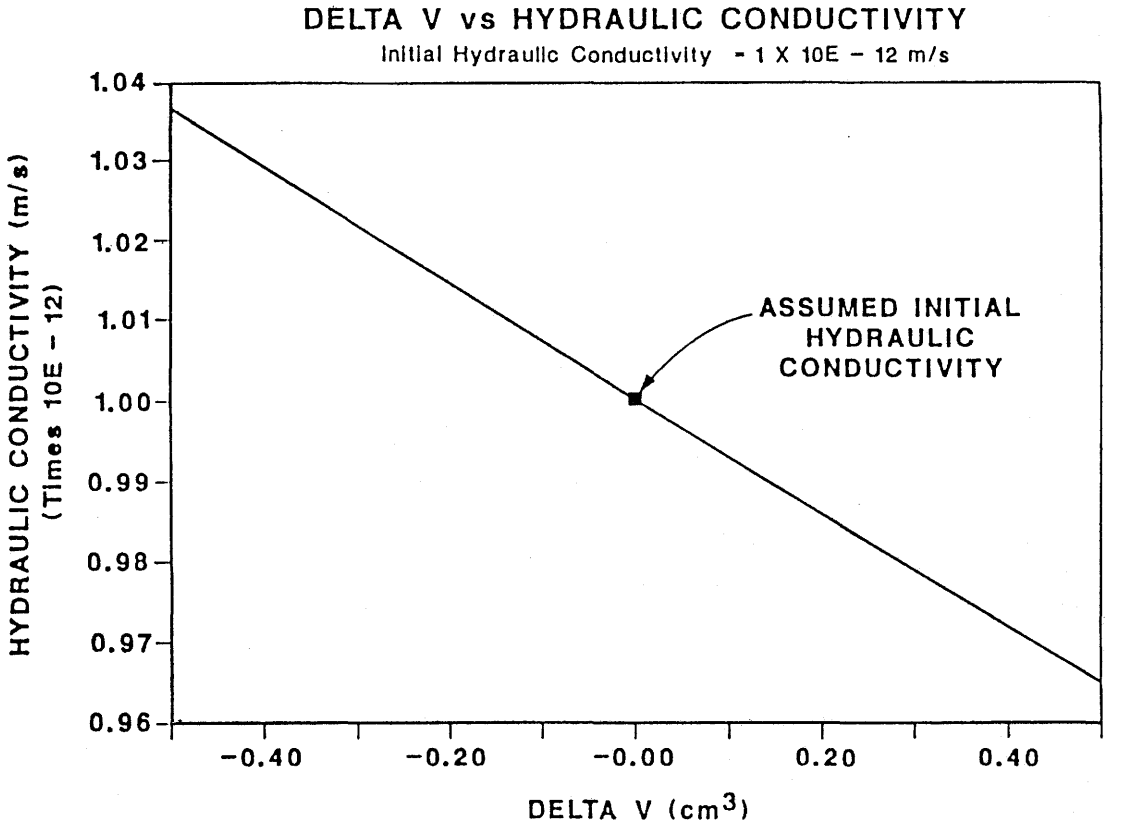

Fig IV:50. Hydraulic Conductivity of a Cement as a Function of Change in Volume (see text)

As part of the "open system" analysis, the volume changes produced from the reaction of one kilogram of each ground water with tobermorite, but without the accompanying precipitation of secondary phases, were calculated and are shown in Fig IV:52 a. The volume changes calculated are equivalent to the volumes of "CSH gel", i.e., tobermorite, dissolved by each ground water. Fig IV:52 b shows the hydraulic conductivities calculated for each volume change, assuming an initial porosity of 30 percent and initial hydraulic conductivity of 10^{-12} meters/second.

Further, in this analysis the dissolution of tobermorite over time was related to changing hydraulic conductivity to obtain an estimate of the longevity of cementitious grout under a conservative but realistic set of hydrologic conditions. The logic here is that in order for water to transport material out of the seal, it first

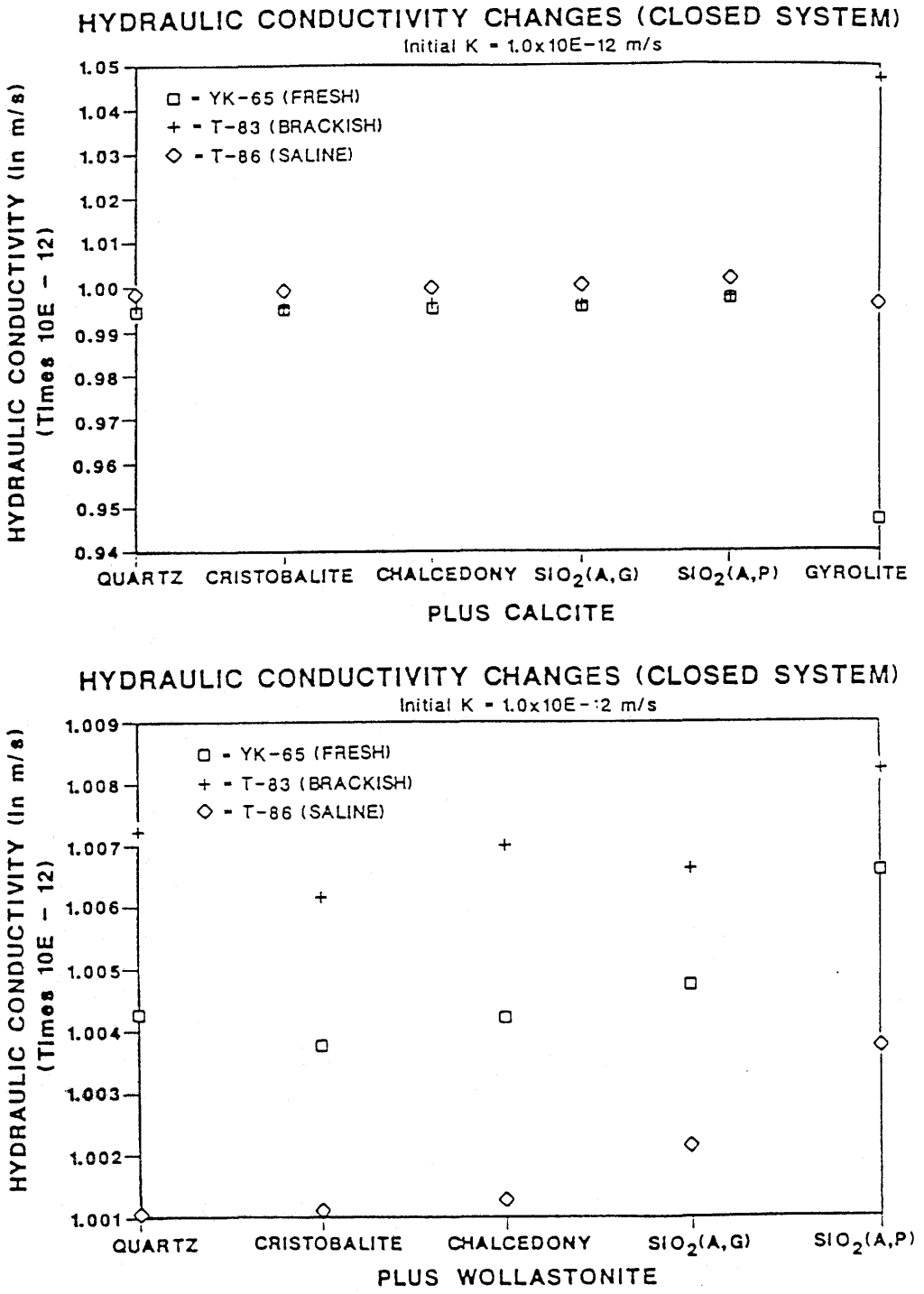

Fig IV:51. Calculated Hydraulic Conductivity Changes For The Ten Secondary Mineral Assemblages In Fig 7 (Closed System)

has to get into the seal. Therefore, the limit on a seal's decrease in performance is determined by: 1) the amount of water travelling through the seal per unit time, which is a function of hydraulic head and hydraulic conductivity, and 2) the solubility of the grout phases. As presented in Section 4.3.2.2., it was assumed that the hydraulic head was equivalent to the depth of the repository (1,000 meters) for the first 1,000 years, at which point the repository horizon was assumed to be resaturated. For conservatism, the head from 1,000 years until

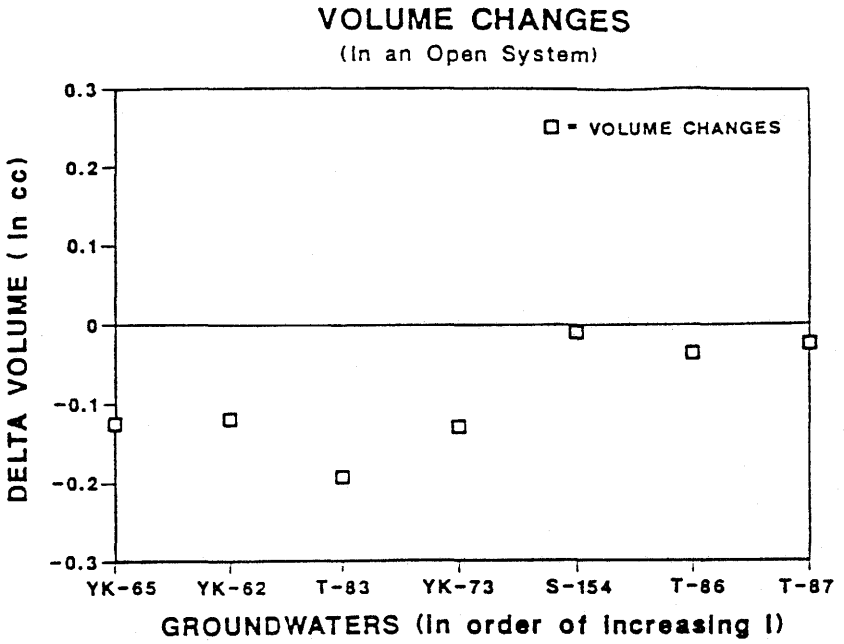

Fig IV:52a. Calculated Volume Changes Resulting From Reaction Of Seven Ground Waters With Tobermorite (Open System). Fresh ground waters are represented by YK-65 and YK-62, brackish ground waters by T-83 and YK-73, and saline ground waters by S-154, T-86, and T-87

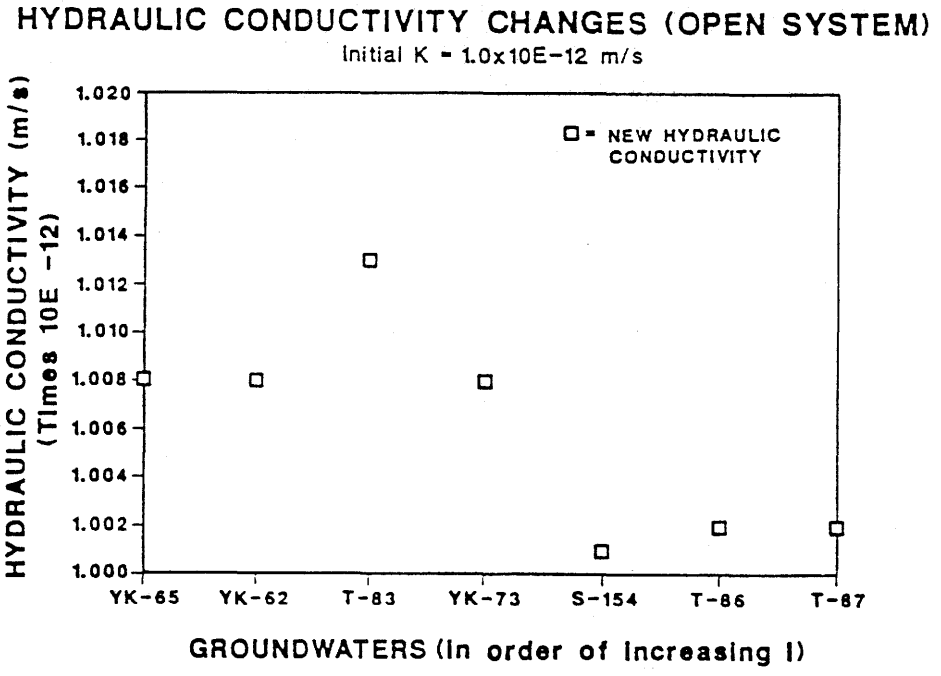

Fig IV:52b. Hydraulic Conductivity Changes For The Seven Ground Waters in Fig IV:52 a (Open System)

failure of the seal was assumed to be one meter. Again, the initial porosity was assumed to be 30 percent and the initial hydraulic conductivity 10^{-12} meters/second.

Fig IV:53 presents the results of the calculations of change in hydraulic conductivity with time. Tobermorite grout appears to be relatively long-lived in saline water T-86, as after two million years there is insignificant change in the hydraulic conductivity of the grout. The seal performs effectively approximately 1.4 million years in brackish water YK-73 and fresh water YK-65. In the worst case, brackish water T-83, the seal performs for about 6000,000 years.

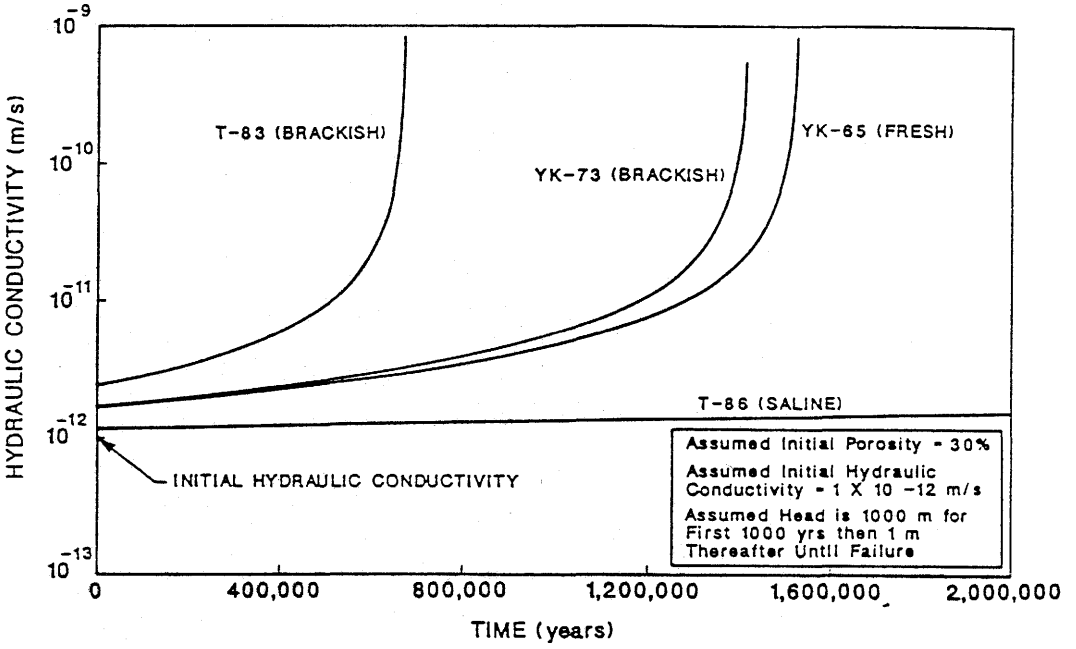

Fig IV:53. Change In Hydraulic Conductivity With Time For Four Gound-water Compositions, From "Open System" Analysys (See Text)

Fig IV:54 shows changes in hydraulic conductivity with time for tobermorite grout in saline water T086 to illustrate the uncertainty in the change-in-porosity versus change-in-conductivity relationship. These curves are shown: average, +1 standard deviation, and -1 standard deviation. Note that even in the worst case ($+1\sigma$) the seal lasts for approximately 900,000 years.

From this analysis, saline ground waters appear to be less reactive with simplified cementitious grout than fresh and brackish waters, i.e., the equilibration of the saline waters with tobermorite (using the PHREEQE code) resulted in the dissolution of smaller amounts of the tobermorite, possibly due to the fact that

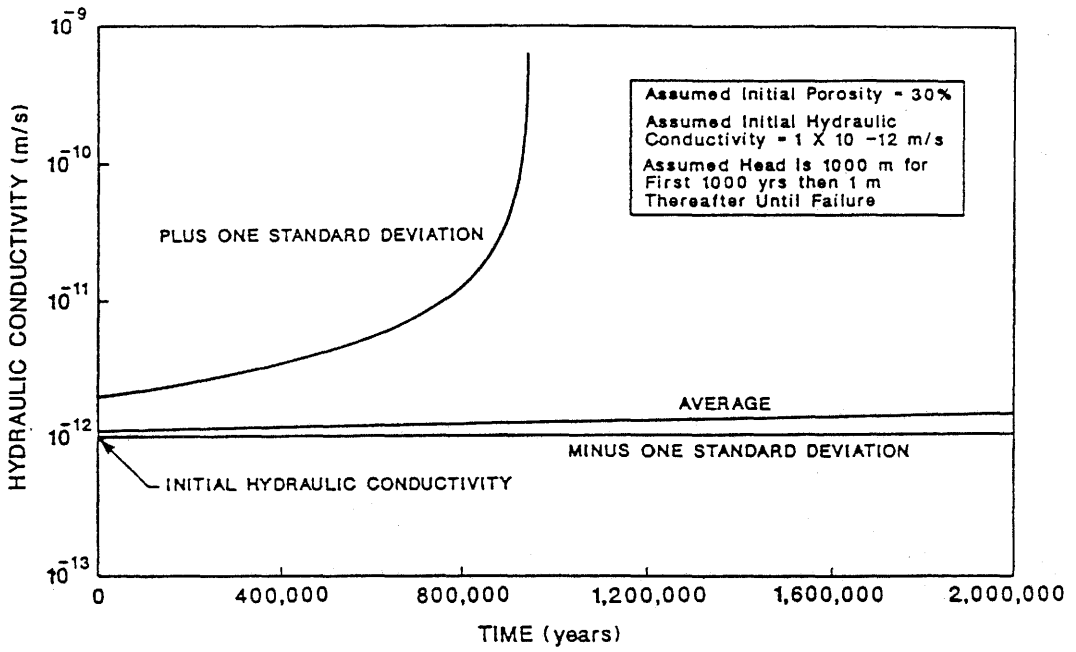

Fig IV:54. Change in Hydraulic Conductivity with Time for Saline Groundwater T-86, Illustrating the Effects of Variability of Data Used in Determining the Relationship Between Changes in Grout Porosity Due to Dissolution and Resulting Changes in Hydraulic Conductivity

water containing a higher solute loading has less capacity to dissolve material if/when chemical complexation is unimportant.This is reflected in the hydraulic conductivity versus time plot in Fig IV:53 which indicates that considerably lower increases in hydraulic conductivity, due to tobermorite dissolution in saline water T-86, may be expected over the first two million years. In the other ground waters, hydraulic conductivity increases sharply from 600,000 years to 1.4 million years.

Discussion of Kinetics

The analyses of cement behaviour described above are based on equilibrium thermodynamics, and the reactions are assumed to be instantaneous. This is a highly conservative approach because no consideration has been given to the lengthy reaction rates that are likely to prevail. The rate of the pertinent reactions will depend on several factors: concentrations of the species involved in the reaction; the nature of the surfaces of the solids (crystal defects, impurities, etc.); degree of supersaturation of species and nucleation mechanisms; and temperature. The first two factors bear on dissolution rates, the second two bear on precipitation rates, and the last affects both dissolution and precipitation. Thus,

kinetic analysis becomes a competing rate problem. To solve the problem, the aspects must be separated and treated independently. It is relatively easy to treat the reaction rate, based on concentrations of species, since concentrations are measurable. The other considerations, although more difficult to analyze, may significantly affect reaction rates. In general, most rate processes conform approximately to the Arrhenius equation:

$$\text{Rate} = A \exp(-\Delta E/RT) \tag{71}$$

where:

R = the gas constant
T = the absolute temperature
A = an empirical constant (for complex systems)
ΔE = an activation energy

Generation of Arrhenius plots was beyond the scope of this investigation; however, it is desirable to perform this type of analysis in subsequent studies.

Observations of ancient cements have provided little information on rates of alteration reactions, because they were not mixed with the same formulas as portland cement. It has been observed, however, that when siliceous aggregates or pozzolan are evident in ancient calcareous cements, phases such as tobermorite are present and apparently long-lived, under some conditions.

It has been shown here that even with the assumption of instantaneous chemical reactions inherent in a thermodynamic analysis of grout longevity, cementitious grout demonstrates promise of being very long-lived. If the evidence of grout phase persistence in ancient cements is also considered, it is reasonable to conclude, on a qualitative basis, that the sluggishness of the reactions involved will ensure that grout longevity will be at least what is predicted by the thermodynamic analysis, and perhaps substantially greater. Further investigation of the kinetics of grout reactions will enable quantification of chemical processes to the extent that much better and more realistic scenarios can be analyzed and evaluated, with the probable result that grout longevity can be projected to long periods of time with much greater confidence than at present.

4.2.3.4 Conclusions

This initial investigation of simplified cement systems and interaction with ground waters of known composition from the Canadian Shield has produced promising results. First, the data indicate that portland cement-based grouts may work very well in some geochemical environments, although perhaps not all. The result that saline ground waters appear less reactive with tobermorite than fresh and brackish waters may be useful. Specifically, saline ground waters are common in granitic terrains and may be typically high in salinity in hydrologic regimes where ground water movement is sluggish and little fresh water enters the system to reduce the salinity. This observation may benefit site selection if or when repository sealing is an important consideration to repository system performance. Moreover, in this investigation, it was also found that in the "closed system" analyses, changes in hydraulic conductivity were extremely small because formation of secondary minerals filled much of the porosity created by dissolution. An apparent finding then is that saline waters common to sluggish hydrologic regimes are conducive to long-term cement grout performance. In addition, if it is necessary to decide between sites which exhibit either saline waters or a slow hydrologic flow regime, then the saline water site may be preferable. This priority stems from the fact that in the "open system" analyses, seal hydraulic conductivity does not increase significantly for many years in saline ground waters, regardless of the potential for flow to occur. If a repository could be located in a zone which satisfies these conditions - saline ground water, low ground water flow, and granitic host rock - a portland cement-based grout may be particularly viable seal material.

More specifically, the results of this investigation show that portland cement-based seals may maintain a useful level of performance for several millions of years and beyond. The "open system" analyses, which in the grout-dissolution models are worst-case scenarios, indicate that hydraulic conductivities of close to 10^{-12} meters/second can be maintained for a million years or more. Moreover, the solid-solid reactions analysis, which models the inversion of grout phases to thermodynamically more stable phases, indicates that absolute worst-case porosity increases result in hydraulic conductivities of approximately 10^{-6} meters/second. This analysis implies that after millions of years, if solid phase transitions occur, then the ultimate worst-case performance of grouted fractures would be equal to that of a siltstone with a transmissivity approaching 10^{-15} meters^2/second. This transmissivity is about 1,000 times less than that for a small

(e.g. three meters thick) conducting zone of clastic debris or sedimentary rock. Thus, even in the very long-term, fractures grouted with portland-based cement are not likely to contribute significantly to total release of radionuclides from the repository system.

4.2.4 Synthesis of modelling and laboratory results

From the modelling, a scenario emerges for long-term cement grout performance:

- A grout seal is emplaced on Fig IV:55 and slowly dissolves for hundreds of thousands or a million years. Due to kinetic constraints, the metastable grout phases persist during this period, inverting to stable forms very slowly, and low hydraulic conductivities (10^{-12} or better) are maintained.

- Dissolution of metastable phases continues and cumulative inversion to stable phases appears to accelerate (Point 2); the stable phases have much lower solubilities than the metastable phases, so grout dissolution progressively decreases, as does the development of porosity due to dissolution.

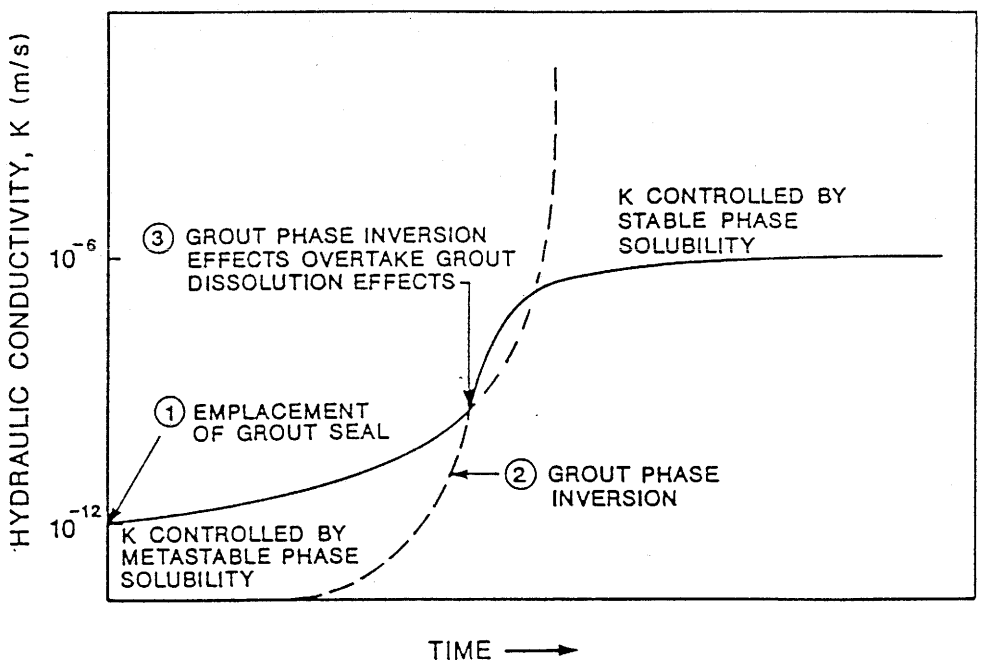

Fig IV:55. Schematic Representation Of Factors Controlling The Hydraulic Conductivity During The Life Of A Grout Seal. Numbered points are keyed to the discussion in Section 4.0

- At some time, the effects of grout phase inversion overtake the effects of grout dissolution (Point 3). The progressive inversion of the grout to stable phases results in large porosity increases, with concomitant increases in hydraulic conductivities, with an upper bounding conductivity equivalent to a sandstone or unconsolidated silty sand.

In summary, cement grout seal will likely maintain a very low hydraulic conductivity on the order of one million years; metastable phases invert to stable phases, resulting in an increase in hydraulic conductivity to that of a sandstone; stable phases persist essentially ad infinitum. This scenario is plausible assuming that dissolution of metastable grout phases is limited for several million years. The rate of inversion of metastable phases to stable phases (kinetics) is important. If inversion occurs before grout dissolves excessively, an assemblage of low solubility stable phases results. This assemblage would likely have an acceptable upper-bound hydraulic conductivity.

Clearly the modelling techniques use simplifying assumptions and thus the above scenario may be speculative. Similarly, the preliminary laboratory leaching data presented also have limitations. The data are the end points from static leaching tests; analysis of time dependent leaching of Ca^{2+}, SI^{4+}, etc., are yet to be completed. The solution-reprecipitation processes in static leach tests which may be controlled by phase solubility limits, are likely to differ significantly from those in dynamic conditions. Taking phase solubility limits into account re-analysis of the static leach data may lead to congruence between the theoretical and laboratory results. Moreover, the effects of clay on the chemical composition of leachates needs evaluation.

The laboratory data determining the effects of superplasticizer on grout stability are also limited. Presently, it appears that the beneficial effects of reduced w/c ratio may not prevail in the low limited w/c range from 0.3 to 0.6. Within this range, which is only practicable with the use of superplasticizer, decreasing w/c (grout porosity) does not appear to enhance the static leaching properties of the grout. This is not inconsistent with the results of the modelling studies. Further laboratory and modelling information is required to allow more effective determination of the effects of initial grout porosity on longevity.

4.2.5 References

Baker, W.H. (ed.), 1982, Grouting in Geotechnical Engineering, ASCE, New-York, 1018 p.

Butler, J.E., 1981, "The Influence of Pore Pressure Upon Concrete," Magazine of Concrete Research, Vol. 33, pp. 3-16

Fleming, G.W., and L.N. Plummer, 1983, "PHRQINTP - An Interactive Computer Program for Constructing Input Data Sets to the Geochemical Simulation Program PHREEQE," U.S. Geological Survey, Water-Resources Investigations Report 83-4236.

Frape, S.K., P. Fritz, and R.H. McNutt, 1984 "Water-Rock Interaction and Chemistry of Ground Water from the Canadian Shield," Geochim. Cosmochim. Acta, pp. 1617-1627.

Hooton, R.D. and P.K. Mukherjee, 1982, "A Review of Cement Based Grouts for Both Repository Sealing and the Construction of the Underground Research Laboratory, "Ontario Hydro Civil Research Department, pp. 98-104.

Parkhurst, D.L., D.C. Thorstenson, and L.N. Plummer, 1980, "PHREEQE - A Computer Program for Geochemical Calculations, "U.S. Geological Survey, Water-Resources Investigations, pp. 80-96.

Powers, T.C., L.E. Copeland, J.C. Hanes, and H.M. Mann, 1954, "Permeability of Portland Cement Paste, "Journal of the American Concrete Institute, November, 1954, pp. 285-298

Sarkar, A.K., M.W. Barnes, and D.M. Roy, 1982, "Longevity of Borehole and Shaft Sealing Materials: Thermodynamic Properties of Cements and Related Phases Applied to Repository Sealing," Technical Report, Battelle Project Management Division, Office of Nuclear Waste Isolation, 52 pp.

Taylor, H.F.W. (ed.), 1964, The Chemistry of Cements, Vol. 1, Academic Press, New York, 460 pp.

4.3 PHYSICAL STABILITY

4.3.1 General

Grouts will be exposed to hydraulic gradients of different magnitude directly after their application in rock fractures and this means that piping and erosion may take place. The study has comprised several series of tests that are reported here in a condensed form.

4.3.2 Clays

4.3.2.1 Scope of study

Three major investigations have been carried out.

* A: Gel front behavior and restistance to flow in the range of 10^{-4} - 10^{-5} m/s for slot widths between 50 and 150 microns. The investigated gels include Tixoton and Tixoton/quartz (50/50) mixtures with different water contents and saturation media, eihter distilled deionized water, synthetic Forsmark water (composition according to Table 16) or brine.

* B: Investigation of critical water pressure for producing piping of gels completely filling 50, 100 and 150 micron wide slots.

* C: Dispersion study of gels applied in 100 and 150 microns wide slots containing distilled water or synthetic Forsmark water. Gel front measured and characterized initially and again after 1 month.

4.3.2.2 Experimental set up

The cells, which had apertures between 50 and 150 microns, were designed for application of clay or cement gels by use of a micrometer and a piston of thin metal foil (Fig IV:56). The gels, d in Fig IV:56, were moved to the edge of the channel containing flowing water.

The flow was controlled and measured, by an electronic system consisting of a pressure cell, pressure gauges, and a series of mass flow meters (HI-TEC P-500 and F-800) (Fig IV:57). The accuracy of the flow meter was ± 0.01 ml/hr while

that of the pressure was ± 0.1 kPa in the range of 0-35 kPa, and ± 0.5 kPa for pressures exceeding 35 kPa. The pressure measurements gave the critical break-through pressure at piping.

The cell was mounted under a polarizing light microscope equipped with lenses with wide focusing depths. The lenses had magnification rates between 40 and 400 times. A video camera and recording unit was attached to the microscope for recording of the piping and erosion events.

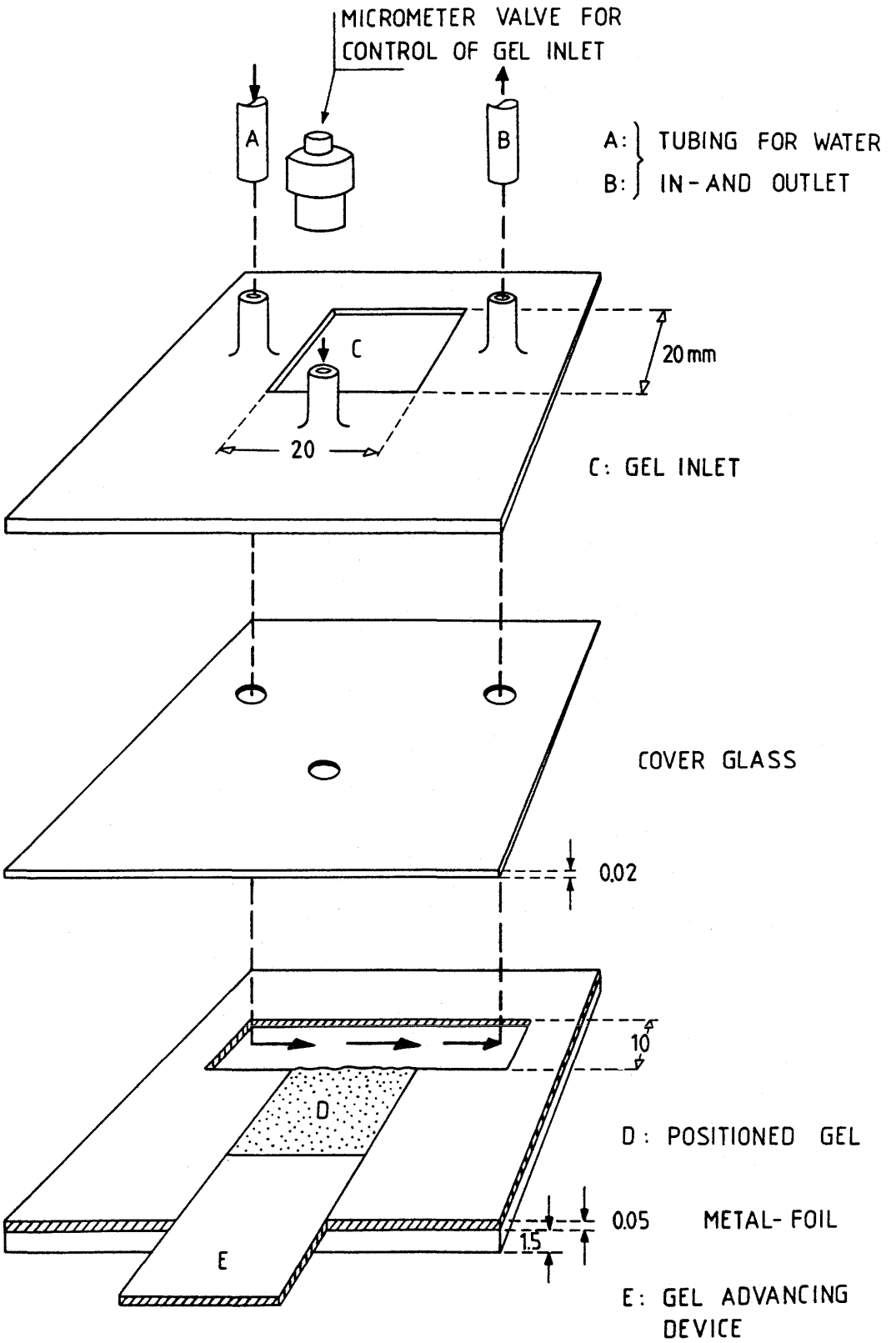

Fig IV:56. Schematic illustration of the cell-design

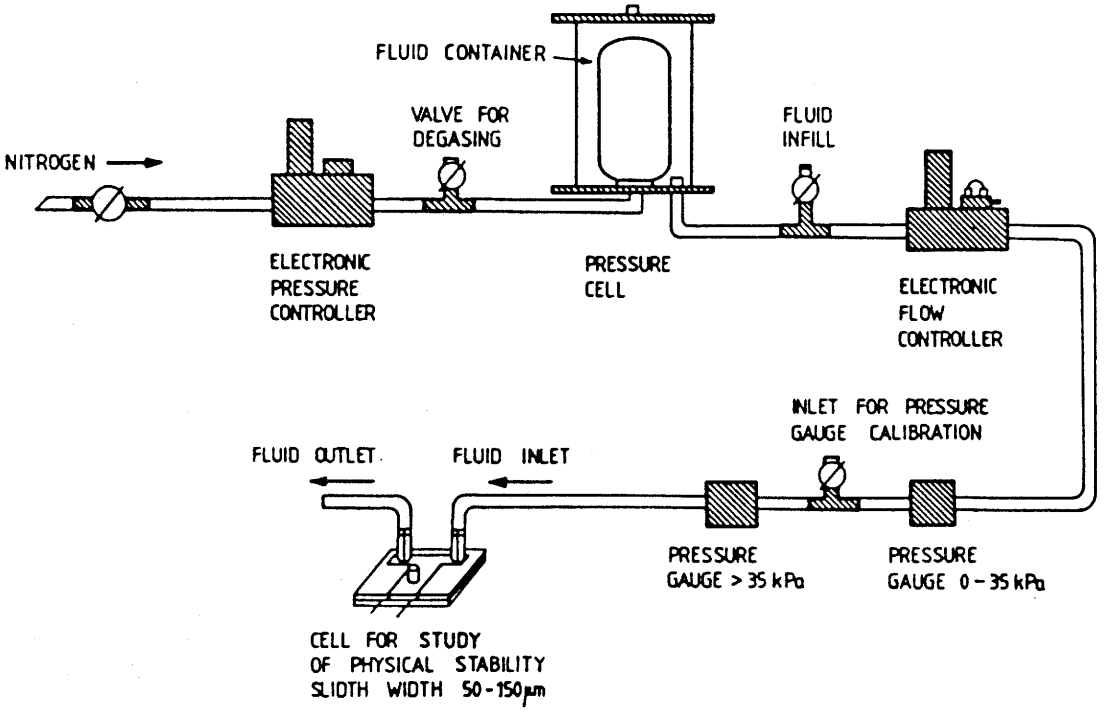

Fig IV:57. Schematic illustration of the pressure and flow controlling unit connected to the cell

Table 16. Chemical composition of synthetic Forsmark water

Chemical component	Content, ppm
Ca^{2+}	950
Mg^{2+}	21.7
Na^{+}	2530
K^{+}	5.4
Cl^{-}	6250

4.3.2.3 Results

Gel front behavior.

20 different clay-based gels have been analyzed with respect to their erodability (Table 17). The critical ratio of flow for erosion was recorded together with the size range of the eroded aggregates and particles. The gels were graded from 1 to 5, where the lowest grade refers to gels with strong cohesive nature and only minor erosion at the gel front even at flow rates of 10^{-4} m/s. The highest grade 5 (+ + + + +) is given to gels with very low resistance to flow and with a high rate of erosion, often yielding aggregates 20-40 microns ripped off from the front at relative low flow rates ($5 \cdot 10^{-5}$ m/s).

The major difference in erosion behavior between the different gels is most likely related to the gel strength. In the homogenous Tixoton gels a distinct front line was formed after initial erosion of the softest parts of the gel. The cohesive nature gave a relatively high critical flow rate, i.e. $5 \cdot 10^{-4}$ m/s. The eroded aggregates generally had a size of 5 and 20 microns. The gels saturated with synthetic Forsmark water, holding less water, were also relatively cohesive. The critical flow rate for initial erosion was rather high, i.e. $>10^{-4}$ m/s, but the aggregates that were torn off were up to 70 microns in size in the 150 micron slot. This resulted in the development of an irregular front line which broke up into frequent aggregates even when the flow rate was reduced to $< 3 \cdot 10^{-5}$ m/s.

The Tixoton/quartz mixtures displayed a somewhat different erosional pattern. The minute quartz particles, <15 microns, seemed to act as reinforcement of the gel. However, this also gave a decrease in cohesion, which caused significant erosion of the gel once this process had been initiated. The particles ripped off ranged in size between 2 and 15 microns for the gels saturatated with distilled water and between 30 and 60 microns for the gels saturated with Forsmark water (cf Table 17).

Piping

The results indicate that the Tixoton/quartz (50/50) mixture has a higher resistance to piping than the pure Tixoton-gel of corresponding water content. Thus, piping occurred in the Tixoton-gel (1.6 x liquid limit) at 20 KPa and a higher

Table 17. Compilation of the reults from performed investigations of the physical stability of gels. D = distilled water, F = synthetic Forsmark water.

Gel mixture	Fluid	w_i, %	Aperture	Piping pressure kPa	Erodability	Particle size, µm	Critical flow, m/s
Tixoton	D	800	50	32.6	+	5-20	$5 \cdot 10^{-4}$
"	D	1000	"	16.8	+ +	"	10^{-4}
"	D	"	"	19.2	+ +	"	"
"	D	"	"	16.4	+ +	"	"
"	D	"	"	19.7	+ +	"	"
"	D	3000	"	<1.0	+ + + +	2-10	10^{-5}
"	F	425	"	6.0	+ + + +	30-40	$3 \cdot 10^{-5}$
"	D	1000	100	23.7	+ +	5-20	$8 \cdot 10^{-5}$
"	D	"	"	20.8	+ +	"	"
"	F	425	"	9.2	+ + + +	40-70	$3 \cdot 10^{-5}$
"	D	1000	150	26.1	+ +	2-15	10^{-4}
"	D	"	"	21.4	+ +	"	"
"	D	"	"	21.9	+ +	"	"
"	F	425	"	8.7	+ + + + +	40-70	$3 \cdot 10^{-5}$
Tixoton/qtz, (50/50)	D	400	100	85.3	+ + +	2-15	$9 \cdot 10^{-5}$
"	F	100	"	61.4	+ + + +	30-50	10^{-4}
"	D	400	150	35.5	+ + + +	2-15	$7 \cdot 10^{-5}$
"	F	100	"	29.8	+ + + +	40-60	10^{-4}
", (30/70)	D	250	100	31.6	+ + + +	2-15	$6 \cdot 10^{-5}$
"	F	80	"	18.2	+ + + + +	40-60	$8 \cdot 10^{-5}$
Portland cmt. 1 min	D + sp	w/c = 0.41	150	<1.0	+ + + + +	5-100	10^{-5}
" 3 min	D + sp	"	"	2.7	+ + + + +	"	"
" 5 min	D + sp	"	"	5.6	+ + + +	5-20	$3 \cdot 10^{-5}$
" 10 min	D + sp	"	"	12.6	+ + +	"	$5 \cdot 10^{-5}$
" 20 min	D + sp	"	"	+80	+	5-10	10^{-4}

value, i.e. between 30 and 85 KPa for the 50/50 mixture in the 100 micron slot, probably as a result of the quartz particles interacting with the walls of the slot.

A higher content of quartz (70%) does not seem to raise the critical pressure for piping but appears to have the negative effect of increasing the erosion rate of the gel once piping has taken place. The channels formed in conjunction with piping become rather wide and significant erosion and transport of particles takes place in them at comparatively low flow rates (10^{-5} m/s).

Pure clay gels saturated with Forsmark water appeared to show a slight decrease in critical pressure for piping. Significant erosion occurred at rather high flow rates (10^{-4} m/s), yielding erosion with aggregates sized 30 to 100 microns.

Spontaneous dispersion in distilled water

The position of the Tixoton/quartz gel front, was not found to have changed significantly one month after application. However, slight dispersion made the initially sharp front fluffy, while the gel behind the front become largely homogenized in this period.

Synthetic Forsmark water changed the character of the Tixoton/quartz gel considerably. A high frequency of microfractures was developed in the front zone and this led to the release of very large aggregates into the free volume of distilled water. The gel volume had also decreased slightly in the slot.

The pure Tixoton gels responded in the same way in contact with Forsmark water. In slots filled with distilled water the front part of the gel became very soft due to dispersion into the free volume of distilled water.

4.3.3 Cement

4.3.3.1 Scope of study

A series of investigations was made with cement in contact with flowing water for determination of the erodability, and with a successively increased water pressure in percolation tests for investigation of the critical water pressure for causing piping in the gel.

4.3.3.2 Experimental set-up

The same equipment and test strategy have been used for the cement gels as for the previously described clay gels (cf Chap. 4.3.2.2)

Gel front behavior

The investigations concerned Portland cement with a water/cement ratio of 0.41 and with 1.5% superplasticizer. The observations were made 1, 3, 5, 10 and 20 minutes after initial mixing (Table 17).

The erosion at the gel front was found to be extensive during the first 5 minutes, thereafter decreasing significantly and being very limited after 20 minutes. The critical flow rates were found to be between 10^{-5} and $5 \cdot 10^{-5}$ m/s for the period 1-10 minutes after mixing and $> 10^{-4}$ m/s after 20 minutes (Table 17).

- Practically all the components in the cement grout were affected by erosion during the initial phase. Thereafter, only minute particles, 5-15 microns in size, were ripped off as the hydratization process proceeded and larger integrated hydrated aggregates were formed. Only discrete, very small particles were eroded after 20 minutes.

Piping

The pressure, which was increased gradually as the hydration proceeded reached a critical level that was very low in the first 5 minutes (Table 17). The piping channels were generally several millimeters wide and they increased rapidly by erosion.

4.3.4 Preliminary conclusions

The following preliminary conclusions were drawn:

* The Tixoton/quartz (50/50) mixture was found to exhibit the highest piping resistance. Higher amounts of quartz in the mixture were found to have a negative effect on the erodability, while the critical piping pressure was still high.

* Pure Tixoton gels, with a water content below about 1500%, were the most erosion-resistant materials with the exception of fully hydrated cement gels.

* Clay gels saturated with synthetic Forsmark water and brine were more easily affected by piping than fresh-water clays. This property is probably only typical of very soft gels with an insignificant shear strength. The erosion was characterized by the release of large aggregates.

* The cement has been found to be very sensitive to piping and erosion during the initial 10-15 minutes of hydration. After this period the cement is hardly affected by water flow rates of up to 10^{-3} m/s along the gel front, and by water pressures of up to about 80 kPa at percolation.

CHAPTER V PILOT FIELD TEST

1 INTRODUCTION

A first attempt to test the efficiency of fracture sealing was made in 1985 at the Tunnel Plug test site at Stripa. It verified that sets of long-extending fractures can be completely sealed and that bentonite grouts with a water content equal to the liquid limit resists water pressures of about 1 MPa. Leakage made it impossible to measure the amount of injected clay accurately and the penetration depth could therefore not be determined with any certainty.

The successively improved injection equipment required testing as part of the preparation of the Pilot Field Test and this pre-test was conducted in Öved, Skåne, in November, 1987. For this test ϕ 86 mm holes with a length of 5 m were drilled in granite, and grouting was made of fine-grained Canadian Portland cement + 10 % silica fume + 1.1 % (dry weight) superplasticizer, w/c being 0.425, using a 40 Hz grouting machine. The main purpose of the test was to check the function and the robustness of the technical equipment, the major conclusions being:

* The injection device is durable at high pressures and operable under field conditions without any leakage even at high pressures. However, it needs to be altered so that the pressure can be controlled much more carefully and recharging made in a few seconds. The absence of leakage means that the amount of injected grout can be accurately determined. It was 0.8 litres in this test.

* Core drilling close to the injection hole showed no coherent cement filling in any of the fractures that intersected the hole, indicating that the pressure had not significantly expanded the fractures. Thus, the grout appeared to have been forced in a finger-like pattern into fractures with an estimated aperture varying between 0 and 200 μm. The volume of the grout that had entered the rock implies that one or a few of the "channels" got filled to several meters distance from the injection hole.

* Despite an unexpected 6 min interruption of the injection procedure, the tested cement slurry was sufficiently liquid to flow in swiftly. With a larger capacity of the grout cylinder and very much faster recharging, the time-dependent increase in viscosity can be minimized and the penetrability improved even more.

The test gave very valuable experience for the planning and performance of the Pilot Test in Stripa. In particular, the use of Lugeon testing for evaluation of approximate fracture apertures and for prediction of grout penetration turned out to be very useful.

2. DESCRIPTION

2.1 PURPOSE

The scope was fourfold:

* To test the sealing efficiency of grouting fine fractures using the dynamic injection technique and clay-based as well as cement grouts

* To verify how far and uniformly the grouts enter fractures

* To check the effect of injection pressure on the efficiency of grout penetration and on fracture response

* To check the general validity of the grout flow theory

2.2 OUTLINE OF THE TEST

Grouting was planned to be made in four 1.5 m long boreholes, by which sealing of shallow rock would be tested, and in two similar 7 m long holes, as well as in two 40 m long ones.The longer holes allowed for higher injection pressures but not for extraction of the rock for identification of the penetration paths. This was planned for the short holes. A seventh 5 m long hole was used for checking the flow model and this hole was instrumented for pressure measurements in the course of sealing. All holes had a diameter of 76 mm.

2.3 TEST STRATEGY

A major point is that the field test should not be a competition between different types of grouts but instead demonstrate that there are different means of sealing fractures of different widths and character by using suitable techniques.

The character of the fracture pattern is a determinant of the potential success of the sealing operation. The rich fissuring of shallow, peripheral rock around a blasted tunnel or shaft suggests that such rock is best sealed by systematic injection in several short boreholes. In the Stripa pilot test the special condition of choosing a site for the short holes that allows for break-up of the rock for identifying the grout was, however, of equal importance. Therefore, planar suitably oriented fractures of long extension should be selected since rock blocks can be removed systematically along such fractures. Naturally, they also offer good oppertunities for identifying injected grout.

The intention was that the four short holes should be located so that one of them would contain relatively wide fractures (100-200 μm eq. ap.), while two of them should represent narrow, i.e. 50-100 μm fractures, and one should hold even thinner fractures.

As to the 7 m holes the same strategy was adopted. Thus, a planar fracture of long extension should be selected and the location of the holes selected so that they contain narrow as well as wider fractures.

The 40 m long holes were included mainly because grouting them would offer a check of the grout flow model. It was required that they do not contain any wide fractures.

2.4 SITE CHARACTERIZATION

The Time Scale area was used for the testing (Fig V:1). The two 76 mm, 40 m long inclined holes S1 and S2 that were drilled in conjunction with LBL:s field research prior to 1980, were used as "long" holes, although it was clear from the available flow data that they are not intersected by significantly water-bearing fractures. The shorter holes were located in the Time Scale primarily because this drift was known to be relatively "wet" and because the rock structure was concluded to be typical of what can be expected in a repository in granite at depth. Thus, we see

from Fig V:2 that there is a set of steeply oriented major fractures, and local flat-lying series of fracture sets.

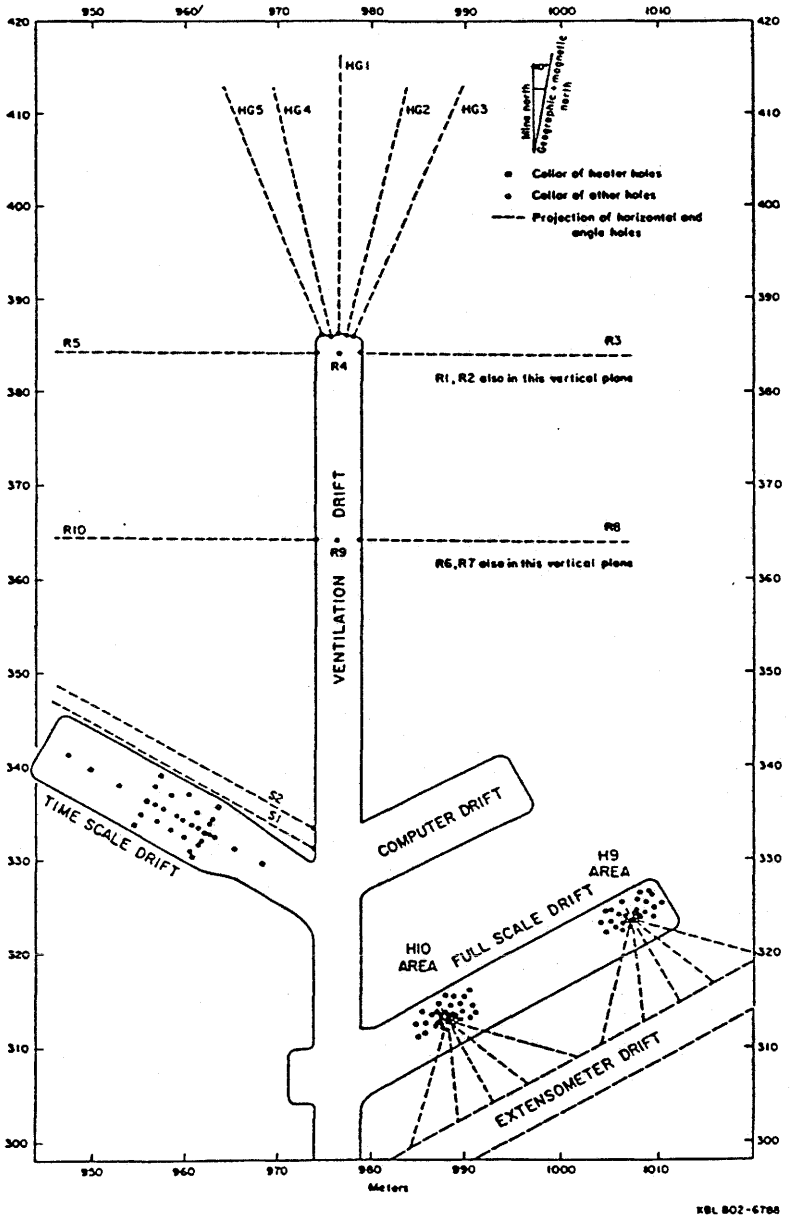

Fig V:1. Plan view of the test drifts, BMT, Time Scale and Full Scale

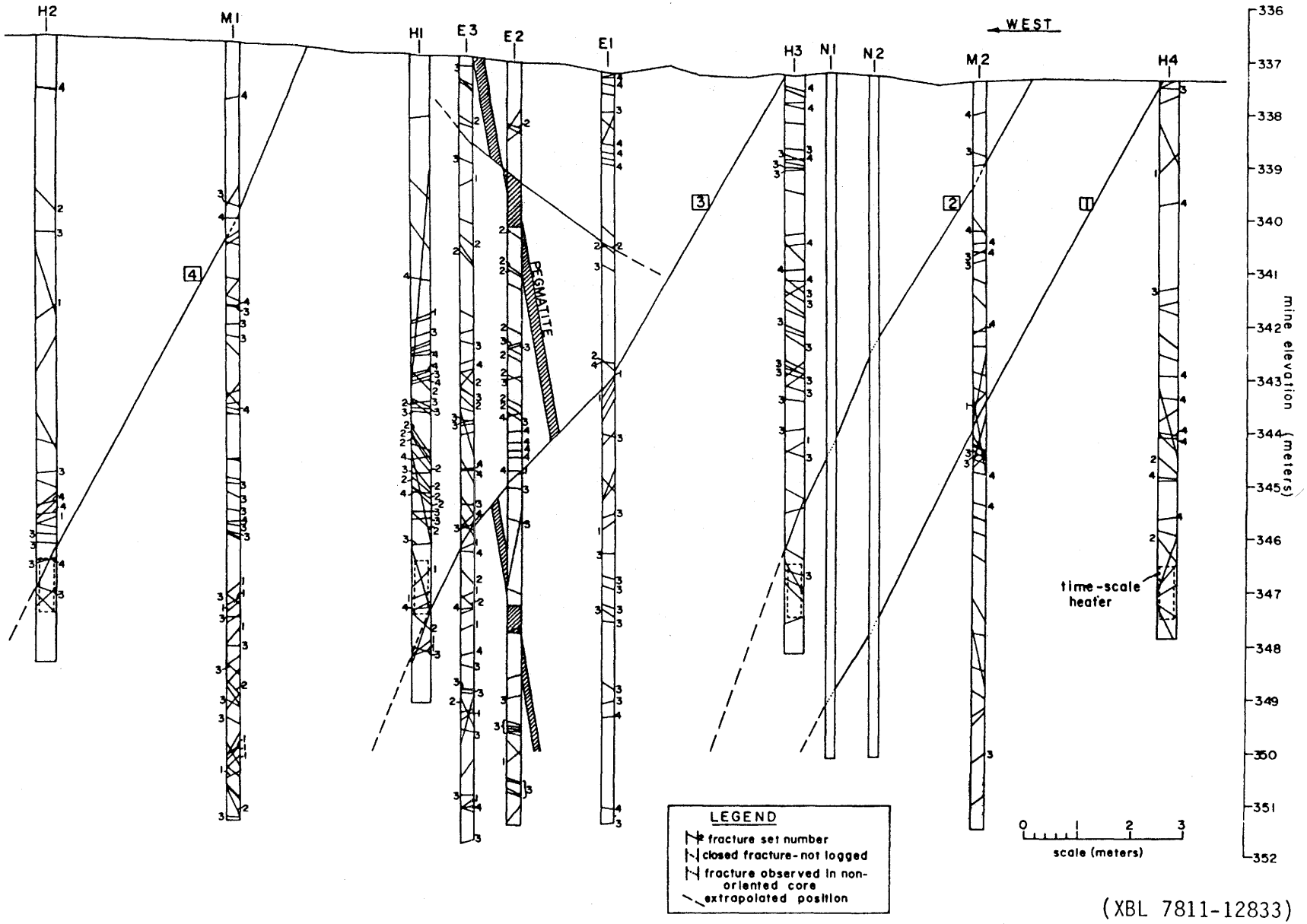

Fig V:2. Centerline profile through Time Scale experiment, showing major subsurface features: Borehole widths not to scale (After LBL).

The holes were placed rather close to one of the steep chlorite-coated fractures at a distance that would imply intersection by the holes at 1-3 m depth. The arrangement is indicated by Fig V:3. As concluded from Fig V:2 it was expected that the degree of fracturing should be very moderate at the tunnel floor, but the often observed phenomenon of richly fissured rock close to periphery of blasted excavating was found also here. It will be documented in the subsequent text.

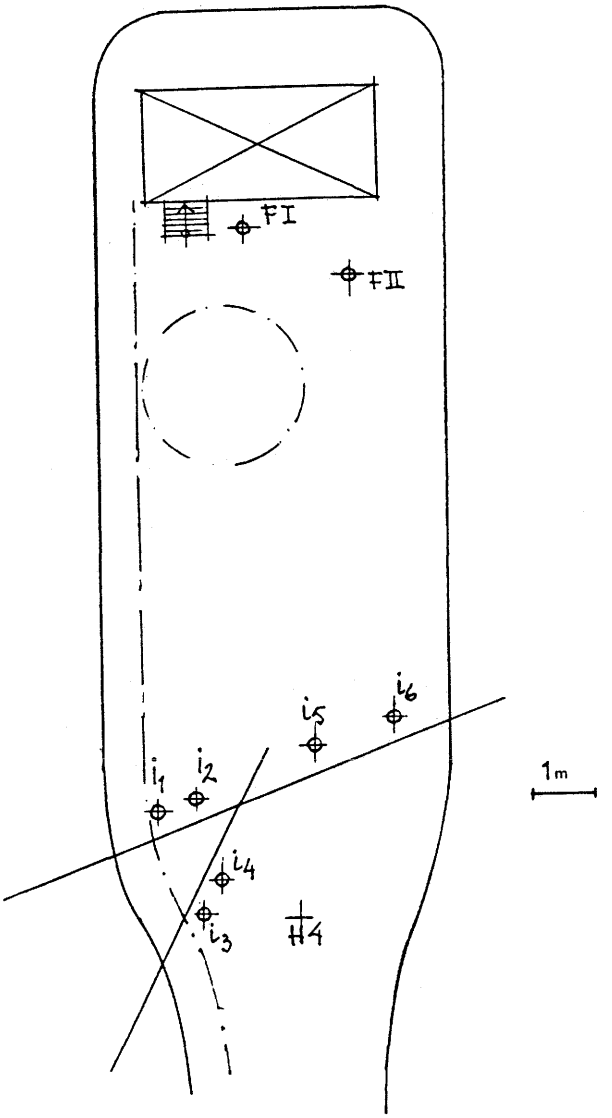

Fig V:3. Location of grouting holes in Time Scale

The major data of the boreholes, which were all core-drilled with 76 mm diameter, and almost vertical except for S1 and S2, are given in Table 18.

Table 18. Borehole data

Borehole	Depth, m
i1	1.5
i2	1.5
i3	1.5
i4	1.5
i5	7.0
i6	7.0
S1	~40
S2	~40

2.5 TEST PROGRAM

2.5.1 General

The test program comprised the following steps:

Activity

1 Core drilling

2 Application of reference bolts for measurements of heave and lateral displacements caused by the groutings.

3 Inflow measurements (S1 and S2)

4 Core mapping

5 Lugeon testing

6 Evaluation of fracture geometry

7 Prediction of grout penetration

8 Grouting
a) application of packer at 0.5 m depth (0,7 m in hole i4)
b) grout injection
c) shut-off reading of grout pressure decay

9 Removal of grout from the holes by core-drilling
10 Lugeon testing
11 Inflow measurements (S1 and S2)
12 Excavation of rock for identification of the location of the grout

2.5.2 Borehole drilling, core mapping

2.5.2.1 Drilling

Drilling technique

At six preselected positions (i1-i6), 76 mm holes were drilled more or less vertically to various depths, penetrating distinct fractured zones of the granite. i1-i4 were drilled to approximately 1.5 m, while i5 and i6 were drilled to 7.0 m depth. The coring was performed by use of a hydraulic Diamec 260 equipment.

The drilling was successful but the precence of closed fractures that "opened" in the course of the drilling occasionally yielded fragmented core sequences. This led to difficulties in the evaluation of the degree and amount of closed and open fractures over certain intervals.

2.5.2.2 Core descriptions

Borehole i1

Lithology

0-51 cm: Grey to reddish grey, coarse-grained granite rich in biotite. Heavily fractured in the upper 30 cm, caused by blasting during construction of the tunnel.

51-71 cm: Brecciated section composed of granite fragments embedded in chlorite mineralized matrix. Pyrite and chalcocite occur frequently, the basal 5 cm of the section being significantly rich in chlorite.

71-150 cm: Slightly reddish medium and coarse-grained granite. Chlorite-sealed microfractures are common.

Fractures

Apart from the upper 30 cm and the frequently occurring closed microfractures there is probably only one fracture that can be interpreted as being open, ie i1:3 at 70 cm depth (Fig V:4). This fracture dips 65 degrees and contains variable amounts of chlorite and calcite. It does also constitute the boundary between the brecciated zone and the underlying granite and strikes N10°W across the tunnel. i2, i5 and i6 also intersect this distinct fracture.

Borehole i2

Lithology

0-77 cm: Grey to slightly reddish grey coarse-grained granite which becomes brecciated in the basal part of the interval and is also significantly richer in chlorite. The brecciation ends abruptly with the same distinct fracture as in i1.

77-155 cm: Slightly reddish medium grained granite with numerous chlorite enriched subparallel bands and sealed fractures.

Fractures

In the upper 77 cm there are only microfractures which have a limited lateral extension, presumably only in the immediate vicinity of the borehole. The most distinct fracture is located at 77 cm depth, i.e i2:8 (Fig V:4). This corresponds to the same fracture as the one found in i1, i.e i1:3. Deeper lying fractures are interpreted as being closed. i2:12 can possibly be slightly open.

Borehole i3

Lithology

0-155 cm: Massive grey to slightly reddish coarse grained granite contaning only a few fractures. The upper 95 cm being massive except for the blast-induced fractures in the uppermost 20 cm.

Fractures

Above 95 cm depth there are hardly any natural fractures. The granite is very massive in the drilled section except for the main fracture at 95 cm depth, i.e. i3:13a (Fig V:4). It dips 50° and strikes N80°E. The fracture plane is irregularly covered by chlorite, epidote and calcite. Still it has a relative smooth surface.

Borehole i4

Lithology

0-150 cm: Grey to slightly reddish coarse-grained granite, rich in biotite. Higher frequency of chlorite enriched microfractures than in i3, especially in the interval 45-90 cm.

Fractures

In total there are 7 significant fractures in the cored section, not including the fractures found within a crushed zone at 77-90 cm and the uppermost fractures produced by blasting. The fractures are interpreted to be more or less open. However, the most distinct fracture occurs at 92 cm, i.e. i4:25 (Fig V:4), which is identical to the i3:13 fractue in the previously described borehole. The basal 45 cm of the borehole does not contain any significant, open fractures.

Borehole i5

Lithology

0-700 cm: Grey to reddish grey, medium to coarse-grained granite containing varying amounts of dark minerals, mainly biotite. Common chlorite-enriched streaks and bands.

Fractures

The cored sequence is characterized by numerous chlorite-sealed subparallel microfractures dipping 25-45 degrees. The lateral extension of these fractures is very limited, they probably exist only in the near vicinity of the borehole. Open and more distinct fractures are found at 62, 85, 110 and 270 cm depth, i.e. i5:31,

i5:32, i5:34 and i5:45 (Fig V:5). However, it is plausible that some of the fractures interpreted as closed may be partly open, since the core was probably broken in the course of coring.

Borehole i6

Lithology

0-70 cm: Grey to reddish grey, coarse-grained granite containing an increasing amount of dark minerals towards the basal part.

70-225 cm: Dark grey to greenish grey fine-grained, partially brecciated section containing a large amount of dark minerals and mineralized bands of chlorite.

225-450 cm: Reddish coarse-grained granite containing numerous closed fractures. Fracture fillings mainly consist of chlorite, calcite and epidote.

450-700 cm: Grey to slightly reddish grey coarse-grained granite containing a few chlorite sealed fractures and enriched bands.

Fractures

The upper 150 cm contains a total of 10 fractures of which at least one or two are open in the interval 50-85 cm, i.e. i6:73-77 (Fig V:5). The major fracture, intersecting the whole tunnel is found at 118 cm depth, i.e. i6-79. It is strongly mineralized with chlorite and therefore not open, at least not in the penetrated section. Beside these, there is only one additional fracture, most likely open, in the borehole, i.e. i6:86 at 290 cm depth. Numerous subparallel 35-50 degrees dipping chlorite-sealed microfractures and lineaments are found in the remaining part between 290 and 700 cm. None of these can be considered to be open to any significant extent.

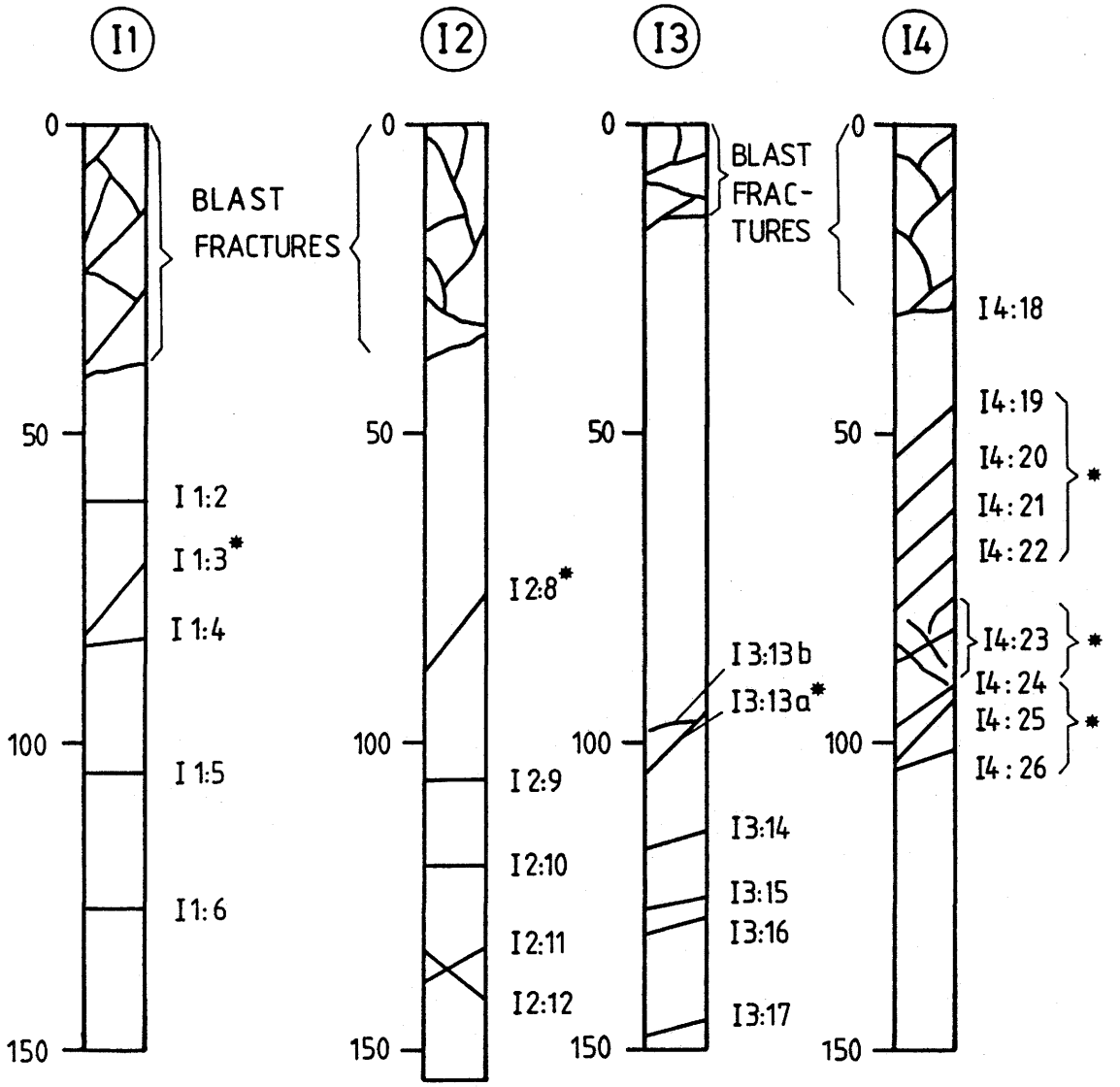

Fig V:4. Fracture-plot of boreholes i1-i4
* Interpreted conductive open fracture or zone.

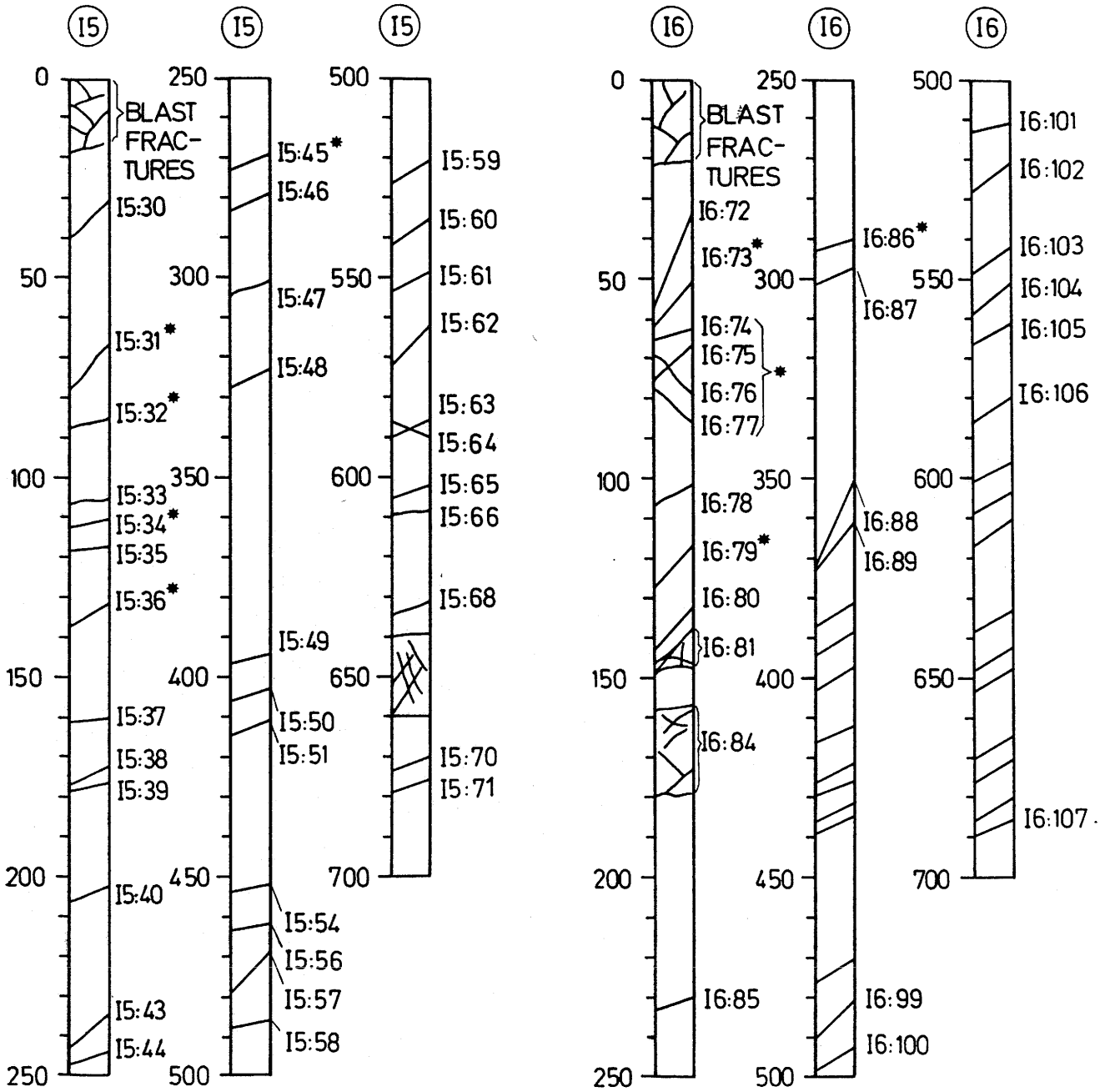

Fig V:5. Fracture-plot of boreholes i5 and i6
* Interpreted conductive open fracture or zone.

2.5.3 Lugeon testing and inflow measurement

In order to be able to locate the water-bearing fractures and estimate the aperture of those fractures that were concluded to be water-bearing according to the core mapping, Lugeon tests and inflow measurements have been made in the boreholes.

Inflow measurements

The primary aim of inflow measurements before and after grouting was to get a simple check of the sealing effect. The measurements involved recording of the rising of the water level in the initially dry holes as a function of time. A week after injection the bentonite and cement were removed from the holes by drilling, using the same equipment as at the core drillings, and the inflow measurements were then repeated.

The rate of inflow decreased with time, an average of the measured inflow during the first 10 hours before injection being shown in Table 19.

Table 19 Results from inflow measurements before grouting

Borehole	Depth m	Inflow, l/h
i1	1.5	0.029
i2	1.5	0.230
i3	1.5	0.200
i4	1.5	23
i5	7.0	23
i6	7.0	0.35

Lugeon testing

The aim of Lugeon testing was to estimate the hydraulic fracture aperture of the groutable fractures in order to form a basis of the predictions of the grout inflow.

The technique used at Lugeon testing was the following: The water-filled hole is sealed by a mechanical packer penetrated by two pipes. One of the pipes is connected to a water tank via a flow measuring device and a regulator. The water tank is pressurized by nitrogen gas. The other pipe is connected to a pressure transducer. The pressure and flow measured by the transducers are then recorded by a plotter.

All 6 short injection holes were tested by this method. In all the holes the packer was first placed 0.5 meters below the rock surface. In some holes the measurement was then repeated at other packer locations in order to get a more detailed picture of the distribution of the hydraulically active apertures.

In the present tests a simplified method was used in which the pressure was adjusted until steady flow was reached. The tests where thus run only during a short time. This simple technique is justified by the short injection time meaning that only the response from a short distance is of interest.

The applied pressure varied between 0 and 280 kPa depending on the rate of inflow, which varied between 0 and 0.3 liters per minute. The applied pressure (p), the measured inflow (Q) and the calculated average hydraulic conductivity of the rock (k) are shown in Table 20.

The average hydraulic conductivity is deduced from Eq.(72):. -

$$k = \frac{Q}{\Delta p \cdot L}\left(\frac{1 + ln\,(L/D)}{2\pi}\right) \qquad (72)$$

where L = length of the borehole (m)
D = diameter of the borehole (m)
Q = inflow (m^3/s)

As shown in Table 20 the rock type varied very much, ranging from almost impermeable fracture-free rock (i1) to highly fractured rock (i4).

Table 20. Results from the Lugeon tests.

Borehole	Depth m	Δ_p (m)	Q (l/m)	k (m/s)
i1	0.5-1.5	16.2	0	$<5\cdot10^{-12}$
i2	0.5-1.5	15.6	0.0052	$3.6\cdot10^{-4}$
i3	0.5-1.5	23.0	0.0043	$2.1\cdot10^{-9}$
i4	0.5-1.5	0	0.294	$>10^{-5}$
	0.7-1.5	0.54	0.289	$7.6\cdot10^{-6}$
	0.9-1.5	2.16	0.283	$2.5\cdot10^{-6}$
	1.1-1.5	24.3	0.0001	$1.2\cdot10^{-10}$
i5	0.5-7	0.54	0.261	$8.4\cdot10^{-7}$
	0.9-7	27.8	0.0001	$6.7\cdot10^{-12}$
	3-7	27.0	0.0001	$1.0\cdot10^{-11}$
	5-7	24.3	0	$<5\cdot10^{-12}$
i6	0.5-7	22.1	0.0034	$5.9\cdot10^{-9}$
	0.9-7	28.1	0.0002	$3.7\cdot10^{-10}$
	3-7	27.0	0	$5\cdot10^{-12}$

2.5.4 Evaluation of fracture geometry

The core mapping, Lugeon testing and inflow measurements have formed the basis for evaluation of the location and geometry of groutable fractures intersecting the boreholes. Most of the water flow could be identified to take place through a few fractures, all large ones being situated within 1 m distance from the tunnel floor. Since it was decided that no grouting was to be made in the upper 0.5 m, only the fractures below 0.5 m depth were considered.

The actual geometry of the fractures is of course difficult to estimate on the basis of these measurements, their probable shape being archipelago-like.

Due to the largely unknown geometry, three different possible fracture models have been considered. The basic one is the classical parallel-plate model, in which the hydraulic fracture aperture can be determined by Eq. (73) which is derived

from Navier-Stokes equations of motion.

$$e_f = \sqrt[3]{\frac{12\mu k L}{g\rho}} \tag{73}$$

where e_f = fracture aperture (m)
μ = dynamic viscosity of water (Pas)
k = average hydraulic conductivity (m/s)
L = studied length (m)
ρ = density of water (kg/m3)

The second case refers to the conditions in which the water is transported between parallel plates with limited width. This case can also be an approximation of an archipelago-like fracture. The formula for the fracture aperture d_f in this case is identical to Eq. (73) except that the relation between the fracture width b and the diameter of the borehole a is included.

$$d_f = \sqrt[3]{\frac{12\mu k L}{g\rho}\,\frac{a}{b}} \tag{74}$$

The relation b/a can also be considered as the relation between the open and total area of the fracture.

The third possible fracture geometry is tube-like openings that can exist where two "impermeable" fractures intersect. The flow can be expressed by equations used for circular tubes, leading to Eq.(75)..

$$r_f = \sqrt[4]{\frac{8\eta\mu k L r_b}{g\rho}} \tag{75}$$

where r_f = tube radius (m)
r_b = borehole radius (m)

All probable fractures have been hydraulically interpreted according to these three geometries (Table 21).

Table 21. The possible geometries of the estimated water-bearing fractures in the boreholes

Bore-hole	Level (m)	Number of fractures	Inclination of fractures	Fracture aperture (μm)		
				e_f	d_f	r_f
i1	-	-	-	<2	<6	<18
i2	0.8	1	35°	20	60	180
i3	0.95	1	45°	16	50	160
i4	0.6	4	45°	100	250	500
	0.8	3	-	100	250	500
	0.95	2	45°-60°	100	250	500
i5	0.7	1	35°	180	450	700
	0.85	1	65°	180	450	700
i6	0.6	3	25°	40	100	250
	0.8		45°			
	2.9	1	75°	16	50	160
S1	every 2 m			<12	<38	<130
S2	every 2 m	1		<12	<38	<130

No Lugeon tests were made in holes S1 and S2. Instead, measurements made by Gale and Witherspoon (1979) were utilized. The fracture apertures in Table 21 are of course very approximate since they are based on idealized geometries, but they still illustrate the actual order of magnitude. The data were used as a basis of the grout inflow calculations.

Beside the fractures accounted for in Table 21 there are some with $e_f < 10$ μm which are left out of the calculations. Holes S1 and S2 have no large fractures.

2.5.5 Prediction of grout inflow

The fracture geometries in Table 21 have served as a basis for prediction of the grout penetration depth into each fracture, and of the amount of penetrating grout into fractures over the full length of each borehole.

Firstly, the expected pressure amplitude and frequency in the borehole must be determined. Calculations and measurements in connection with the slot injection tests have shown that the pressure amplitude is 3-5 MPa in the pipe connected to the machine. The pressure waves are quite irregular but can be approximated by a sinusoidal curve with a frequency between 40 and 200 Hz.

The inner tube diameter is 2.5 cm while the diameter of the boreholes is 7.6 cm. This widening of the area will decrease the amplitude of the pressure by a factor δ according to Eq. (76)

$$\delta = \frac{2}{1 + \frac{A_2}{A_1}} \qquad (76)$$

where A_2/A_1 is the ratio between the borehole area and the tube area. Thus the amplitude will be only 20 % of the original, i.e. to 0.6-1.0 MPa.

The change in amplitude along the borehole can be calculated according to Eq (35) in Chapter III. Sensitivity analyses of the effect of changes in frequency and borehole length show that at short holes (1 m) there will be no decrease in pressure amplitude in the range 40 Hz $< f <$ 200 Hz but rather an increase. At longer holes the attenuation is very much a function of the frequency. As an example the calculated attenuation at the 5 meter test hole in Stripa is shown in Fig V:6.

The figure shows that at low frequencies, the amplitude is strongly increased while at high frequencies the amplitude can be significantly decreased at certain levels. The real pressure wave is, as mentioned, a mixture of different frequencies meaning that it is difficult to predict the actual pressure distribution. However, on the basis of the performed calculations, it is logical to believe that the variations in amplitude must be moderate. In future calculations it is therefore assumed that there is no change in amplitude along the borehole, as confirmed also by the measurements in the 5 m test hole.

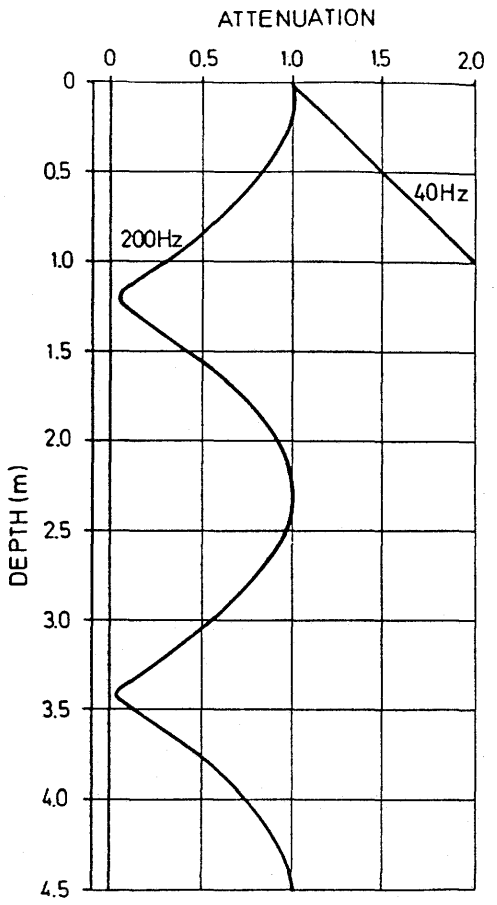

Fig V:6. The calculated attenuation in the test hole in Stripa at two different frequencies.

Once the amplitude of the pressure wave in the fracture opening is known it is possible to calculate the rate of the penetrating grout front according to Eq. (53) and the amplitude of the oscillating shear strain according to Eq. (45) in Chapter III. These calculations are made using the following parameter values:

m = 1.0 Pa (bentonite)
m = 0.17 Pa (cement)
n = 1
E_v = $2.1 \cdot 10^9$ Pa
E_r = $5 \cdot 10^9$ Pa
h_1 = $2 \cdot 10^6$ Pa (static pressure)
h_o = $5 \cdot 10^5$ Pa (dyn pressure ampl.)
w = 251 s^{-1}
ρ_v = 1100 kg/m^3 (bentonite)
ρ_v = 1900 kg/m^3 (cement)
d = the fracture aperture from Table 21

As mentioned in Chapter IV the major problem in making the calculations is the change in oscillating strain at increased penetration depth and the dependence on the initial value of *m*. In the present calculations the same technique has been utilized as in the slot injection tests meaning that the values of *m* and *n* at the oscillating shear deformation $\gamma = 1.0$ have been applied. The penetration depth L_1 and the penetrating volume *V* were calculated for the three fracture geometries discussed in Chapter V:2.5.4. The total volume of expected grout inflow in each hole is also shown in Table 22.

Table 22. The calculated penetration depth and the inflow volume of the fractures treated in Table 21

Hole	L_1 cm			V cm^3			Materiel
	e_f	d_f	r_f	e_f	d_f	r_f	
I 1	3	8	70	0.016	-	-	Bentonite
I 2	28	90	360	4.8	5.3	11.5	Bentonite
I 3	64	160	880	21	13	54	Cement
I 4	400	1100	3000	20 dm^3	16 dm^3	27 dm^3	Cement
	400	1100	3000	15 dm^3	12 dm^3	21 dm^3	
	400	1100	3000	10 dm^3	8 dm^3	14 dm^3	
ΣI 4				45 dm^3	46 dm^3	62 dm^3	
I 5	760	1600	4000	65 dm^3	28 dm^3	32 dm^3	Cement
I 6	56	170	560	120	140	200	Bentonite
	64	160	880	21	13	54	
ΣI 6				141	153	254	
S 1	40	130	800	5	6	27	Cement
ΣS 1				100	120	540	
S 2	15	36	250	1.1	0.5	2.7	Bentonite
ΣS 2				22	10	54	

3 RESULTS OF GROUTING TESTS

3.1 MEASURED GROUT INFLOW AND PRESSURE RESPONSE

Grout flow

The different grouts used at the grouting test were:

a) Pure Tixoton: Tixoton bentonite, w = 790 % (= 1.5 w_L)
b) Tixoton/quartz: 50 % Tixoton / 50 % quartz filler, w = 400 % (= 1.6 w_L)
c) Cement: Cement+10 % Silica Fume+1% Super Plasticizer, w/c=0.36

The percentage of CSF and SP and the w/c are expressed as parts of the total dry weight of cement and CSF. The percentage of Tixoton and quartz and the water content is expressed in terms of the total dry weight of Tixoton and quartz. Table 23 shows the main data of the grouting phase of the experiment.

At the grouting of holes i4 and i5, where refill of the grout cylinder (described in Chapter IV:3.3.1) was needed, outflow of cement grout from the tunnel floor was observed. At i4 the first outflow was seen after the first restart and at i5 the first outflow was seen immediately after the injection start (Fig V:7).

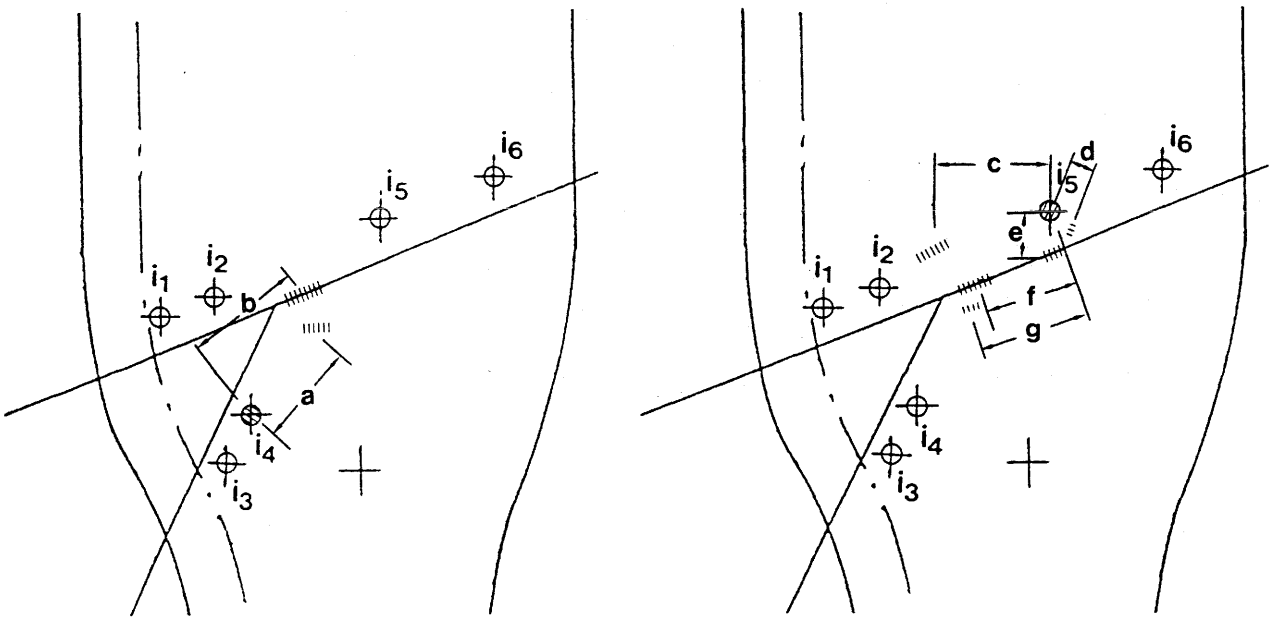

Fig V:7 Observed outflow of cement grout on tunnel floor during injection Left: hole i4, a=130 cm, b=165 cm. Right: hole i5, c=190 cm, d=4 cm, e=57 cm, f=175 cm, g=210 cm

Table 23 Data from the groutings

Hole	Grout	Injection time (sec)			Piston movem (cm^3)	Compr (cm^3)	Estimated grout inflow (cm^3)
		P1[1]	P2[1]	P3[1]			
i1	Pure Tixoton	25	25	20	37	>5	5-25
i2	Tixoton/quartz	25	5	50	29	>5	5-25
i3	Cement	15	10	40	76	>5	40-70
i4	"	13[2]	-	-	5055	>5	~ 5 dm^3
i5	"	5[3]	-	-	6754	>20	~ 6.5 dm^3
i6	Tixoton/quartz	25	10	45	127	>20	70-100
S1	Cement	-	-	65	461 -50[4]	>200	50-200
S2	Tixoton/quartz	-	-	65	633 -450[5]	>200	0

1) Different pressure levels, explained below
2) Cylinder refilled three times
   Injection times: 0.2 + 4.0 + 4.5 + 4.5 = 13.2 sec
3) Cylinder refilled four times. Each injection took less than 1 second. Total injection time: abt. 5 sec
4) Packer moved 12 mm out of hole (= 54 cm^3)
5) Packer moved 100 mm out of hole (=454 cm^3)

For each injection hole the following data are listed: type of grout, injection times at each pressure level, total piston movement during injection, compression in inlet valve and hole due to incomplete filling and estimated volume of injected grout.

Pressure response

Typical pressures during injection for the three different pressure levels used (P1, P2, P3) are:

P1: P_{stat} = 1.1 MPa, P_{dyn} = 2.5 MPa, P_m = 1.3 MPa, F = 50 Hz.
P2: P_{stat} = 2.8 MPa, P_{dyn} = 3.0 MPa, P_m = 3.0 MPa, -"- .
P3: P_{stat} = 3.3 MPa, P_{dyn} = 3.5 MPa, P_m = 3.5 MPa, -"- .

Where P_{stat} is the static pressure level, P_{dyn} is the dynamic peak height from the static level and P_m is the mean pressure level.

Examples of pressure recordings from the injections are shown in Figs V:8-9.

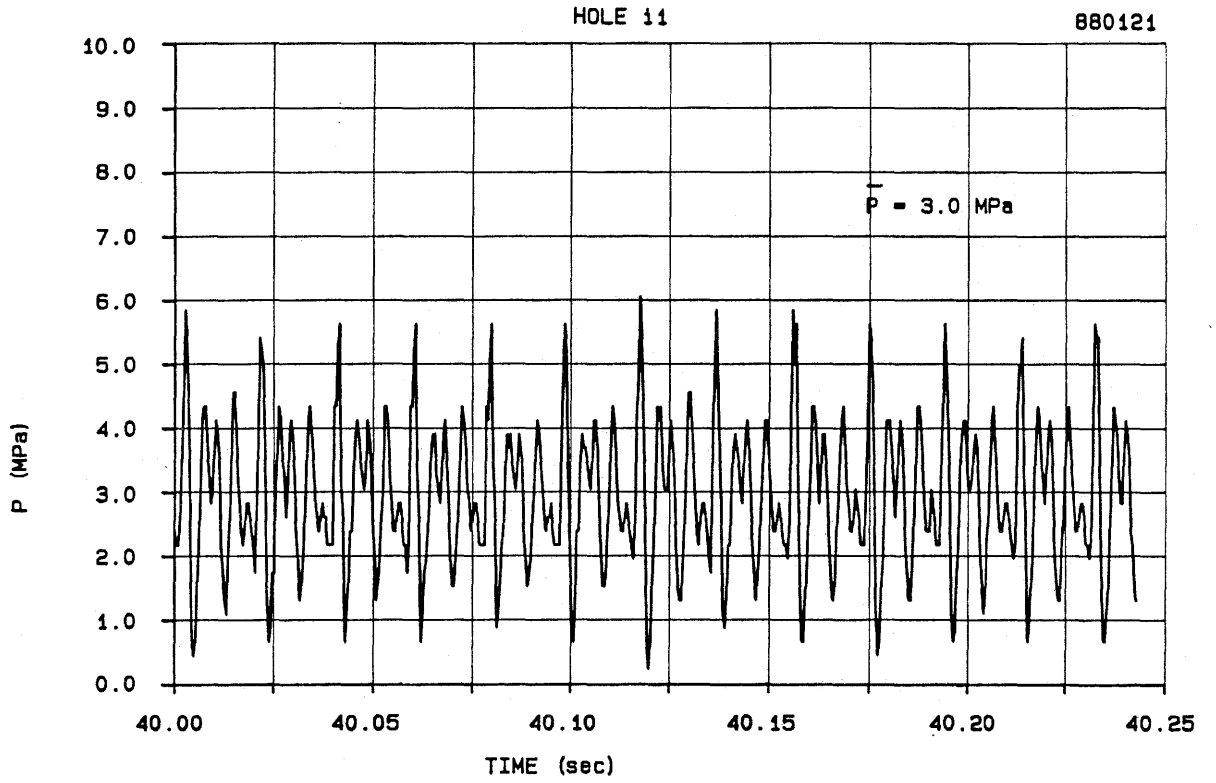

Fig V:8 Pressure recorded during grouting of hole i_1. Pressure level P_2

During the grouting of one hole, all the others were water-filled and sealed off by a packer at the top with a pressure gauge attached. No pressure response was noticed in any of the neighboring holes, however. Immediately after the grouting of each hole a pressure gauge was attached to the injection point and the pressure decline after injection recorded. The results are listed for all injection holes in Fig V:10. For holes i4 and i5 there was no pressure observed. In hole i1 the pressure dropped to zero during night, when no observations were made, and for hole S2 the pressure stabilized at about 0.5 MPa, being the ambient groundwater pressure.

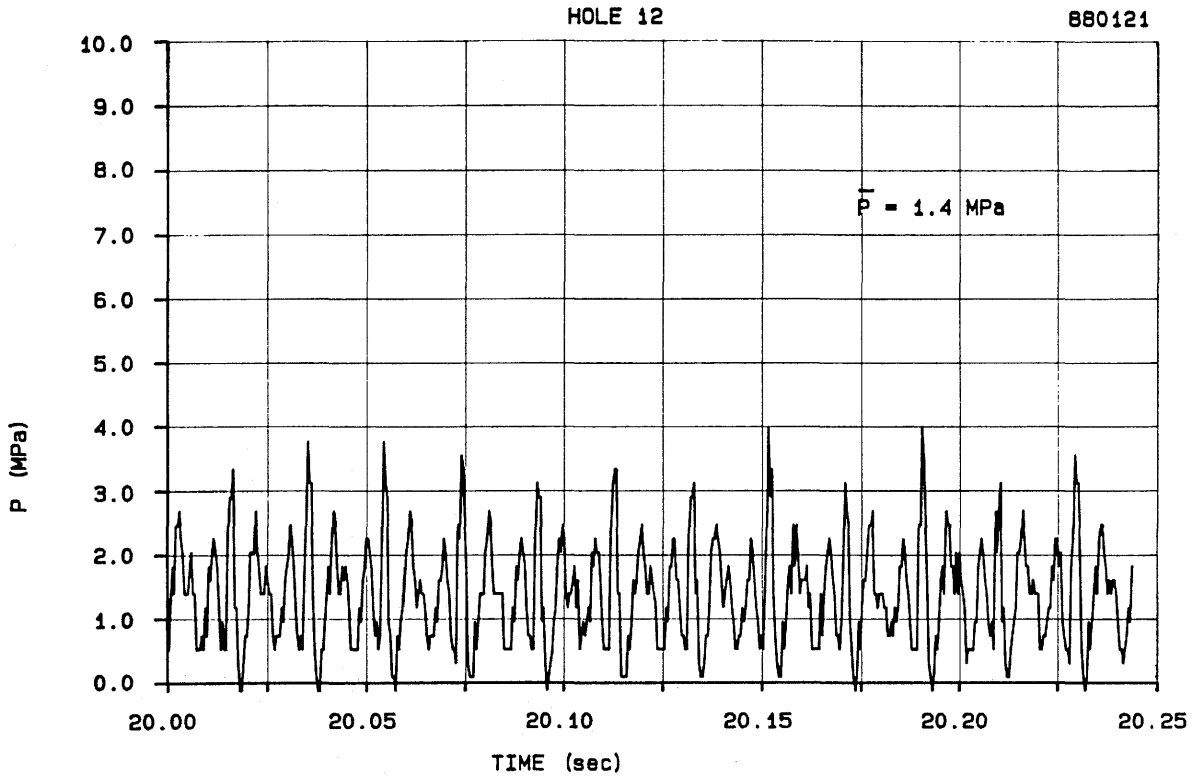

Fig V:9 Pressure recorded during grouting of hole i2. Pressure level P_1

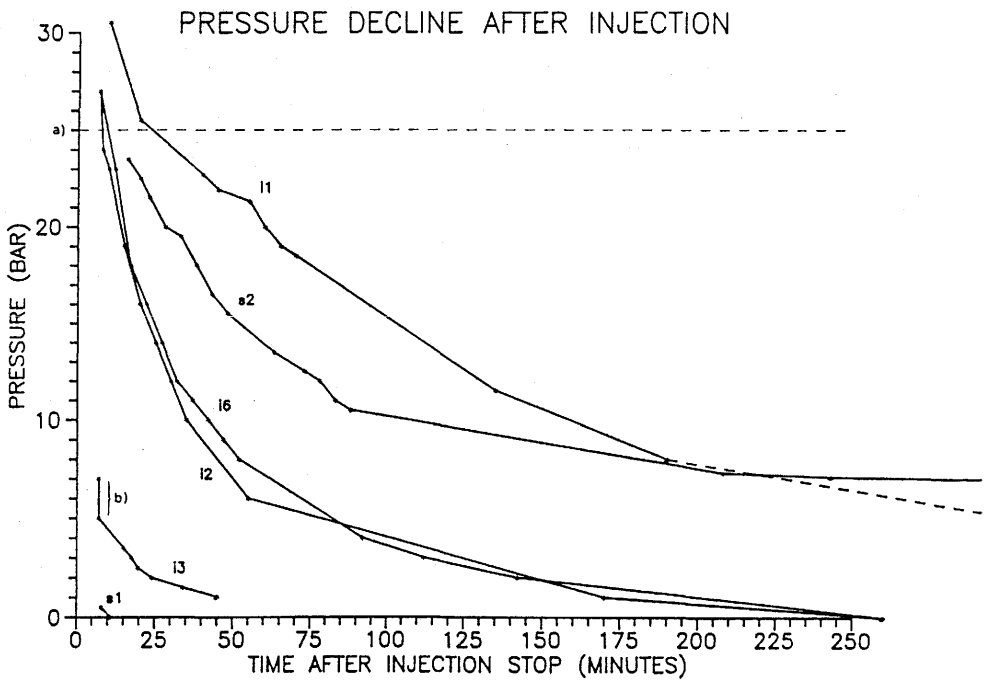

Fig V:10 a) All pressures exceeding 2.5 MPa (scale max) are estimated.
b) Leakage at pressure gauge.

Rock deformations

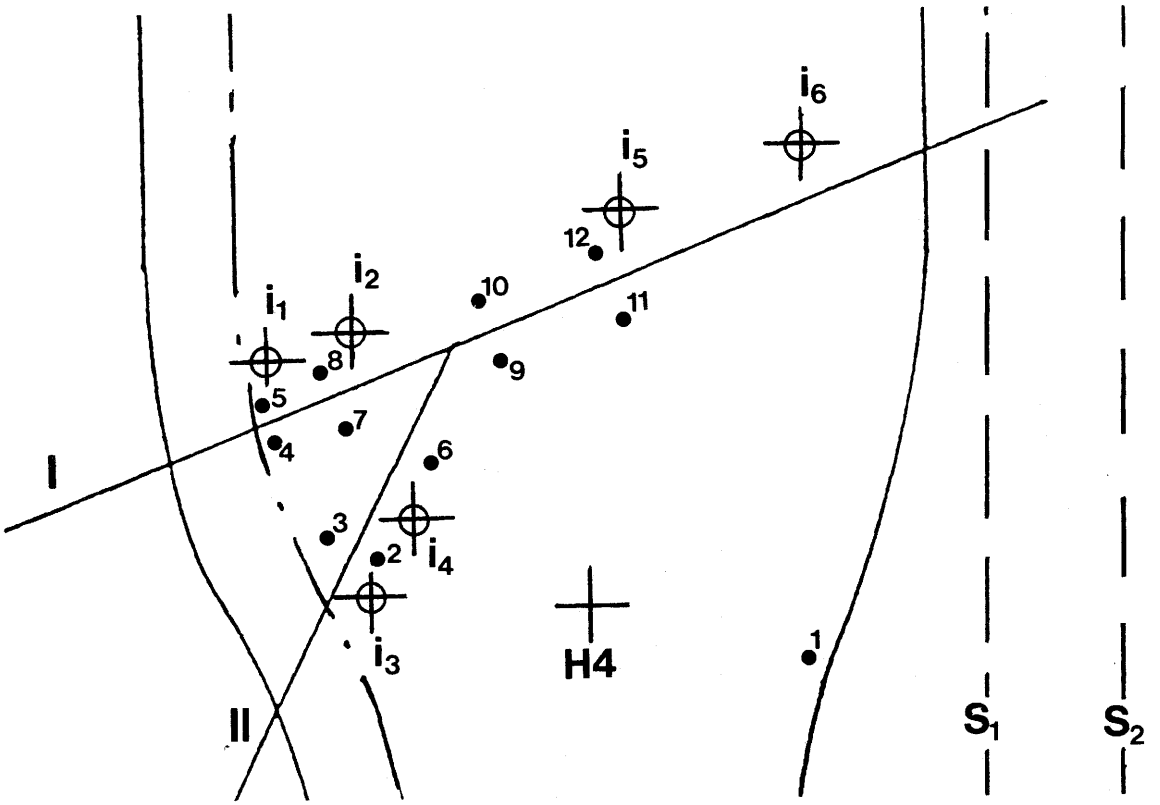

Fig V:11 Positions of the rock dowels

Before the groutings started a number of rock dowels were fixed on the tunnel floor (Fig V:11) and their vertical positions and horizontal distances were carefully measured by VIAK AB both before and after the grouting in order to determine possible rock deformations. The results are listed in Table 24.

The results showed that significant rock heave had occurred only for dowels no 10 and 12. The subsequent rock excavation showed that they were placed on a loose wedge-shaped granite block, formed by two intersecting fractures . The horizontal movements between dowels 9 and 10 and dowels 11 and 12 were also caused by the movement of the loose block.

Table 24 Recorded rock strain caused by the grouting

Dowel no	Heave [1] (mm)		Dowels	Horizontal distance-increase (mm)
1[3]	0.00			
2	+0.05			
3	+0.01		2-3	-0.05
4	+0.01			
5	+0.00		4-5	-0.02
6	+0.10			
7	-0.02		6-7	-0.07
8	+0.00			
9	-0.06		9-10	+0.50
10	+2.62			
11	+0.04			
12	+1.26		11-12	-0.17

1) Differences smaller than 0.1 mm are not significant
2) All figures significant
3) Fix point

3.2 VALIDITY OF FLOW MODEL

The amplitude of the oscillating pressure, which was measured at different levels in the 5 m test hole, was only 15-20 % of the pressure measured in the tube close to the injection machine. Fig V:12 shows, as an example, the pressure waves measured close to the injection machine and at 3.9 m depth. The decrease is in good agreement with Eq. (76). No significant differences in pressure at different levels could be observed, which confirms the conclusions in Chapter V:2.5.6.

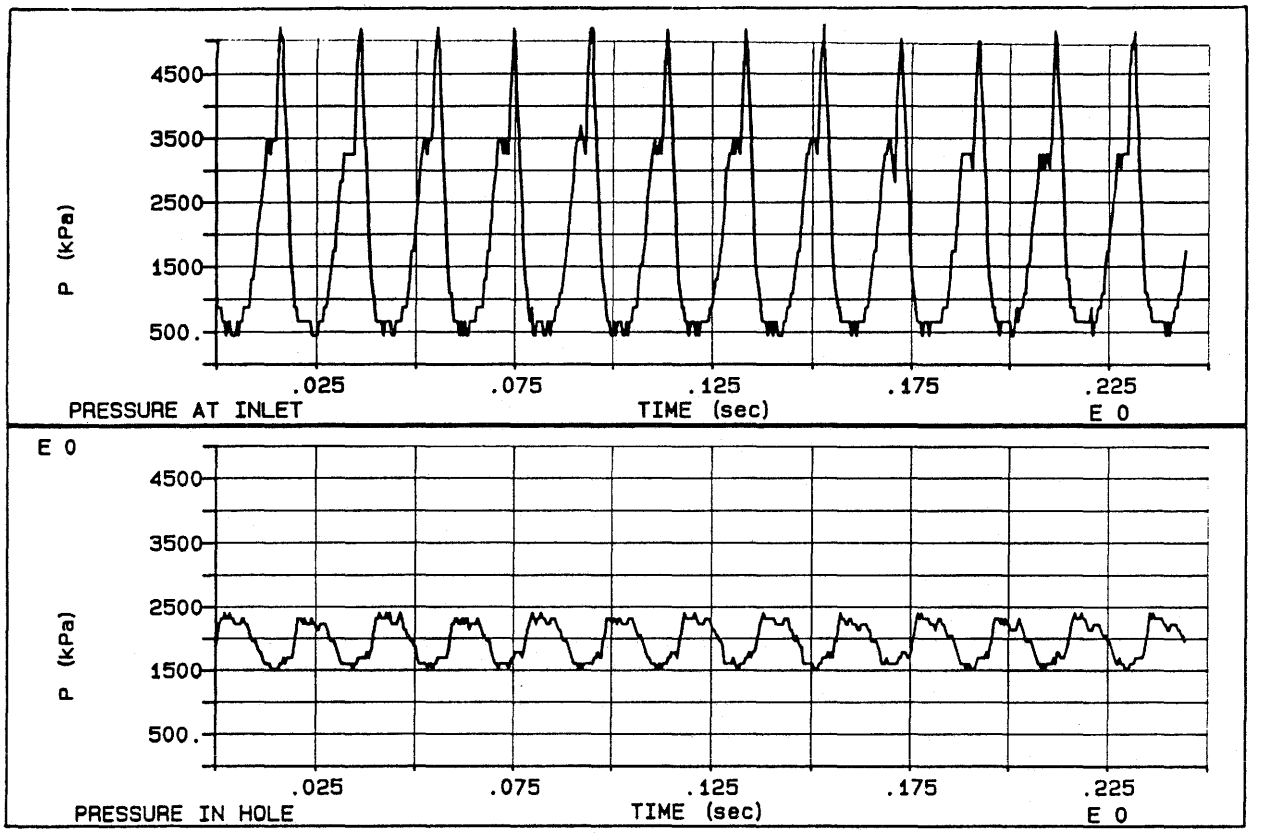

Fig V:12 Example of the decrease in amplitude in the borehole caused by the difference in diameter between the borehole and the tube close to the injection machine

The inflow measurements are not very accurate for volumes smaller than 25-50 cm^3 due to the probable presence of air bubbles in the grout-filled bore hole. Thus, the inflow into i1, i2 and i3 are difficult to evaluate. However, the measured amounts were quite low in these holes and the calculated amounts are definitely of the right order of magnitude (Table 25). Holes i4 and i5 had such large fractures that the predicted penetration length indicated that the grout had to come up

through the floor. This also happened in these holes. Hole i6 offered a possibility of very accurate checking of the agreement between predicted and actual grout inflow. Here, the actual injected grout volume was about half the predicted one.

Table 25 A comparison between the predicted and the measured volumes of penetrated grouts

Hole	Grout	Calculated inflow cm^3	Measured inflow cm^3
i1	Bentonite	0	5-25
i2	Bentonite/quartz	5-12	5-25
i3	Cement	13-54	40-70
i4	Cement	45-62 dm^3	>5 dm^3
i5	Cement	28-65 dm^3	>6.5 dm^3
i6	Bentonite/quartz	141-254	70-100
S1	Cement	100-540	50-200
S2	Bentonite/quartz	10-54	~0

The documentation of grout distribution from breaking up the tunnel floor and the measured sealing effect also gave valuable information on the validity of the flow model. Grout from holes i4 and i6 was found several meters from the holes, which supports the predictions, in principle. In the narrow fractures in holes i2 and i6, bentonite was found 25 and 50 cm from the holes and possible bentonite spots about 1 meter off. The low permeability measured after the injections in hole i5 indicates that fractures with a hydraulic aperture (e_f) as small as 16 μm have been grouted at a distance of 2.9 meters.

Although there is no perfect agreement between the predicted and measured grout inflows it is obvious that the flow models can be used for a reasonably safe prediction of the grout penetration.

3.3 SEALING EFFECT

To evaluate the effect of the grouting, the inflow and Lugeon tests were repeated one week afterwards. Before these measurements could be made the cement and bentonite had to be removed from the boreholes. The cement-filled holes were re-bored using the same crown, thus preventing any cement film from being left on the borehole surface. The same drilling equipment was then used to empty the bentonite-filled holes. Unfortunately, the reboring of hole i4 failed so no measurements could be made in this hole.

The results from the inflow measurements have a limited value since they also include the upper ungrouted 0.5 m zone. Table 26 shows the measured inflow after injection compared to the inflow before the injection.

Table 26 Results from inflow measurements before and after injection.

Borehole	Depth	Inflow l/h	
		Before injection	After injection
i1	1.5	0.029	0.0029
i2	1.5	0.230	0.230
i3	1.5	0.200	0.029
i4	1.5	23	
i5	7.0	23	0.15
i6	7.0	0.35	0.35
S1	40	0.396	0.347
S2	40	0.502	0.520

The high inflow into hole i2 after injection is probably caused by both shallow leakage through the ungrouted zone and secondary disturbing effects from injection in hole 5.

The long holes S1 and S2 were very tight, with inflows around 0.01 l per hour and meter before the grouting. It had no positive effect on the permeability and it thus

seems that these holes did not contain any groutable fractures. The Lugeon tests had in fact shown that no fractures with a hydraulic aperture (e_f) larger than 10 µm were present in these holes, meaning that the possibility for grouts to penetrate was very small unless all water in a two-meter section was carried by one "channel" only.

The Lugeon tests supplied better information of the sealing efficiency since the ungrouted areas of the holes were sealed off. Table 27 shows the results after grouting compared to the measurements before that event.

Table 27 shows that the hydraulic conductivity has decreased to about 10^{-10} m/s in holes i3, i5 and i6, irrespectively of the original value. Hole i2 gave the highest permeability after grouting, which can partly be explained by an external disturbing effect from the later injection of hole i5.

It is concluded that the dynamic injection technique can reduce the average bulk hydraulic conductivity of granitic rock to about 10^{-10} m/s using clay as well as cement as grouting material.

Table 27 The measured flow and the evaluated average hydraulic conductivity at the Lugeon tests before and after injection.

Bore-hole	Depth	Before injection			After injection			Injected material
		Δp (m)	Q (l/m)	k (m/s)	Δp (m)	Q (l/m)	k (m/s)	
i1	0.5-1.5	16.2	0	$<5 \cdot 10^{-12}$	19.4	0	$<5 \cdot 10^{-12}$	Bentonite
i2	0.5-1.5	15.6	0.0052	$3.6 \cdot 10^{-9}$	21.2	0.0022	$9.8 \cdot 10^{-10}$	Bentonite/quartz
i3	0.5-1.5	23.0	0.0043	$2.1 \cdot 10^{-9}$	23.2	0.0002	$8.2 \cdot 10^{-11}$	Cement
i4	0.5-1.5	0	0.294	$>10^{-5}$	-	-	-	Cement
i5	0.5-7	0.54	0.261	$8.4 \cdot 10^{-7}$	20.0	0.005	$3.6 \cdot 10^{-10}$	Cement
i6	0.5-7	22.1	0.0034	$5.9 \cdot 10^{-9}$	21.1	0.0002	$1.4 \cdot 10^{-10}$	Bentonite/quartz

3.4 DOCUMENTATION OF FLOW PATHS

3.4.1 Methods

The search for grout traces began approximately 10 days after the injection was performed. A total volume of 4.5 m^3 rock material was excavated around the five boreholes i2, i3, i5 and i6. The excavation started with removing the rock around i5 since this enabled us to proceed laterally towards i2 and i6 from this position. The technique involved the use of a hand-operated percussion rock-drilling machine with 35 mm crown diameter (Fig V:13, left). A number of 30-45 cm deep holes were strategically drilled with the aim to split and remove the rock along the potential grout-containing fractures. The rock was subsequently broken up by inserting a hydraulically operated Darda rock expander with a maximum expansion pressure of 32 MPa (Fig V:13, right).

Findings of blue bentonite-based, and yellow cement-based grouts were thouroghly mapped and sampled. The most distal findings were carefully measured and transport paths identified.

Fig V:13. Rock excavation technique. Left: Percussion drilling of 30-40 cm deep boreholes around i5. Right: Positioning the hydralic operated Darda expander

3.4.2 Results

3.4.2.1 Borehole i5

Already after removing the upper 20-30 cm of the blast-affected rock it was found that the fractures i5:34 and i5:36 had received large amounts of yellow-colored cement grout. The cement was mainly found as patches on the fracture planes (Fig V:14).The grout seemed to have originated from i5:34 and protruded from there up and into the i5:36 fracture (Fig V:14; Fig V:15). This was actually evidenced when more of the overlying rock was removed. The intersection of the two fractures also led to the formation of a separate wedge-formed granite block extending towards i2. Hole i5:34 intersects the upper part of the i2 borehole at 20 cm depth (Fig V:15).

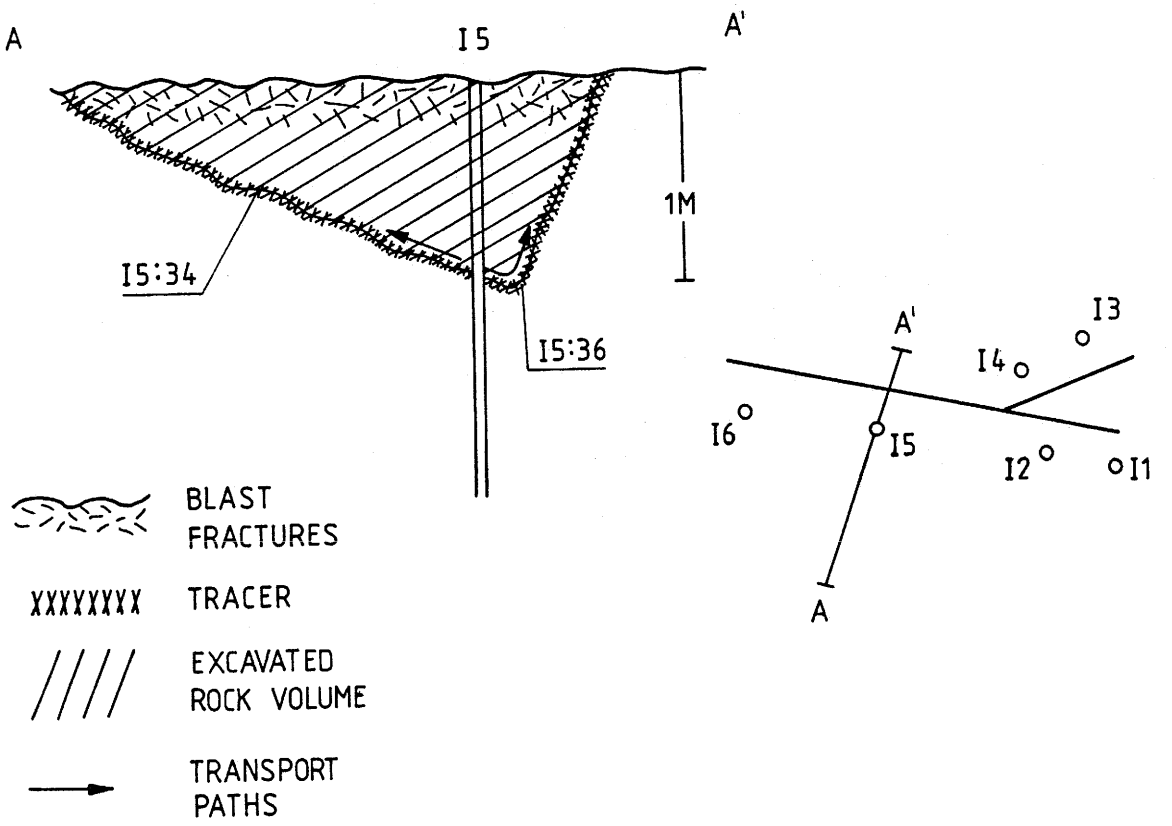

Fig V:14. Section A-A' describing the occurrence of yellow traces in i5:34 and i5:36

The grout was found at a maximum distance of 270 cm from the borehole i2, in the major fracture i5:36. Thinner fractures, more or less vertically dipping and intersecting the i5:34 and i5:36 fracture, were found to contain patches of cement, which were locally rather homogenous (Fig V:18; Fig V:16, B in Fig. V:17).

Fig V:15 Outline of the pit after removing the granite between the i5:34 and i5:36 fractures. The water at the bottom had flowed in from the unsealed tunnel walls.

Fig V:16. Minor fractures containing yellow cement grout at 80-90 cm depth, 20-30 cm from the i5 borehole.

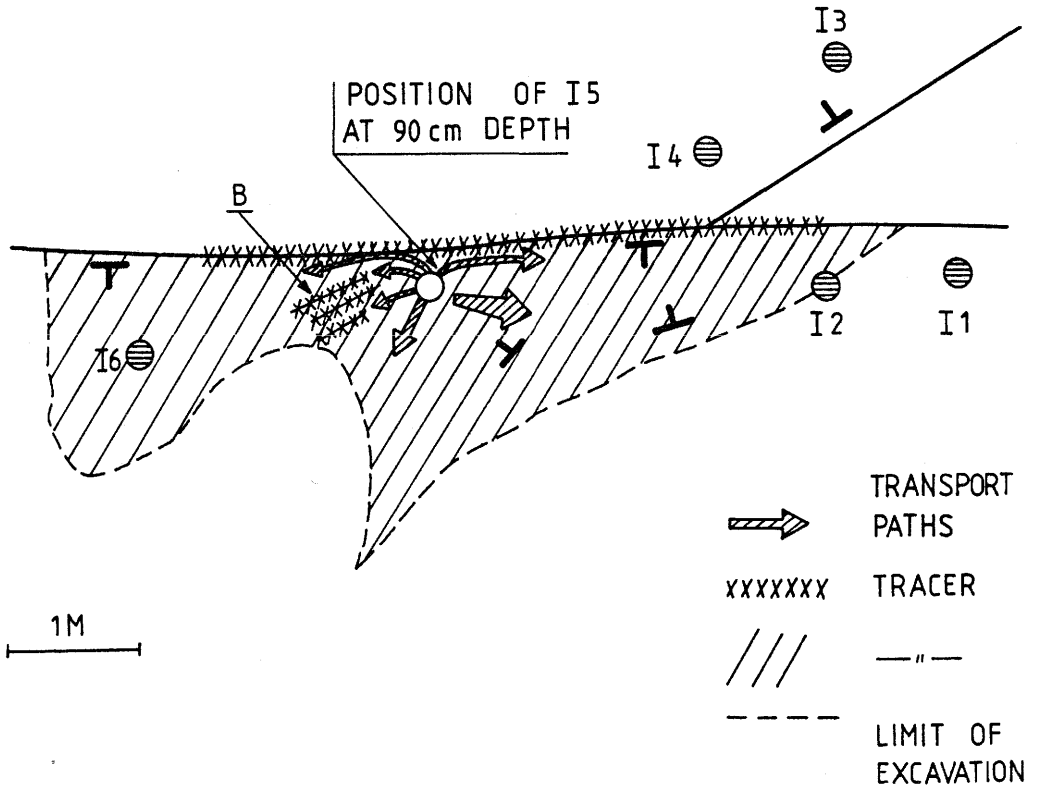

Fig V:17. Migration paths and their relative magnitude, in plane view, of i5.

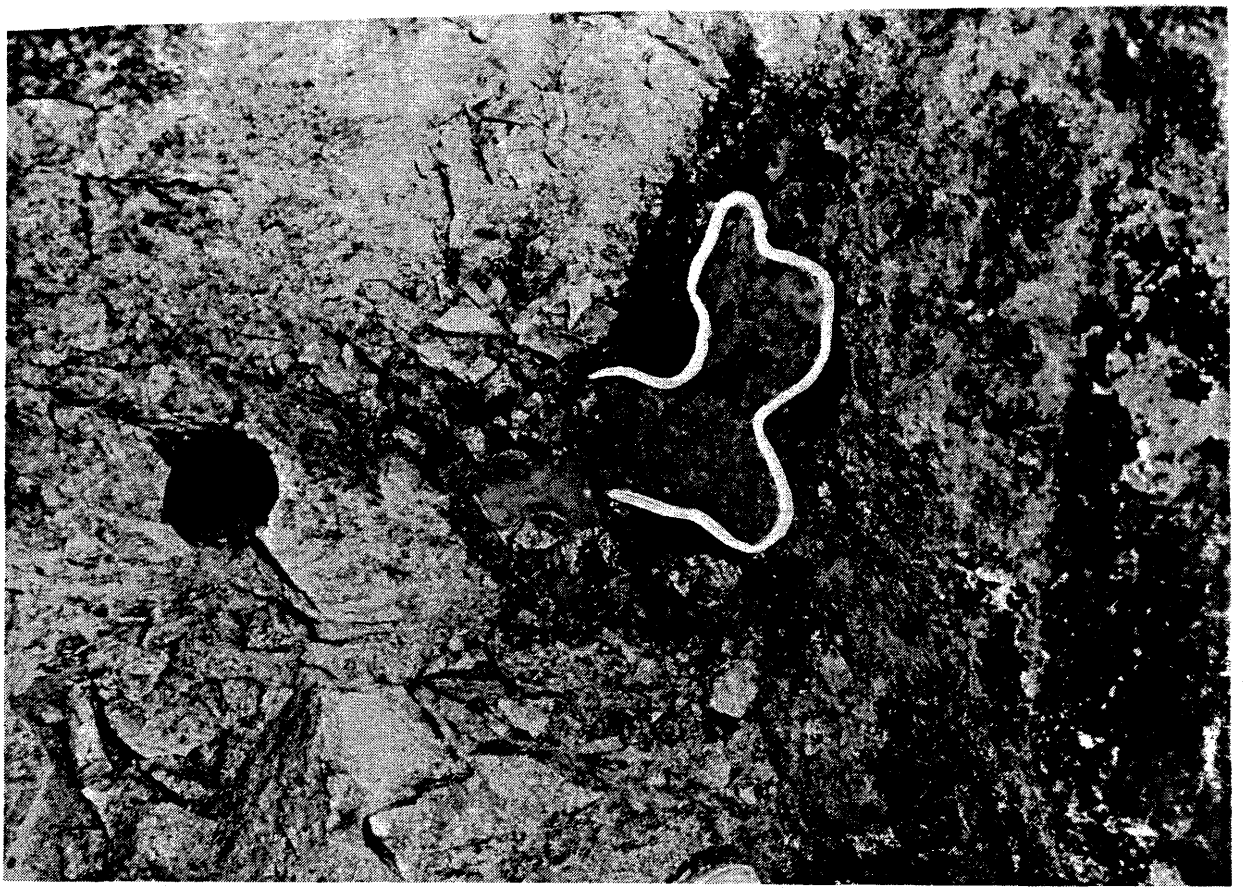

Fig V:18. Patches of yellow cement on i5:36 at 50 cm depth. i5 borehole at the left center

3.4.2.2 Borehole i2

The measured volume of blue bentonite grout that entered the fractures at i2 was somewhere between 5 and 25 cm^3, of which the major part most likely followed the i2:8 and i5:34 fractures. When removing the rock it was also found that the upper 60 cm consisted of massive, more or less fracture-free granite, except for the uppermost part that contained a number of blast-fractures. However, at 70 cm depth there was evidence of blue grout in thin fractures within 5 cm of the borehole-penetrated section. At a distance of approximately 25 cm from the borehole the same bluish color appeared as small spots on a vertically standing thin fracture that wedged out beyond that point (Fig V:19).

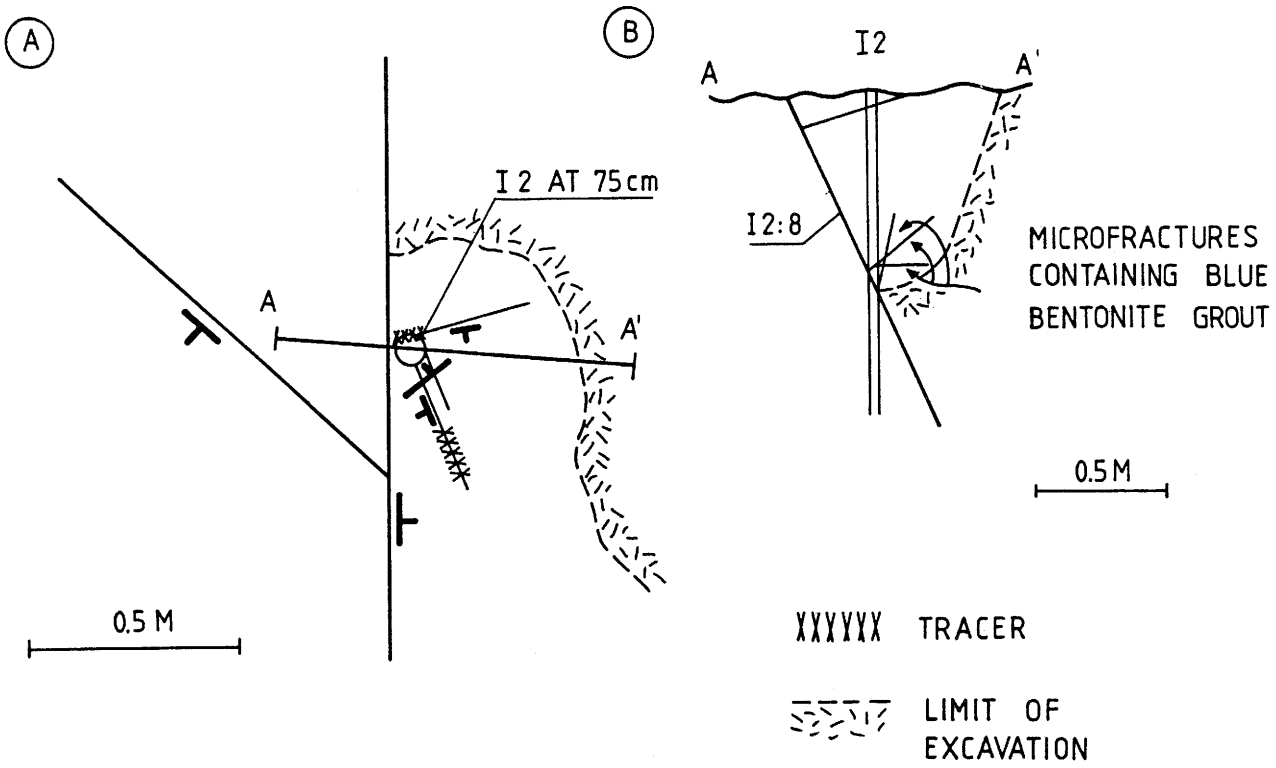

Fig V:19 A: Plane view of i2 and occurrence of blue bentonite tracers and position of cross-section A-A'. B: Characteristics of Cross-section A-A'.

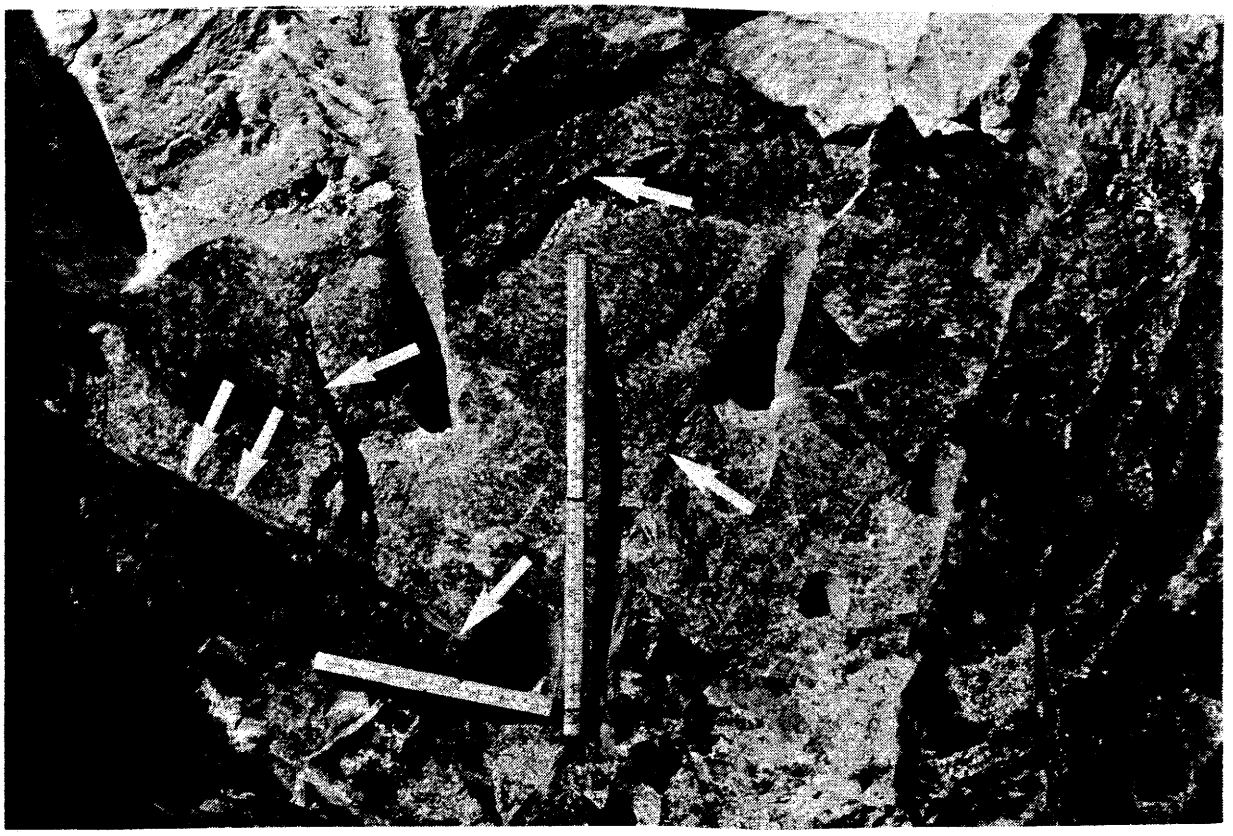

Fig V:20 White arrows pointing on findings of bluish bentonite around i6. Maximum depth of the pit is approximately 80 cm at the borehole position.

3.4.2.3 Borehole i6

Around i6 the granite was found to be extremely well confined by high rock stresses and therefore very difficult to remove without causing destruction of possible bentonite-carrying fractures. The major fracture i6:79 was also found to be closed and sealed by thick chlorite mineralizations, which directed the search towards the i6:72-77 fractures between 30 and 85 cm depth (Fig V:5).

At 35 cm depth along the i6:72 fracture plane a significant amount of bluish bentonite was found. Blue spots were also recognized in the fracture in the borehole at 61 cm depth and bentonite was traced laterally to a maximum distance of 40 cm (Fig. V:20; Fig. V:21).

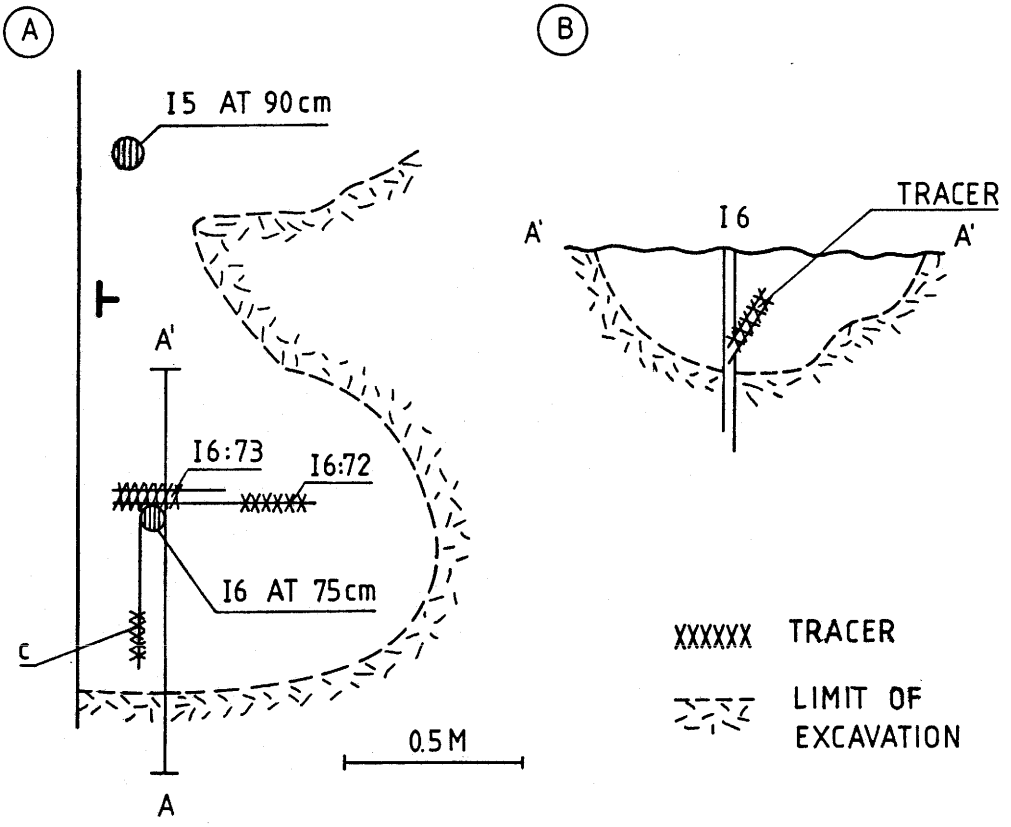

Fig V:21. A: Plane view of i6 and position of cross-section A-A'. B: Characteristics of cross-section A-A'

The blue bentonite occurred as channels, mainly in very thin microfractures with minor lateral extension. The maximum transport distance was found to be 40-50 cm after entering the fracture at the borehole intersection at 60-65 cm depth. Bluish bentonite was also found in i6:73 and a perpendicularly striking fracture not visible in the borehole (C in Fig V:21), indicating a transport path from the i6:72 fracture.

3.4.2.4 Borehole i4

The injected cement in i4 was not possible to extract by drilling. The attempt to do so resulted in a 40 cm thick suspension of cuttings, water and yellow tracer remaining in the upper part of hole. Since this would flow out over the surrounding rock at continued excavation of this part it would prevent proper identification of protruded cement in fractures. It was therefore decided to primarily focus on the investigation of i3. This hole behaved similarly to the i2 and i6 boreholes on grouting.

However, it could be observed, when removing the upper parts of the granite around i3, that the grout from i4 had followed the i4:25 fracture to an approximate distance of 120 cm from the fracture-borehole intersection. The grout from i4 was also observed in an intersecting set of N80°E striking and 25 degrees dipping shallow fractures (Fig V:22).

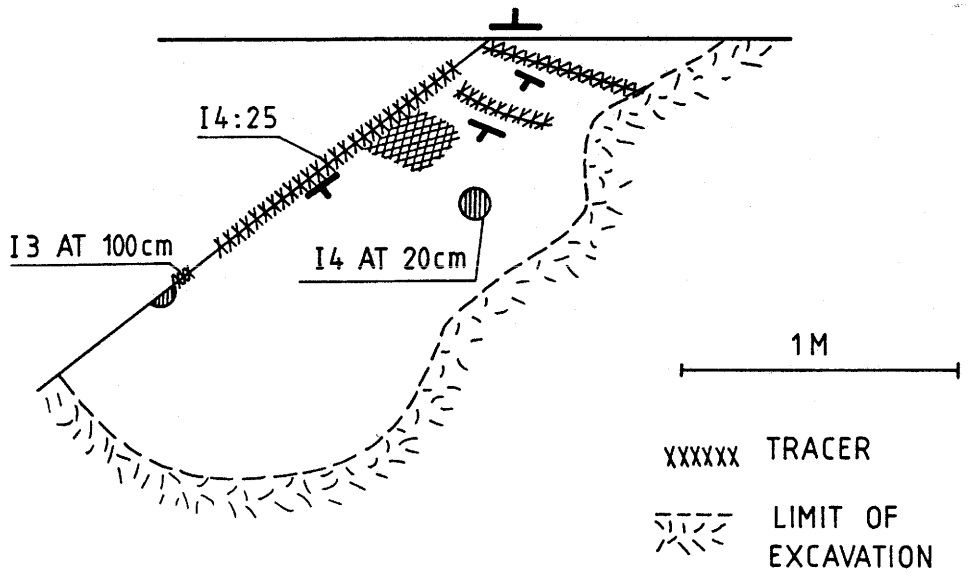

Fig V:22. Plane view of i3 and i4 with marked tracer occurrence

3.4.2.5 Borehole i3

The rock in the upper 100 cm of the borehole consisted of massive granite containing closed microfractures and this led to difficulties in excavating the rock mass. At 100 cm depth the borehole penetrated the dominant fracture i3:13a, the same as i4:25, which was the only fracture that was open in this borehole. Only a minor amount of yellow cement was found in the area adjacent to the borehole intersection. A 1-2 cm wide channel was found to extend approximately 5 cm up along the fracture-plane (Fig V:23). It does also seem to have partly followed the intersection of a minor fracture i3:13b and i3:13a.

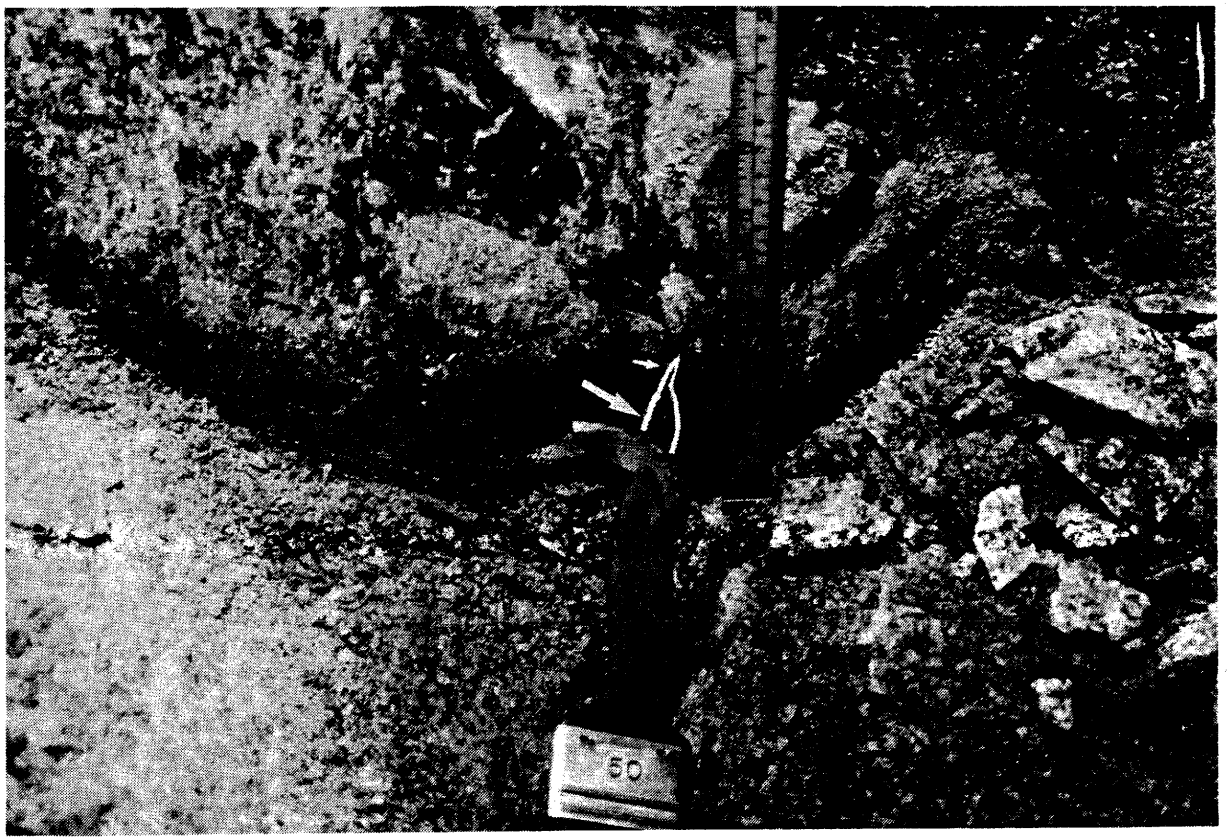

Fig V:23. Yellow cement on the i3:13a fracture-plane at 100 cm depth.

4 CONCLUSIONS AND RECOMMENDATIONS

4.1 GENERAL

The Pilot Test was concluded to be succesful on the following grounds:

* The grouting equipment was found to be thoroughly field-adapted and practical. Its complete tightness made it possible to evaluate the injected grout with sufficient accuracy.

* Both types of grout were found to penetrate fractures with apertures down to 10-20 µm. The grout penetrated such narrow fractures to several decimeters from the respective hole as demonstrated by the excavation.

* Groutable rock became effectively sealed.

* Piping did not occur on Lugeon testing after grouting.

* Except for one hole, where the shallow rock consisted of almost free-lying rock slabs,the rock was not fractured or distorted even at grouting pressures of several megapascals despite the small distance between the packer and the free surface.

* The flow model is valid, in principle, which means that relevant laboratory-derived flow parameters have been selected and that the effect of grouting can be predicted for different hole geometries, including larger holes.

4.2 RECOMMENDATIONS

A technique now appears to be available for successful grouting of fine fractures. Since very promising grout materials are also at hand it is suggested to continue the project by applying the investigated grouting techniques on a full scale. It is recommended also to develop the technique further, in order to make it applicable

also to very fractured shallow roof and walls of tunnels, where the grouting pressure must be kept low.

GENERAL REFERENCES

1. De Wiest, R.J.M, 1965, "Geohydrology", New York, John Wiley and Sons.

2. Pusch, R., Erlström, M., and Börgesson, L., 1985, "Sealing of Rock Fractures, A Survey of Potentially Useful Methods and Substances", SKB Technical Report 85-17.

3. Pusch, R., Erlström, M., and Börgesson, L., 1987, "Piping and Erosion Phenomena in Soft Clay Gels", SKB Technical Report 87-09.

4. Pusch, R., Hökmark, H., and Börgesson, L., 1987, "Outline of Models of Water and Gas Flow Through Smectite Clay Buffers", SKB Technical Report 87-10.

5. Pusch, R., and Karnland, O., 1988, "Hydrothermal Effects on Montmorillonite, A Preliminary Study", SKB Technical Report 88-15.

6. Wylie and Streeter, 1978, "Fluid Transients", Mc Graw-Hill Inc.